Elsevier Editorial System(tm) for Lithos
Manuscript Draft

Manuscript Number: LITHOS4424R1

Title: Ultra-oxidized rocks in subduction mélanges? Decoupling between oxygen fugacity and oxygen availability in a Mn-rich metasomatic environment

Article Type: SI:HP & UHP metamorphism

Keywords: manganese; oxidation; oxygen fugacity; subduction; mantle wedge; slab; eclogite

Corresponding Author: Dr. Simone Tumiati,

Corresponding Author's Institution: Università di Milano

First Author: Simone Tumiati

Order of Authors: Simone Tumiati; Gaston Godard; Silvana Martin; Nadia Malaspina; Stefano Poli

Abstract: The manganese ore of Praborna (Italian Western Alps) is embedded within a metasedimentary sequence belonging to a subduction mélange equilibrated at high-pressure (HP) conditions (ca. 2 GPa) during the Alpine orogenesis. The pervasive veining of the ore and the growth of "pegmatoid" HP minerals suggest that these Mn-rich rocks strongly interacted with slab-derived fluids during HP metamorphism. These rocks are in textural and chemical equilibrium with the veins and in contact with sulphide- and magnetite-bearing metabasites at the bottom of the sequence. They contain braunite (Mn2+Mn3+6SiO12), quartz, pyroxmangite (Mn2+SiO3), and minor hematite, omphacite, piemontite and spessartine-rich garnet. Sulphides are absent in the Mn-rich rocks, whereas sulphates (barite, celestine) occur together with As- and Sb-oxides and silicates. This rock association provides an excellent natural laboratory to constrain the redox conditions in subducting oceanic slab mélanges at HP and fluid-present conditions. Similarly to Fe-bearing minerals, Mn oxides and silicates can be regarded as natural redox-sensors. A thermodynamic dataset for these Mn-bearing minerals is built, using literature data as well as new thermal expansion parameters for braunite aud pyrolusite, derived from experiments. Based on this dataset and the observed assemblages at Praborna, thermodynamic calculations show that these mélange rocks are characterized by ultra-oxidized conditions (ΔFMQ up to +12.7) if the chemical potential of oxygen (or the oxygen fugacity fO2) is accounted for. On the other hand, if the molar quantity of oxygen is used as the independent state variable to quantify the bulk oxidation state, the ore appears only moderately oxidized and comparable to typical subduction-slab mafic eclogites. Such an apparent contradiction may happen in rock systems whenever oxygen is improperly considered as a perfectly mobile component. In the Earth's mantle, redox reactions take place mainly between solid oxides and silicates, because O2 is a negligible species in the fluid phase. Therefore, the description of the redox conditions of most petrological systems requires the introduction of an extensive variable, namely the oxygen molar quantity (nO2). As a consequence, the oxygen chemical potential, and thus fO2, becomes a dependent state variable, not univocally indicative of the redox conditions of the entire rock column of a subduction zone, from the dehydrating oceanic crust to the overlying mantle wedge. On a more general basis, the comparison of fO2 retrieved from different bulk compositions and different phase assemblages is sometimes challenging and should be undertaken with care. From the study of mélange rocks at Praborna, the distribution of oxygen at subduction zones could be modelled as an oxidation gradient, grading from a maximum in the subducted altered oceanic crust to a minimum in the overlying peridotites of the mantle hanging-wall.

ABSTRACT

The manganese ore of Praborna (Italian Western Alps) is embedded within a metasedimentary sequence belonging to a subduction mélange equilibrated at high-pressure (HP) conditions (ca. 2 GPa) during the Alpine orogenesis. The pervasive veining of the ore and the growth of "pegmatoid" HP minerals suggest that these Mn-rich rocks strongly interacted with slab-derived fluids during HP metamorphism. These rocks are in textural and chemical equilibrium with the veins and in contact with sulphide- and magnetite-bearing metabasites at the bottom of the sequence. They contain braunite ($Mn^{2+}Mn^{3+}{}_6SiO_{12}$), quartz, pyroxmangite ($Mn^{2+}SiO_3$), and minor hematite, omphacite, piemontite and spessartine-rich garnet. Sulphides are absent in the Mn-rich rocks, whereas sulphates (barite, celestine) occur together with As- and Sb-oxides and silicates. This rock association provides an excellent natural laboratory to constrain the redox conditions in subducting oceanic slab mélanges at HP and fluid-present conditions. Similarly to Fe-bearing minerals, Mn oxides and silicates can be regarded as natural redox-sensors. A thermodynamic dataset for these Mn-bearing minerals is built, using literature data as well as new thermal expansion parameters for braunite aud pyrolusite, derived from experiments. Based on this dataset and the observed assemblages at Praborna, thermodynamic calculations show that these mélange rocks are characterized by ultra-oxidized conditions (ΔFMQ up to +12.7) if the chemical potential of oxygen (or the oxygen fugacity fO_2) is accounted for. On the other hand, if the molar quantity of oxygen is used as the independent state variable to quantify the bulk oxidation state, the ore appears only moderately oxidized and comparable to typical subduction-slab mafic eclogites. Such an apparent contradiction may happen in rock systems whenever oxygen is improperly considered as a perfectly mobile component. In the Earth's mantle, redox reactions take place mainly between solid oxides and silicates, because O_2 is a negligible species in the fluid phase. Therefore, the description of the redox conditions of most petrological systems requires the introduction of an extensive variable, namely the oxygen molar quantity (nO_2). As a consequence, the oxygen chemical potential, and thus fO_2, becomes a dependent state variable, not univocally indicative of the redox conditions of

the entire rock column of a subduction zone, from the dehydrating oceanic crust to the overlying mantle wedge. On a more general basis, the comparison of fO_2 retrieved from different bulk compositions and different phase assemblages is sometimes challenging and should be undertaken with care. From the study of mélange rocks at Praborna, the distribution of oxygen at subduction zones could be modelled as an oxidation gradient, grading from a maximum in the subducted altered oceanic crust to a minimum in the overlying peridotites of the mantle hanging-wall.

Highlights:

- The manganese-rich rocks of Praborna are high-pressure metacherts belonging to a slab mélange.
- Rocks are veined pervasively suggesting a strong interaction at HP with slab-derived fluids.
- Mn-rich mineral associations suggest ultra-high fO_2 conditions up to ΔFMQ +12.7.
- In terms of quantity of O_2, the same rocks display a moderate oxidation state.
- The decoupling between intensity and extensity of O_2 in metasomatic rocks is highlighted.

Ultra-oxidized rocks in subduction mélanges? Decoupling between oxygen fugacity and oxygen availability in a Mn-rich metasomatic environment

Simone Tumiati[a,*], Gaston Godard[b], Silvana Martin[c], Nadia Malaspina[d] and Stefano Poli[a]

[a] *Dipartimento di Scienze della Terra "Ardito Desio", Università degli Studi di Milano, via Mangiagalli 34, I-20133 Milano, Italy; simone.tumiati@unimi.it*

[b] *Institut de Physique du Globe de Paris, Sorbonne Paris Cité, Université Paris Diderot, UMR 7154 CNRS, 1 rue Jussieu, F-75252 Paris, France*

[c] *Dipartimento di Geoscienze, Università degli Studi di Padova, via Giotto 1, 35137 Padova, Italy*

[d] *Dipartimento di Scienze dell'Ambiente e del Territorio e di Scienze della Terra, Università degli Studi di Milano Bicocca, piazza della Scienza 4, 20126 Milano, Italy*

ABSTRACT

The manganese ore of Praborna (Italian Western Alps) is embedded within a metasedimentary sequence belonging to a subduction mélange equilibrated at high-pressure (HP) conditions (ca. 2 GPa) during the Alpine orogenesis. The pervasive veining of the ore and the growth of "pegmatoid" HP minerals suggest that these Mn-rich rocks strongly interacted with slab-derived fluids during HP metamorphism. These rocks are in textural and chemical equilibrium with the veins and in contact with sulphide- and magnetite-bearing metabasites at the bottom of the sequence. They contain braunite ($Mn^{2+}Mn^{3+}_6SiO_{12}$), quartz, pyroxmangite ($Mn^{2+}SiO_3$), and minor hematite, omphacite, piemontite and spessartine-rich garnet. Sulphides are absent in the Mn-rich rocks, whereas sulphates (barite, celestine) occur together with As- and Sb-oxides and silicates. This rock association provides an excellent natural laboratory to constrain the redox conditions in subducting oceanic slab mélanges at HP and fluid-present conditions. Similarly to Fe-bearing minerals, Mn

oxides and silicates can be regarded as natural redox-sensors. A thermodynamic dataset for these Mn-bearing minerals is built, using literature data as well as new thermal expansion parameters for braunite aud pyrolusite, derived from experiments. Based on this dataset and the observed assemblages at Praborna, thermodynamic calculations show that these mélange rocks are characterized by ultra-oxidized conditions (ΔFMQ up to +12.7) if the chemical potential of oxygen (or the oxygen fugacity fO_2) is accounted for. On the other hand, if the molar quantity of oxygen is used as the independent state variable to quantify the bulk oxidation state, the ore appears only moderately oxidized and comparable to typical subduction-slab mafic eclogites. Such an apparent contradiction may happen in rock systems whenever oxygen is improperly considered as a perfectly mobile component. In the Earth's mantle, redox reactions take place mainly between solid oxides and silicates, because O_2 is a negligible species in the fluid phase. Therefore, the description of the redox conditions of most petrological systems requires the introduction of an extensive variable, namely the oxygen molar quantity (nO_2). As a consequence, the oxygen chemical potential, and thus fO_2, becomes a dependent state variable, not univocally indicative of the redox conditions of the entire rock column of a subduction zone, from the dehydrating oceanic crust to the overlying mantle wedge. On a more general basis, the comparison of fO_2 retrieved from different bulk compositions and different phase assemblages is sometimes challenging and should be undertaken with care. From the study of mélange rocks at Praborna, the distribution of oxygen at subduction zones could be modelled as an oxidation gradient, grading from a maximum in the subducted altered oceanic crust to a minimum in the overlying peridotites of the mantle hanging-wall.

Keywords: manganese, oxidation, oxygen fugacity, subduction, mantle wedge, slab, eclogite

Highlights:

- The manganese-rich rocks of Praborna are high-pressure metacherts belonging to a slab mélange.

- Rocks are veined pervasively suggesting a strong interaction at HP with slab-derived fluids.
- Mn-rich mineral associations suggest ultra-high fO_2 conditions up to ΔFMQ +12.7.
- In terms of quantity of O_2, the same rocks display a moderate oxidation state.
- The decoupling between intensity and extensity of O_2 in metasomatic rocks is highlighted.

1. Introduction

The reduction-oxidation (redox) conditions of rocks are known to affect phase relationships, speciation of volatile elements, trace element partitioning, diffusivity, electrical conductivity and mechanical properties (Arculus, 1985). Redox conditions are traditionally described using the intensive variable oxygen fugacity (fO_2). Variability in fO_2 at subduction zones has been debated since a long time (Gill, 1981; Wood et al., 1990; Foley et al., 2011). Compared to the asthenospheric and lithospheric mantles, relatively high fO_2 has been proposed for subducted slab materials, sub-arc mantle and arc magmas (Hirschmann, 2009; Kelley and Kottrell, 2009; Malaspina et al., 2009, 2010; Groppo and Castelli, 2010; Evans, 2012). However, trace-element and isotope systematics, aimed to constrain the variation of fO_2 in the mantle (Canil, 2002; Lee et al., 2005, 2010), challenge such conclusion, emphasizing a discrepancy between the fO_2 calculated by oxygen thermobarometry and that inferred from V/Sc data on arc lavas.

The redox conditions of rocks could be also expressed in terms of ratios of cations occurring in different oxidation states, such as Fe^{2+} and Fe^{3+}. However, paucity of thermodynamic data on Fe^{3+} end-members of minerals and analytical difficulties in retrieving Fe^{3+}/Fe^{2+} in fine-grained, texturally complex volatile-rich rocks have hindered so far the quantitative assessment of redox conditions in the slab-mantle mixing zone in terms of Fe^{3+}/Fe^{2+} ratio (Bebout, 2007). On the other hand, Mn-rich nodules and crusts, though volumetrically very limited, are nearly ubiquitous on the seafloor (Manheim, 1978) and contain highly oxidized Mn^{4+}-bearing phases, such as amorphous MnO_2, pyrolusite, birnessite, and todorokite (e.g., Ostwald and Frazer, 1973). Upon metamorphism, a variety of Mn^{3+} and Mn^{2+} oxides and silicates may form in subduction mélanges, depending on *P*–

77 *T–X* conditions (e.g., Dasgupta, 1997; Tumiati et al., 2010). The variable oxidation states of
78 manganese make Mn minerals extremely useful sensors to constrain redox conditions of rocks.
79 The present study takes advantage of the manganese ore of Praborna, cropping out in the Italian
80 western Alps, and consisting of Mn-rich metasediments embedded within meta-ophiolites (Tumiati
81 et al., 2010). This ore displays a complex variety of Mn- and Fe-rich mineral assemblages, formed
82 at eclogite-facies conditions in a subduction mélange. Swarms of stockwork high-pressure (HP)
83 veins are cutting the Mn-rich rocks, suggesting an interaction with slab-derived fluids at very high
84 fluid-rock ratio, as expected for such very thin, veined, metasedimentary sequences (Bebout et al.,
85 2013). Praborna represents an excellent natural laboratory for the study of the behaviour of the
86 component oxygen in terms of mobility in oceanic slab mélanges subducted at HP conditions and
87 flushed by fluids. This particular case should be considered as paradigmatic, because it draws the
88 attention to the choice of the independent parameter capable of describing the redox conditions of
89 rocks in a metasomatic environment.
90
91 **2. Concepts and definitions**
92 Oxidation and reduction are defined in general chemistry as loss and gain of electrons, respectively.
93 Since oxygen is the most common electron acceptor in natural systems, because of its high
94 electronegativity, oxidation and reduction generally mean gain and loss of oxygen, by exchange
95 with the external medium. Thus, the redox condition of rocks is described by considering a variable
96 that can potentially rule this exchange. Exception done for a few works (e.g., Chinner, 1960; Evans,
97 2006), the variable traditionally considered in Earth sciences is the oxygen fugacity (fO_2). However,
98 O_2 is not expected to be a major gaseous/fluid species in the Earth's interior, and the chemical
99 potential of oxygen (either μO or μO_2) could appear more appropriate. In this study, we use both
100 variables fO_2 and μO_2 considered as equivalent.
101 The fugacity of a gaseous species is the theoretical partial pressure that this gas would have if it
102 would obey the ideal-gas law ($P \times V = n \times R \times T$). This means that fugacity is equal to partial

pressure only in ideal gases (i.e., for $P \rightarrow 0$ bar). At higher pressures, gases strongly diverge from the ideal gas law, and a fugacity coefficient ($\Phi = f / P$) is introduced accounting for the non-ideal behaviour. The fugacity of a gas is in turn a function of the chemical potential of the relative component. For the component O_2, this relationship is expressed by the following equation:

$$\mu O_2 = G^0_{f,T,O2} + R \times T \times \ln fO_2/f^0O_2$$

where

- μO_2 (J•mol^{-1}) is the chemical potential of the component O_2 at P and T of interest;
- $G^0_{f,T,O2}$ (J•mol^{-1}) is the molar Gibbs energy of formation of pure oxygen (O_2) at P^0 = 1 bar and T;
- R (J•K^{-1}•mol^{-1}) is the gas constant;
- fO_2 (bar) is the fugacity of pure oxygen at P and T of interest;
- f^0O_2 is the fugacity of pure oxygen at the standard-state pressure P^0 (f^0O_2 = 1 bar at all T).

As for any other component of a petrological system, μO_2, and thus fO_2, is ideally homogenous in all phases at equilibrium and independent of the phase abundance; in other terms, it is an intensive variable. The O_2 molar quantity (nO_2) is the conjugate extensive variable of μO_2, since the product ($\mu O_2 \times nO_2$) has the dimension of an energy (J•mol^{-1} × mol = J), similarly to other couples of intensive and extensive variables like ($P \times V$) and ($T \times -S$).

While considering an oxidised system, the set of basis vectors that generate the compositional vector space (i.e. the set of independent components) could be either {Si, Fe, Mn, ..., O} or {SiO_2, FeO, MnO, ..., O_2}. We have chosen here the latter set of independent components, so that μO_2 and nO_2 have to be considered instead of μO and nO. In that case, nO_2 represents the coordinate for the basis vector O_2; it equals zero when all Fe and Mn occur in their divalent oxidation state, i.e. as FeO and MnO (see Fig. 7).

The choice to describe a redox system in terms of intensive variables (fO_2 or μO_2) is entirely valid only if O_2 can be considered a “perfectly mobile” component. As already explained by Korzhinskii (1959, p. 16), the behaviour of a chemical component in a rock system could be “inert” or

129 "perfectly mobile", depending on its mobility between the system and an external medium. As an
130 example, during a fluid-rock interaction, where the system is the rock and the external medium is a
131 fluid phase flushing the rock, those rock components that are not readily transported by the fluid are
132 considered inert or "immobile", whereas components that can dissolve into the fluid can be
133 considered "mobile" and rapidly react with the surrounding rock. On this principle, the quantity of
134 inert components has a fundamental role to attain the equilibrium, while it can be neglected for
135 mobile components. Therefore, from a thermodynamic point of view, during the equilibration
136 between a rock and a fluid phase, the molar quantity of material should be considered as an
137 independent state variable for inert components, whereas chemical potential must be used as an
138 independent state variable for perfectly mobile components (Korzhinskii, 1959).
139 A complication arises when we consider the component O_2 in the Earth's interior, because redox
140 reactions take place mainly between solid oxides and silicates, where oxygen is bonded to relatively
141 inert components such as FeO (forming, for example, Fe_2O_3) and MnO (forming, for example,
142 Mn_2O_3), while it occurs in very limited amounts in fluids. Therefore, O_2 cannot be considered
143 unequivocally a perfectly mobile component. It could well be that, in many cases, O_2 is better
144 regarded as an inert component, so that nO_2, rather than μO_2, becomes an independent
145 thermodynamic state variable imposed upon the system.
146 Considering the variable nO_2 instead of μO_2 modifies the inspection of phase relationships (e.g.,
147 Hillert, 1985). In particular, when a molar quantity is introduced as an axis instead of its conjugate
148 chemical potential, two one-phase fields will separate from each other, thus leaving room for the
149 two-phase field, and their distance will be equal to the difference in the molar quantity between the
150 two phases (Fig. 1). In addition, when molar quantities other than nO_2 are not constant, μO_2 (and
151 fO_2) is not a simple, monotonically increasing function of the quantity of oxygen. Therefore, the
152 reconstruction of the extensive property (nO_2) from the intensive variable (fO_2 or μO_2) can be a
153 very inaccurate procedure in natural, multi-component systems (see Malaspina et al., 2009, 2012).
154

3. The Praborna manganese ore

Slices of Mn-rich metasediments are commonly hosted in meta-ophiolites of the Western Alps. Praborna (Saint-Marcel valley, Italy; Fig. 2) is the largest Mn deposit in the Zermatt-Saas unit, which is interpreted as part of the Jurassic oceanic lithosphere of the Tethys, subducted during the Alpine orogeny (e.g., Dal Piaz, 2001). In the Zermatt-Saas unit, Mn-rich rocks from Lago di Cignana (Valtournanche) preserve coesite (Reinecke, 1998) and microdiamonds (Frezzotti et al., 2011), suggesting that the oceanic sediments underwent ultrahigh-*P* (UHP) metamorphism. HP metamorphic peak conditions of 2.1 GPa and 550 °C were recorded also in the meta-ophiolite of the Saint-Marcel valley (Martin et al., 2008), which are the country rocks of the Praborna deposit.

The disused mine of Praborna, known since 1415 CE (Castello, 1982), is world-famous for its peculiar rocks and minerals. In particular, it is the type locality of five mineralogical species, namely piemontite, braunite, romeite, strontiomelane, and manganiandrosite-(Ce) (Ciriotti et al., 2009 and references therein). The Praborna deposit displays a continuous change in mineralogy from the basal contact with metabasites (now glaucophanites) towards the upper contact with Mn-poor metasediments (Figs. 2, 3), and consists of boudinaged Mn-rich metasediments cropping out in a "mélange" composed of serpentinite, ophicarbonate breccias, metagabbro and metabasalt with N-MORB affinity (Fig. 2; Martin and Kienast, 1987; Martin et al., 2008; Tumiati et al., 2010). Swarms of stockwork HP veins cut the Mn-rich rocks especially near the basal contact (Fig. 3), suggesting an interaction with slab-derived fluids. On the basis of the mineralogical composition, several "levels" have been recognized (Martin and Kienast, 1987; Tumiati et al., 2010). Basal levels and veins contain braunite (the ore mineral), piemontite and jadeite-rich Mn-bearing omphacite, whereas upper levels are characterised by the abundance of garnet ± pyroxmangite ± jadeite-poor clinopyroxene. Quartz is generally abundant in all the levels. In Table 1, we report representative mineral compositions of the basal and upper levels, the HP veins and the SiO_2-undersaturated assemblages found at Praborna. Other details concerning mineralogy and petrography of the ore are provided in Section 5, as Supplementary Material (SM), and in Tumiati et al. (2010).

4. Materials and methods

Several thin sections of the basal and upper levels (Table SM-1 in the Supplementary Material) have been analysed at the petrographic and scanning electron microscopes. Chemical analyses reported in Table 1 were performed using the Cameca SX100 (Paris) and JEOL 8200 (Milano) wavelength-dispersive electron microprobes (EMP), at 15-kV accelerating potential, 15-nA sample current and 1-μm beam diameter. Standards used were albite (Na), diopside (Ca, Mg and Si), Fe_2O_3 (Fe), orthoclase (Al and K), $MnTiO_3$ (Mn and Ti), Cr_2O_3 (Cr) and barite (Ba). A counting time of 30 s was applied for all elements.

The Fe^{3+}/Fe_{TOT} and Mn^{3+}/Mn_{TOT} ratios in minerals have been calculated by stoichiometry. Because of the relative electronegativity of Fe and Mn, the pair Fe^{3+}–Mn^{2+} is more stable than the pair Fe^{2+}–Mn^{3+}, which has never been reported in minerals (Sherman, 1990). In fact, values of standard redox potential (or electromotive force) are 0.77 V for the pair Fe^{3+}–Fe^{2+} and 1.51 V for Mn^{3+}–Mn^{2+}. Therefore, the charges were calculated iteratively, by adjusting first Fe^{3+}/Fe_{TOT}, and then, if necessary, Mn^{3+}/Mn_{TOT}. In any case, this study is mainly focused on simple manganese oxides and silicates characterized by fixed Mn^{3+}/Mn_{TOT}, so that uncertainties related to this procedure do not affect the conclusions provided here.

For more complex phases, crystal chemistry has been evaluated mostly using the principal component analysis (PCA). In particular, this method was used to unravel substitution vectors in solid solutions. PCA is a statistical procedure that transforms a number of possibly correlated variables into the same number of uncorrelated variables given by the eigenvectors of the covariance matrix, and called principal components. The first principal component (F1) account for as much of the variability in the data as possible, and thus corresponds to the highest eigenvalue of the covariance matrix; each of the succeeding components (F2, F3…) accounts for as much of the remaining variability as possible. For other details and examples of PCA applied to EMP data, refer to Tumiati et al. (2005 A, 2005 B, 2008, 2013).

Raman spectroscopy of selected samples has been carried out using a green (514 nm) laser radiation, at the *Muséum National d'Histoire Naturelle* of Paris. In particular, Raman spectroscopy was required for the identification of the HP $MnSiO_3$ polymorph pyroxmangite.

5. Mineralogy and petrography of the Praborna ore

5.1 Basal levels

The basal levels (Fig. 3; Table 1) are in contact with glaucophanite made up of glaucophane + garnet + chloritoid + chlorite + paragonite and showing pseudomorphs after lawsonite (Martin et al., 2008). These basal levels mainly contain braunite ($Mn^{2+}Mn^{3+}{}_6SiO_{12}$) and piemontite (Fig. 3), minor quartz, omphacite, garnet, phengite and pyroxmangite, the HP polymorph of $Mn^{2+}SiO_3$ (Fig. 4A; see Raman spectrum of sample SM93 in Fig. 5). Hematite is the stable iron oxide (Fig. 4a), while magnetite was never observed. Rutile and As-bearing apatite (Fig. 6a) are common accessories. Sulphides were not observed, although they are reported in the host metabasites of the Saint-Marcel valley, where Fe–Cu ores have been exploited in the past centuries (mines of Servette and Chuc; e.g. Martin et al., 2008; Tumiati et al., 2008).

Omphacite in these levels is dark purple and known as a semiprecious stone called *violan* (Bondi et al., 1978). It is a solid solution of jadeite (up to Jd_{64}), diopside and aegirine, with minor contents in johansennite ($CaMn^{2+}Si_2O_6$) and namansilite ($NaMn^{3+}Si_2O_6$), often showing a complex zoning. PCA indicates that the main substitution vector in omphacite, represented by the first principal component F1 (79.55 % of the total eigenvalues), concerns augite (elements Ca, Mg, Fe^{2+}, Mn^{2+}) vs. jadeite + aegirine + namansilite (elements Na, Al, Fe^{3+}, Mn^{3+}). The second principal component F2 (18.98 % of the eigenvalues) mainly represents the jadeite (Al) and namansilite (Mn^{3+}) vs. aegirine (Fe^{3+}) substitution.

Omphacite always coexists with braunite and piemontite, forming cm-sized boudinaged bands hosted by massive quartz. Braunite crystals can contain included and/or exsolved barite and hollandite ($BaMn^{3+}{}_2Mn^{4+}{}_6O_{16}$), suggesting a possible presence of Ba in the initial braunite. Tumiati

et al. (2010) reported up to 194 ppm (µg/g) of Ba in these crystals, in addition to other trace elements (e.g. 2015 ppm Cu, 1101 ppm Zn, 272 ppm Sr, 2543 ppm Co and 404 ppm Ni). Piemontite is typically Sr-bearing and shows oscillatory zoning, following the coupled piemontite-(Sr) vs. Fe-epidote substitution. Tumiati et al. (2010) have shown that the Sr-rich parts of piemontite contain up to 459 ppm As, 361 ppm Zn, 937 ppm P, 508 ppm Ni and 767 ppm Ba. In some samples, epidote-group minerals display Mn-poor cores and Mn-rich piemontite rims. The transition between the two compositions is gradual without an obvious solution gap, and follows the substitution $Mn^{3+}_{+2}Al^{3+}_{-1}Fe^{3+}_{-1}$.

Garnet is a solid solution of spessartine and grossular with minor contents in calderite ($Mn^{2+}_3Fe^{3+}_2Si_3O_{12}$) and pyrope. The garnet crystals are generally only slightly zoned in these levels.

5.2 High-P veins

Veins crosscutting the basal levels are quartz-rich and contain piemontite, omphacite, braunite (Fig. 4b; Table 1), pyroxmangite and hematite. Piemontite is euhedral and commonly displays oscillatory zoning with REE and Sr substituting for Mn following the exchange 2 Ca^{2+}_A + 1 Mn^{3+}_M = 2 Sr^{2+}_A + 1 REE^{3+}_M (first eigenvector of the PCA; 80.4% of the total eigenvalues). The maximum contents in REE and Sr observed are 0.24 atoms per formula unit (a.p.f.u.) (Ce/La = 2.36) and 0.17 a.p.f.u., respectively (for 12.5 equivalent O). These oscillatory zones are sharp and superimposed to a weaker and more regular zoning involving Fe^{3+} *vs*. Mn^{3+}, suggesting an increase of the piemontite endmember from core to rim (second eigenvector of the PCA; 15.0% of the total eigenvalues).

Veins often contain pink Mn-bearing phengite, known as *alurgite*. Occasionally, As and Sb silicates and oxides occur, in particular ardennite (a rare hydrous silico-arseniate of aluminium and manganese; Fig. 6B) and the calcium antimonate romeite (Fig. 6c).

A quartz-rich vein, between the basal braunite/piemontite-rich and the upper garnet-rich levels (Fig. 3), contains emerald-green omphacite (Jd_{70}), minor Cr-rich phengite and (Cr, REE)-rich epidote-group minerals. Accessory minerals are Cr-bearing hematite (up to 3.51 wt% Cr_2O_3) and braunite

(up to 0.52 wt% Cr_2O_3). As-bearing apatite (up to 9.22 wt% As_2O_3), native Au and REE-vanadates (wakefieldite; M. Merlini pers. comm.; details provided elsewhere) have been found as accessory phases.

5.3 Upper levels

Upper levels (Fig. 3; Table 1) are dominated by garnet and quartz associated with hematite, pyroxmangite (Fig. 4c; see Raman spectrum of sample 1601 in Fig. 5) and/or an aegirine-rich Mn-bearing clinopyroxene known as *schefferite*. Garnet is zoned with grossular- and/or calderite-rich core and spessartine-rich rim (cf. also Cenki-Tok and Chopin, 2006). In the Fe^{3+}-rich core, Cr is present up to $Uv_{1.1}$ (0.022 a.p.f.u. per 12 equivalent O; 0.32 wt% Cr_2O_3). The epidote-group mineral manganiandrosite-(Ce) occurs instead of piemontite as an accessory phase (Cenki-Tok et al. 2006). Sb-rich pyrophanite ($MnTiO_3$) was also observed (Fig. 6d).

In one sample, dominated by tephroite, hausmannite and rhodochrosite, we observed a peculiar quartz-free assemblage, where braunite and pyroxmangite show resorption microstructures (Fig. 4d; Table 1).

6. Thermodynamic modelling

At Praborna, the occurrence of omphacite + quartz and of pyroxmangite (e.g. Maresch and Mottana, 1979) confirms that these Mn-rich metasediments equilibrated at HP conditions in the eclogite facies. Jadeite-rich omphacite in equilibrium with quartz occurs also in the pervasive veins that crosscut the basal layers, suggesting that an interaction with vein-forming fluids occurred also at HP. These fluids are likely derived from the dehydration of the slab and flushed the mélange rocks, like the serpentinite and glaucophanite now cropping out at the bottom of the sequence. This is the best of all possible environments to be considered, for verifying the mobility of the component oxygen in the slab. The importance of fO_2 in controlling the phase relationships of Mn-rich systems was first recognised by Muan (1959) and Huebner (1967), who demonstrated that, analogously to

the Fe–O system, Mn-oxides can be used as oxygen buffers because Mn shows changes in the oxidation state from +2 to +4. Also, the presence of piemontite requires very high fO_2 to be stabilized over garnet, as experimentally demonstrated by Anastasiou and Langer (1977), and Keskinen and Liou (1979). However, such systems have been rarely adopted as redox sensors in HP rocks, because the available experimental data are currently restricted to the $MnO–SiO_2–O_2$ and $Al_2O_3–MnO–SiO_2–O_2$ systems at 0.4–2.5 GPa (Abs-Wurmbach et al., 1983; Abs-Wurmbach and Peters, 1999).

At Praborna, the basal levels are characterised by the assemblage braunite + quartz, the stability of which requires very high fO_2 ($\Delta FMQ = \log (fO_2^{sample} / fO_2^{fayalite+magnetite+quartz}) = +11$ at 0.8 GPa and 500 °C, estimated by Brown et al., 1978). These high fO_2 values have been interpreted as indicative of highly oxidized rocks, inheriting the fO_2 of the sedimentary protolith. In this section, we quantify the μO_2, fO_2 and nO_2 variables at Praborna, using a specific thermodynamical dataset customized for Mn-rich systems and presented in Appendix.

6.1 Modelling of the $MnO–SiO_2–O_2$ system

The $MnO–SiO_2–O_2$ is the simplest petrological system that describes the phase relations between Mn-silicates and oxides. Pure phases belonging to this system are: quartz, manganosite ($Mn^{2+}O$), tephroite ($Mn^{2+}{}_2SiO_4$), pyroxmangite ($Mn^{2+}SiO_3$), rhodonite ($Mn^{2+}SiO_3$), hausmannite ($Mn^{2+}Mn^{3+}{}_2O_4$), braunite ($Mn^{2+}Mn^{3+}{}_6SiO_{12}$), bixbyite ($Mn^{3+}{}_2O_3$) and pyrolusite ($Mn^{4+}O_2$). Solid solutions are not expected in this system. Using literature (Table A-1 in Appendix) and new experimentally derived thermodynamic data for these phases (Table A-2 and A-3 Appendix), we were able to construct two diagrams (Figs. 7a and 7b), calculated at P = 2.1 GPa and T = 550 °C, i.e. at the metamorphic conditions recorded by the slab lithologies in the Saint-Marcel valley (Martin et al., 2008). Diagrams 7a and 7b consider, respectively, the component O_2 as "perfectly mobile" (i.e., μO_2 and fO_2 are intensive independent state variables) and "inert" (nO_2 is an extensive independent state variable). We recall that in these diagrams and in the following calculations, nO_2

311 is set to zero value for rocks in which all Fe and Mn occur exclusively in their divalent oxidation
312 state. Therefore, nO_2 could be regarded as extra moles of the component O_2 relative to a Fe^{3+}- and
313 Mn^{3+}-free reference composition (see also Section 2).
314 Figure 7a displays log (fO_2/1 bar) – μO_2 vs. X_{SiO2} (=SiO_2/($Mn^{2+}O$+SiO_2)). The bulk Mn^{3+}/Mn_{tot}
315 ratio is also reported (shaded areas in Fig. 7a and black dotted isopleths in Fig. 7b). For comparison,
316 reference redox buffers, such as, hematite + magnetite, pyrite + Fe-sulphate and piemontite + garnet
317 are shown in Figure 7a, where they are expressed as ΔFMQ, i.e. with reference to the fayalite +
318 magnetite + quartz buffer (FMQ).
319 The braunite + quartz + pyroxmangite assemblage of the basal levels at Praborna is stable for
320 almost the entire X_{SiO2} range (except for very low SiO_2 contents, where quartz disappears) at very
321 high fO_2 (ΔFMQ = +12.7), above the hematite–magnetite buffer and slightly above the piemontite–
322 garnet buffer. This is consistent with the occurrence of piemontite and hematite in basal levels
323 (Figs. 4a, b).
324 The upper levels of Praborna are characterised by the equilibrium between pyroxmangite, quartz,
325 garnet and hematite (Figs. 3, 4c), which are stable at ΔFMQ < +12.7 and X_{SiO2} > 0.5 according to
326 Figure 7a. In one quartz-free sample, we observed the assemblage braunite + hausmannite +
327 tephroite (blue fields in Figs. 7a, b; see also Fig. 4d) with relics of pyroxmangite. This latter
328 assemblage can be attained only for X_{SiO2} < 0.33 and log (fO_2/1 bar) between FMQ+4.1 and
329 FMQ+9.7. A further constraint is given by the occurrence of sulphates at Praborna (e.g. barite and
330 celestine), and the absence of sulphides. Chalcophile elements, such as Sb and As, partitionate into
331 silicates, phosphates and oxides (Fig. 6), suggesting that the fO_2 at Praborna is higher than the
332 pyrite–$FeSO_4$ buffer (i.e. ΔFMQ > +5.7), even in the most retrograde assemblages. Values of log
333 (fO_2/1 bar) in the range from FMQ+5.7 to FMQ+12.7 widely exceed those previously evaluated for
334 subduction environments (see Introduction and Section 7.2 below).
335 Figure 7b is the ternary chemography of the system $Mn^{2+}O$–SiO_2–O_2. Compositions are portrayed
336 in barycentric mole fractions. This diagram plots the relative positions of the phase assemblages

shown in Figure 7a, therefore unravelling the relationships between μO_2 (or fO_2) and the conjugate variable nO_2 (see also Fig. 1). In terms of nO_2, the most reduced possible assemblages (i.e., the poorest in component O_2) consist of tephroite + manganosite, pyroxmangite + tephroite, and quartz + pyroxmangite, depending on $XSiO_2$ (Fig. 7a). These associations fall on the join SiO_2–$Mn^{2+}O$, where nO_2 is null and $Mn^{3+}/Mn_{tot} = 0$. On the other hand, the most oxidized assemblage (i.e., the richest in component O_2) is braunite + bixbyite, for which nO_2 and Mn^{3+}/Mn_{tot} range from 0.16 to 0.20 and from 0.86 to 1.00, respectively, depending on the phase proportions. The assemblage bixbyite + hausmannite and bixbyite + hausmannite + braunite can therefore have the same Mn^{3+}/Mn_{tot} ratio, provided that the abundance of hausmannite is sufficiently low. The Mn^{3+}/Mn_{tot} ratio and nO_2 values are directly proportional only on the $Mn^{2+}O$–O_2 subspace of the chemographic diagram. As a consequence, the equilibrium tie-lines of Figure 7b, which delimit the phase fields with identical chemical potentials, crosscut the nO_2 and Mn^{3+}/Mn_{tot} isopleths at high angle. This translates into a decoupling between μO_2, nO_2 and Mn^{3+}/Mn_{tot}, when comparing Figures 7a and 7b. To better understand this concept, we reported a hypothetical metasomatic path represented by the black arrow of Figure 7b. Evolution of the bulk composition along this path from the starting point to the ending point induces a change of the assemblage hausmannite + braunite + tephroite (blue field: $Mn^{3+}/Mn_{tot} = 0.70$; $\mu O_2 = -267$ kJ•mol^{-1}; $nO_2 = 0.13$) to the assemblage braunite + pyroxmangite + quartz (red field: $Mn^{3+}/Mn_{tot} = 0.30$; $\mu O_2 = -219$ kJ•mol^{-1}; $nO_2 = 0.03$). Counter-intuitively, it is therefore possible to *increase* μO_2 (and fO_2), while nO_2 and Mn^{3+}/Mn_{tot} actually *decrease*. In this case, oxidation in terms of an increase of the intensive variable μO_2 (or fO_2) actually corresponds to a decrease in nO_2 and Mn^{3+}/Mn_{tot}, and thus to a bulk reduction. The Mn^{3+}/Mn_{tot} ratio is also depicted in Figure 7a by greyscale tones grading from black ($Mn^{3+}/Mn_{tot} = 1$) to white ($Mn^{3+}/Mn_{tot} = 0$), showing that the same Mn^{3+}/Mn_{tot} ratio can be found at different μO_2 conditions. Figures 7a and 7b show that the decrease in fO_2 from the basal (red) to the upper (blue) levels of Praborna does not necessarily correspond to an increase in bulk Mn^{3+}/Mn_{tot} as one would expect. The Mn^{3+}/Mn_{tot} ratio is also a function of phase abundances, which cannot be evaluated

using μO_2 (or fO_2) diagrams. Therefore, the high fO_2 values observed at Praborna cannot be considered a straightforward sign of high degrees of oxidation.

6.2 Comparison with the FeO–SiO₂–O₂ system

The peculiarity of the MnO–SiO_2–O_2 system is mostly related to the occurrence of braunite, a compound that does not have an analogue in the well known FeO–SiO_2–O_2 system. In order to explore differences and similarities between Mn- and Fe-bearing assemblages, we have constructed a four-component, FeO–MnO–SiO_2–O_2, compositional space shown in Figure 8. Analogously to Figure 7b, also in this diagram the quantity of the component oxygen (nO_2) is treated as an independent state variable, and fO_2 (expressed as ΔFMQ in the figure) is dependent. Every Mn-bearing phase has a corresponding Fe-bearing phase, except braunite. While hematite and magnetite can coexist with quartz, hausmannite and bixbyite cannot, because of the stability of braunite. In Figure 8, the high-fO_2 phase assemblage braunite + pyroxmangite + quartz + hematite of the basal levels (red volume) can be accessed from the low-fO_2 braunite + hausmannite + tephroite + hematite assemblage of the upper levels (blue volume) just by adding silica (e.g. via a metasomatic agent), even decreasing nO_2, similarly to what displayed in Figure 7b. The grey plane in Figure 8 represents the surface where nO_2 is constant and is drawn to highlight the decoupling between oxygen intensity (fO_2) and extensity (nO_2). Moving along this plane it is possible to cross ultra-high fO_2 (e.g. red volume, ΔFMQ = +12.7) and ultra-low fO_2 (e.g. light green, ΔFMQ = -18.1) assemblages at constant nO_2, which means without changing the bulk "redox budget" (Evans, 2006) of the rock.

Therefore, although the braunite + pyroxmangite + quartz + hematite assemblage of the basal levels of Praborna shows an ultra-oxidized redox state in terms of intensive redox parameters (ΔFMQ = +12.7), it could have the same quantity of O_2 component as magnetite- and even ultra-reduced wüstite-bearing assemblages.

7. Discussion

In this section, we re-discuss the concept of oxidation degree of slab rocks, emphasizing the choice between intensive (μO_2 or fO_2) and extensive (nO_2) parameters to describe properly redox conditions. In general, we will demonstrate that the oxidation degree of rocks is definitely a relative concept, dependent on the variable used to describe it.

7.1 Oxygen chemical potential versus oxygen molar quantity: is oxygen a "perfectly mobile" or an "inert" component?

The rocks of Praborna clearly suggest that even in the presence of pervasive flux of fluids, the homogenization of μO_2 was not attained. In fact, if oxygen had been perfectly mobile, μO_2 (and fO_2) would have been constant but, on the contrary, while the country-rock pyrite-magnetite-bearing glaucophanite records $\Delta FMQ < +2.6$ (Fig. 7a), the adjacent basal Mn-rich quartzites attain $\Delta FMQ \geq +12.7$. Moreover, we recognised a mineralogical variability between the basal and upper levels, reflecting ΔFMQ down to +5.7. These observations suggest that, in these rocks, oxygen can hardly be considered a "perfectly mobile" component, as defined by Korzhinskii (1959); thus, the description of the redox conditions of such petrological systems should not be described by μO_2 (or fO_2) as an *independent* state variable. The introduction of its conjugate variable nO_2 is instead required, μO_2 becoming *dependent* of nO_2. Figures 7a, 7b and 8 warn against the undiscriminating use of μO_2 (or fO_2) as univocal indicator of the redox state of a rock system. Especially in multi-component and metasomatic systems, the nO_2 and μO_2 (or fO_2) could be well decoupled.

In order to enlighten this concept, we can make a comparison with a more intuitive analogue: *P* and *V* is a couple of intensive and extensive variables similar to μO_2 and nO_2, respectively. Pressure *P* (like μO_2 or fO_2) is generally considered as an independent variable imposed upon the system by its environment, to which the system responds by adapting the conjugate variable *V* (similarly to nO_2), in order to reach the state of equilibrium. However, in a few particular cases, like fluid inclusions, *V*

414 is imposed by the surroundings, which may induce local *P* heterogeneities, like overpressures at the
415 inclusion scale; in that case, *V* should be considered as the independent variable and *P* the conjugate
416 dependent variable. This occurs when volumes cannot adjust as easily as pressures. In our case,
417 nO_2, in part inherited from the sedimentary protolith, cannot adjust itself easily – in other terms, O_2
418 not a "perfectly mobile" component. This generates local μO_2 heterogeneities, and nO_2 should be
419 considered as the independent variable that determines the redox state.
420
421 *7.2 Consequences for fO_2 estimates in subduction zones*
422 In a multi-component system, the chemical potential of each component, including oxygen, is
423 ideally homogeneous, i.e. equal in all the phases at equilibrium. As seen in Figures 7a, 7b and 8,
424 different mineralogical associations will be characterised by different chemical potentials, including
425 μO_2, and thus fO_2, even when they display the same nO_2 or the same Fe^{3+} and Mn^{3+} contents. In
426 fact, two variables in a conjugate pair, such as μO_2 (or fO_2) and nO_2, are coupled, i.e. both increase
427 or both decrease, only if all the other molar quantities are kept at constant values. The addition of
428 SiO_2 or FeO components, for example via a metasomatic process, can produce assemblages
429 characterised by different fO_2 without necessarily changing the redox budget. This consideration
430 warns against the indiscriminate comparison of fO_2 data for rocks characterized by different bulk
431 composition or simply by different mineral assemblages, because it may lead to apparent redox
432 heterogeneities, wherever μO_2 cannot be considered as an independent variable (i.e., where O_2 is
433 not "perfectly mobile" and therefore rocks could be not in equilibrium to each other). Therefore,
434 heterogeneities in fO_2 do not necessarily require the mobility of redox species.
435 In subduction zones, fO_2 corresponding to a range of ΔFMQ from 0 to +2 has been estimated on
436 carbonate-bearing mantle-wedge peridotite from the Sulu UHP terrane (China) by Malaspina et al.
437 (2009), whereas eclogites from the same area are characterised by ΔFMQ from +2.5 (Cao et al.,
438 2011; massive lawsonite eclogite) to ca. +4 (Cao et al., 2011; foliated clinozoisite + glaucophane
439 eclogite) and ca. +4.5 (amphibole eclogite; Mattinson et al., 2004). Difference in fO_2 between

peridotite and eclogite are reported also in the Western Gneiss Region of Norway, where Malaspina et al. (2010) estimated ΔFMQ of -2–0 for garnet websterites, while Donohue and Essene (2000) and Boundy et al. (2002) estimated ΔFMQ in the range +2.5– +3.0 for eclogite-facies marbles.

Although it is unclear, at present, whether heterogeneities in fO_2 in the slab (see also Foley, 2011) should be ascribable to differences in chemical–mineralogical composition, to lack of μO_2 equilibration, or to differences in redox budget, the case of Praborna appears paradigmatic and suggests that metasomatic processes could lead to ultra-high fO_2 conditions despite a modest, if any, bulk oxidation in terms of nO_2,

In order to compare the Praborna metasediments with other slab rocks and the corresponding mantle wedge, we need to evaluate the oxidation states of representative rocks in terms of nO_2. Unlike for μO_2 (or fO_2), the quantification of nO_2 depends on the mineral abundances. Typically, nO_2 may vary in an oxygen buffer assemblages (i.e., oxygen can be added or subtracted) without a change of μO_2 (or fO_2). For example, the addition of oxygen to a hematite + magnetite assemblage leads thus to an increase in the abundance of hematite, an increase of Fe^{3+}/Fe_{tot} and an increase of nO_2, without changing fO_2, as long as both minerals are present. The system is therefore buffered at constant fO_2 (and μO_2).

Estimates of nO_2 provided below take into account the mineral mode in different subduction-related rock types. They should be regarded as an attempt to assess the magnitude of the redox budget of the subducting slab pile and its overlying mantle wedge. Concerning HP rocks, only few analytical data allowing a mass balance of the component oxygen are reported in literature. We profit of the case of HP rocks from Sulu (China), a unique region where the Fe^{3+} contents of garnet and clinopyroxene have been measured both in wedge peridotite (Malaspina et al., 2009; 2012) and in slab eclogite (Proyer et al., 2004).

For peridotite mineral assemblages, the contribution of garnet to nO_2 (cf. Fig. 7b and 8) is the amount of excess oxygen with reference to a Fe^{3+}-free system, provided by the skiagite ($Fe^{3+}{}_2Fe^{2+}{}_3Si_3O_{12}$) component. In the following idealized mass balance, oxygen (O_2) is not regarded

as a phase or species but merely as a component and therefore can be made explicit:

$1.00 \times (FeO)_{0.59}\bullet(SiO_2)_{0.35}\bullet(O_2)_{0.06}$ [skiagite] =

$0.71 \times (FeO)_{0.67}\bullet(SiO_2)_{0.33}$ [fayalite] + $0.24 \times (FeO)_{0.50}\bullet(SiO_2)_{0.50}$ [ferrosilite] + 0.06 O_2 (Eq. 1).

This equation, after Luth et al. (1990), has been rewritten here expressing compounds as molar fractions of the independent components SiO_2, FeO, MnO and O_2 (see Section 2; Spear et al., 1982), allowing a direct comparison of the excess O_2 with different barycentric representations (Figs. 7b and 8). In the discussion below, we will use the same convention to express chemical compositions of minerals and rocks.

According to Eq. 1, one mole of pure skiagite would lead to 0.06 mole of excess O_2. Because Malaspina et al. (2009) reported garnet containing up to 6 mol% of skiagite, one mole of garnet from Sulu peridotite contributes for the 6 percent of 0.06 mole of O_2, i.e. for 3.6 millimoles of excess O_2.

In mafic eclogites, a model redox mass balance for skiagite can be written as:

$1.00 \times (FeO)_{0.59}\bullet(SiO_2)_{0.35}\bullet(O_2)_{0.06}$ [skiagite] = $+1.37 \times (FeO)_{0.43}\bullet(Al_2O_3)_{0.14}\bullet(SiO_2)_{0.43}$ [almandine] - $0.39 \times (Al_2O_3)_{0.5}\bullet(SiO_2)_{0.5}$ [kyanite] - 0.04 SiO_2 [quartz/coesite] + 0.06 O_2 (Eq. 2).

The coefficients for O_2 are the same in Equations 1 and 2, suggesting that in both mafic and ultramafic rocks the excess oxygen is 0.06 mole of O_2 per 1 mole of skiagite component.

Profiting of the garnet composition reported by Proyer et al. (2004), containing up to 5 mol% of skiagite, the contribution of one mole of garnet from Sulu eclogite is therefore the 5 percent of 0.06 moles of O_2 (v. Eq. 2), i.e. 3.0 millimoles of excess O_2 per 1 mole of garnet.

As peridotitic and eclogitic garnets display comparable skiagite content (~5% in eclogite and ~6% in peridotite), the *n*O_2s for one mole of garnet are also comparable (3.6 and 3.0 millimoles in

peridotite and eclogite, respectively).

The contribution of clinopyroxene to the bulk oxidation can be evaluated on the basis of the aegirine ($NaFe^{3+}Si_2O_6$) component, which can be expressed in the following way, for peridotite (Eq. 3) and eclogite (Eq. 4) assemblages respectively.

$$1.00 \times (Na_2O)_{0.13}\bullet(FeO)_{0.27}\bullet(SiO_2)_{0.53}\bullet(O_2)_{0.07}\ [\text{aegirine}] = 0.80 \times (Na_2O)_{0.17}\bullet(Al_2O_3)_{0.17}\bullet(SiO_2)_{0.67}\ [\text{jadeite}] - 0.80 \times (FeO)_{0.50}\bullet(SiO_2)_{0.50}\ [\text{ferrosilite}] + 0.13 \times (FeO)_{1.00}\bullet(SiO_2)_{1.00}\bullet(Al_2O_3)_{-1.00}\ [\text{Fe Tschermak}] + 0.80 \times (FeO)_{0.67}\bullet(SiO_2)_{0.33}\ [\text{fayalite}] + 0.07\ O_2 \qquad \text{(Eq. 3).}$$

$$1.00 \times (Na_2O)_{0.13}\bullet(FeO)_{0.27}\bullet(SiO_2)_{0.53}\bullet(O_2)_{0.07}\ [\text{aegirine}] = 0.80 \times (Na_2O)_{0.17}\bullet(Al_2O_3)_{0.17}\bullet(SiO_2)_{0.67}\ [\text{jadeite}] + 0.53 \times (FeO)_{0.50}\bullet(SiO_2)_{0.50}\ [\text{ferrosilite}] - 0.13\ SiO_2\ [\text{quartz/coesite}] - 0.27 \times (Al_2O_3)_{0.5}\bullet(SiO_2)_{0.5}\ [\text{kyanite}] + 0.07\ O_2 \qquad \text{(Eq. 4).}$$

Similarly to equalities involving garnet in Equations 1 and 2, the coefficients of O_2 in Equations 3 and 4 are identical and independent on the system chosen, accounting for 0.07 mole of excess O_2 per 1 mole of pure aegirine. Clinopyroxene from Sulu peridotite contains 5 mol% of aegirine endmember (Malaspina et al., 2012), while clinopyroxene from eclogite contains 6 mol% of aegirine (Proyer et al., 2004). Therefore, one mole of clinopyroxene contributes to 3.5 and to 4.2 millimoles of excess O_2 in peridotites and mafic eclogites, respectively.

On the basis of the above considerations, a bimineralic eclogite composed of 50 mol% of garnet and 50 mol% of clinopyroxene would be characterized by 3.6 millimoles of excess O_2 per mole of a rock, whose composition is expressed as molar fractions of oxides. On the other hand, assuming 5 mol% of garnet and 5 mol% of clinopyroxene, a peridotite would be characterized by 0.36 millimoles of excess O_2 per mole of rock, which means one order of magnitude less.

Metasedimentary rocks at Praborna display nO_2 that can be estimated on the basis of the proportions between pyroxmangite, braunite and quartz (see Fig. 7b). Considering the bulk

chemical and mineralogical compositions reported by Tumiati et al. (2010), we estimated average contents of ca. 95 mol% of quartz and 5 mol% of pyroxmangite + braunite. Although the available data are not sufficient to determine the pyroxmangite/braunite ratio, we can estimate that the braunite abundance equals that of pyroxmangite, being the first mineral more abundant in the basal levels and the second in the upper levels. Braunite and pyroxmangite can be written respectively as $(MnO)_{0.74}•(SiO_2)_{0.11}•(O_2)_{0.16}$ and $(MnO)_{0.50}•(SiO_2)_{0.50}$ (see Fig. 7b). Therefore, only braunite can contribute to the excess O_2 of the Mn-rich metasediments of Praborna, at the rate of 2.5% of 0.16 moles of excess O_2, i.e. 4.0 millimoles of excess O_2 per 1 mole of rock. This value is nearly identical to the excess O_2 of the Sulu eclogite, suggesting that the Mn-rich metasediments of a subduction mélange can display towards the mantle an oxidizing power comparable to that of slab rocks, despite the presence of ultra-high fO_2 mineral assemblages.

As a consequence, a likely scenario for the slab-mantle interface in natural geodynamic environments is illustrated in Figure 9. Mass transport and metasomatism are supported by chemical gradients, notably by gradient in nO_2 across rocks of the subduction channel towards the mantle hanging-wall. Dehydration processes trigger fluid flow, which is localized in shear zones, and open fractures and pervasive microfractures. While ΔFMQ is likely very inhomogeneous, reflecting the different bulk chemical–mineralogical compositions and the limited mobility of oxygen, the oxidation degree of the subduction channel, expressed in terms of nO_2, is expected to be much smoother. In the conceptual model of Figure 9, a sort of metasomatic front develops from the slab to the overlying mantle wedge passing through a transitional layer of mélange rocks. Although fluids cannot transport oxygen as a major volatile species, they are expected to promote mass transfers and to affect the attainment of equilibrium and kinetics of reactions (Lasaga and Rye, 1993; Marschall and Schumacher, 2012). Therefore, oxygen is expected to be transported, especially along fractures and veins (see inset of Fig. 9), possibly through mechanisms of dissolution-reprecipitation of O-enriched oxides and silicates. The front is possibly sustained also by the strong inverse thermal gradient across the slab surface, which is evaluated to be in the order

of -20 °C/km (Arcay et al., 2007). Whether a thermophoretic effect at the slab–mantle interface is able to contribute to the O_2 component redistribution or mass-transport is driven mainly by chemical potential gradients and to advective processes (e.g., Gerya and Yuen, 2003; Marschall and Schumacher, 2012) is an open challenge for understanding rock diversity at subduction zones.

8. Conclusions

Praborna HP veined Mn-rich rocks record environmental conditions typical for a subducting slab setting. Although veining and growth of "pegmatoid" HP minerals might suggest an open system, characterized by large fluid-rock ratios, the extremely high fO_2 deduced from Mn–Fe-rich mineral assemblages clearly indicates that oxygen can hardly be considered as a perfectly mobile component. As a consequence, μO_2, and therefore fO_2, should not be regarded as long-range properties, indicative of the redox state of the entire rock column of a subduction zone, from the dehydrating oceanic crust to the overlying mantle wedge. On a more general basis, the comparison of fO_2 retrieved from different bulk compositions and phase assemblages may suggest redox heterogeneities in subduction zones, even if the distribution of oxygen is expected to be much more continuous, ranging from a maximum in the mafic eclogites, derived from the altered oceanic basalts and gabbros, and in the sediments of the slab, down to a minimum in the overlying peridotites of the mantle hanging-wall.

Acknowledgements

The authors are indebted to the reviewers H. Marschall and A. Korsakov for their useful suggestions. M. Fialin and A. Risplendente supported the work at EMP. F. Zorzi and S. Carbonin, and N. Masciocchi and G. Tagliabue are acknowledged for the acquisition and the refinement of XRD data of braunite and pyrolusite, respectively. P. Mietto, C. Micaglio and E. A. Perseil are thanked for providing some interesting samples. D. Smith is acknowledged for the access to Raman

facility. This work was supported by the Italian Ministry of Education, University and Research (MIUR) [PRIN-2012R33ECR].

Appendix A. Thermodynamic calculations and supplementary data

Phase diagrams of Figures 6 and 7 have been drawn on the basis of thermodynamic calculation performed with the Perple_X computer package (http://www.perplex.ethz.ch; Connolly, 1990) using a specifically compiled thermodynamic dataset of Mn-rich minerals and oxygen buffers (see Table A-1). Thermodynamic parameters are available in the literature apart from the thermal expansion coefficients of braunite and pyrolusite, unknown as far as we are aware, and which we derived experimentally from their cell-volume changes during heating (cf. Tables A-2 and A-3). The dataset used has proven to be robust in reproducing the results of the HP experiments of Abs-Wurmbach et al. (1983).

Thermal expansion of braunite

Braunite at Praborna is invariably polycrystalline. Consequently, powder X-ray diffraction methods rather than single crystal methods were used to measure the thermal expansion of this mineral. Average composition of 11 analyses can be expressed on the basis of 8 cations and 12 O as (standard deviation in parenthesis):

$Mn^{3+}_{5.92(8)}\ Mn^{2+}_{0.82(6)}\ Mg_{0.13(2)}\ Fe^{3+}_{0.06(3)}\ Ca_{0.05(2)}\ Al_{0.03(1)}\ Si_{0.99(5)}\ O_{12}$.

Powder diffraction patterns were recorded on a Philips X'Pert PRO automatic powder diffractometer, using a normal focus Cu X-ray tube operating at 40 kV and 40 mA**.** The vertical goniometer in Bragg-Brentano geometry (with 240 mm radius) was equipped with a first divergence slit, a Soller slit and a 0.2 mm receiving slit upstream of a curved graphite diffracted-beam monochromator PW3123/10. For high temperature data collection, the diffractometer was equipped with a heating camera Anton Paar HTK16.

The powder was spread as a thin film directly on the platinum thermocouple (heating strip) and the beam impingement area was restricted to a narrow central section of the strip, so that thermal gradients through and across the sample were minimized. The expansion of Al_2O_3 NIST standard reference material 676 was used for temperature calibration. We estimate the uncertainty of temperature measurement at the sample to be 10 °C.

A first data collection performed in continuous mode in the 16–120° 2θ range revealed the good crystallinity and the purity of the phase. Successively, data were collected with a step increment of 0.02° and a step counting time of 5 seconds in the 90–120° 2θ range.

The position of each Bragg peak was measured by means of "X'pert high score" program and indexed by comparison with the calculated pattern obtained by GSAS program (Larson and Von Dreele, 1994). Angular values and respective crystallographic planes were used to refine lattice parameters *a* and *c* by means of the XLAT program (Rupp, 1988). Diffractometer alignment was repeatedly checked by carrying out data collection of NBS640B silicon standard and obtaining *a* values of 5.4308(1) and 5.4310(1) Å.

In Table A-2, we reported the molar volume of braunite at *T* ranging from 25 to 600 °C. These data have been fitted with the expression reported in Table A-1, in order to obtain the volumetric expansion parameter *b1*.

Thermal expansion of pyrolusite

Although pyrolusite has proven to be unstable at the investigated conditions, this mineral was included in calculations because it belongs to the investigated petrological system. Thermal expansion data were collected in Bragg-Brentano mode on a Bruker AXS D8 Advance, operating in θ:θ geometry equipped with Nickel filtered Cu-Kα radiation and a position-sensitive Lynxeye detector. Generator settings were 40 kV and 40 mA. Reagent-grade MnO_2 was deposited in the aluminium sample holder of a custom-made heating chamber, operating in air, supplied by *Officine*

619 *Elettrotecniche di Tenno*, Ponte Arche, Italy. A series of scans, lasting ca. 30 min each, were
620 collected in isothermal conditions, in the *T* range 100–600 °C at 50 °C steps.
621 Cell parameters were refined by the whole pattern structureless refinement technique (Le Bail et al.,
622 1988) with the aid of the TOPAS-R program (V. 3.0, Bruker AXS, Karlsruhe, Germany). Estimated
623 standard deviations were computed under the assumption that, in the absence of systematic effects,
624 errors followed a normal distribution. Similarly to braunite, cell volume data (Table A-3) have been
625 fitted with the expression reported in Table A-1, in order to obtain the volumetric expansion
626 parameter *b1*.
627
628 **References**

629 Abs-Wurmbach, I., Peters, T., Langer, K., Schreyer, W., 1983. Phase relations in the system Mn–
630 Si–O: an experimental petrological study. Neues Jahrbuch für Mineralogie Abhandlungen
631 14, 258-279.
632 Abs-Wurmbach, I., Peters, T., 1999. The Mn-Al-Si-O system: an experimental study of phase
633 relations applied to parageneses in manganese-rich ores and rocks. European Journal of
634 Mineralogy 11, 45-68.
635 Anastasiou, P., Langer, K., 1977. Synthesis and physical properties of piemontite, $Ca_2Al_{3-p}Mn^{3+}_p(Si_2O_7/SiO_4/O/OH)$. Contributions to Mineralogy and Petrology. 60, 225-245.
637 Arcay, D., Tric, E., Doin, M.P., 2007. Slab surface temperature in subduction zones: Influence of
638 the interpolate decoupling depth and upper plate thinning processes. Earth and Planetary
639 Science Letters 255, 324-338.
640 Arculus, R.J., 1985. Oxidation status of the mantle–Past and present. Annual Review of Earth and
641 Planetary Sciences13, 75–95.
642 Bebout, G.E., 2007. Metamorphic chemical geodynamics of subduction zones. Earth and Planetary
643 Science Letters 260, 373–393.

644 Bebout, G.E., Agard, P., Kobayashi, K., Moriguti, T., Nakamura, E., 2013. Devolatilization history
645 and trace element mobility in deeply subducted sedimentary rocks: Evidence from Western
646 Alps HP/UHP suites. Chemical Geology 342, 1-20.
647 Bondi, M., Mottana, A., Kurat, G., Rossi, G., 1978. Cristallochimica del violano e della schefferite
648 di St. Marcel (Valle d'Aosta). Rendiconti della Società Italiana di Mineralogia e Petrologia.
649 34, 15-25.
650 Boundy, T.M., Donohue, C.L., Essene, E.J., Mezger, K., Austrheim, H., 2002. Discovery of
651 eclogite facies carbonate rocks from the Lindås Nappe, Caledonides, Western Norway.
652 Journal of Metamorphic Geology 20, 649-667.
653 Brown, P., Essene, E.J., Peacor, D., 1978. The mineralogy and petrology of manganese-rich rocks
654 from St. Marcel, Piedmont, Italy. Contributions to Mineralogy and Petrology. 67, 227-232.
655 Canil, D., 2002. Vanadium in peridotites, mantle redox and tectonic environments: Archean to
656 present. Earth and Planetary Science Letters 195, 75–90.
657 Cao, Y., Song, S.G., Niu, Y.L., Jung, H., Jin, Z.M., 2011. Variation of mineral composition, fabric
658 and oxygen fugacity from massive to foliated eclogites during exhumation of subducted
659 ocean crust in the North Qilian suture zone, NW China. Journal of Metamorphic Geology
660 29, 699-720.
661 Castello, P., 1982. Il giacimento di Praborna (S. Marcel-AO). Rivista Mineralogica Italiana. 3, 87-
662 92.
663 Cenki-Tok, B., Ragu, A., Armbruster, T., Chopin, C., Medenbach, O., 2006. New Mn- and rare-
664 earth-rich epidote-group minerals in metacherts: manganiandrosite-(Ce) and
665 vanadoandrosite-(Ce). European Journal of Mineralogy 18, 569–582.
666 Cenki-Tok, B., Chopin, C., 2006. Coexisting calderite and spessartine garnets in eclogite-facies
667 metacherts of the Western Alps. Mineralogy and Petrology 88, 47-68.
668 Chinner, G. A., 1960. Pelitic gneisses with varying ferrous/ferric ratios from Glen Clova, Angus,
669 Scotland. Journal of Petrology 1, 178-217.

670 Ciriotti, M. E., Fascio, L., Pasero, M., 2009. Italian type minerals: Edizioni Plus, Pisa.
671 Connolly, J.A.D., 1990. Multi-variable phase diagrams: an algorithm based on generalized
672 thermodynamics. American Journal of Science 290, 666-718.
673 Dal Piaz, G.V., 2001. History of tectonic interpretations of the Alps. J. Geodyn. 32, 99-114.
674 Dapiaggi, M., Tiano, W., Artioli, G., Sanson, A., Fornasini, P., 2003. The thermal behaviour of
675 cuprite: An XRD-EXAFS combined approach. Nuclear Instruments and Methods in Physics
676 Research B 200, 231-236.
677 Dasgupta, S., 1997. P-T-X relationships during metamorphism of manganese-rich sediments:
678 Current status and future studies. Geological Society Special Publication 199, 327-337.
679 Donohue, C.L., Essene, E.J., 2000. An oxygen barometer with the assemblage garnet-epidote. Earth
680 and Planetary Science Letters 181, 459-472.
681 Evans, K.A., 2006. Redox decoupling and redox budgets: Conceptual tools for the study of earth
682 systems. Geology. 34, 489-492.
683 Evans, K.A., 2012. The redox budget of subduction zones. Earth-Science Reviews 113, 11-32.
684 Foley, S., 2011. A reappraisal of redox melting in the Earth's mantle as a function of tectonic
685 setting and time. Journal of Petrology 52, 1363-1391.
686 Frezzotti, M.L., Selverstone, J., Sharp, Z.D., Compagnoni, R., 2011. Carbonate dissolution during
687 subduction revealed by diamond-bearing rocks from the Alps. Nature Geosciences 4, 703-
688 706.
689 Geller, S., Espinosa, G.P., 1970. Magnetic and crystallographic transitions in Sc^{3+}, Cr^{3+}, and Ga^{3+}
690 substituted Mn_2O_3. Physical Review B 1, 3763-3769.
691 Gerya, T., Yuen, D.A., 2003. Rayleigh-Taylor instabilities from hydration and melting propel 'cold
692 plumes' at subduction zones. Earth and Planetary Science Letters 212, 47-62.
693 Gill, J., 1981. Orogenic Andesites and Plate Tectonics: New York, Springer-Verlag.
694 Greeff, C.W., Boettger, J.C., Graf, M.J., Johnson, J.D., 2006. Theoretical investigation of the Cu
695 EOS standard. Journal of Physics and Chemistry of Solids 67, 2033-2040.

696 Groppo, C., Castelli, D., 2010. Prograde P-T Evolution of a Lawsonite Eclogite from the Monviso
697 Meta-ophiolite (Western Alps): Dehydration and Redox Reactions during Subduction of
698 Oceanic FeTi-oxide Gabbro. Journal of Petrology 51, 2489-2514.
699 Hazen, R.M., 1985. Comparative crystal chemistry and the polyhedral approach. Reviews in
700 Mineralogy 14, 317-345.
701 Heines, J., Leger, J.M., Hoyau, S., 1995. 2^{nd}-order rutile-type to $CaCl_2$-type phase-transition in
702 beta-MnO_2 at high-pressure. Journal of Physics and Chemistry of Solids 56, 965-973.
703 Hillert, M., 1985. Principles of phase diagrams. International Metals Review 30, 45-67.
704 Hirschmann, M.M., 2009. Ironing out the oxidation state of Earth's mantle. Science 325, 545–546.
705 Holland, T.J.B., 1989. Dependence of entropy on volume for silicate and oxide minerals: A review
706 and a predictive model. American Mineralogist 74, 5-13.
707 Holland, T.J.B., Powell, R., 1998. An internally consistent thermodynamic data set for phases of
708 petrological interest. Journal of Metamorphic Geology 16, 309-343.
709 Huebner, J., 1967. Stability relations of minerals in the system Mn–Si–C–O [Ph.D. thesis]:
710 Baltimore, John Hopkins University.
711 Irani, K.S., Sinha, A.P.B., Biswas, A.B., 1958. Entropy of hausmannite to spinel transformation.
712 Proceedings of the Physical Society 71, 270-271.
713 Kazanc, S., Çiftci, Y.Ö., Çolakoğlu, K., Ozgen, S., 2006. Temperature and pressure dependence of
714 the some elastic and lattice dynamical properties of copper: a molecular dynamics study.
715 Physica B 381, 96-102.
716 Kelley, K.A., Cottrell, E., 2009. Water and the oxidation state of subduction zone magmas. Science
717 325, 605–607.
718 Keskinen M., Liou, J.G., 1979. Synthesis and stability relations of Mn-Al piemontite,
719 $Ca_2MnAl_2Si_3O_{12}(OH)$. American Mineralogist 64, 317-328.

720 Konrad-Schmolke, M., O'Brien, P.J., Zack, T.,2011. Fluid migration above a subducted slab –
721 Constraints on amount, pathways and major element mobility from partially overprinted
722 eclogite-facies rocks (Sesia Zone, Western Alps). Journal of Petrology 52, 457-486.
723 Korzhinskii, D.S., 1959. Physicochemical basis of the analysis of the paragenesis of minerals: New
724 York, Consultants bureau, inc.
725 Krist, P., Bohem, J., Gerber, R., Kelland, D.R., 1992. OGMS of cryogenically enhanced magnetics.
726 IEEE Transactions on Magnetics 28, 2412-2414.
727 Langer, K., Tillmanns, E., Kersten, M., Almen, H., Arni, R.K., 2002. The crystal chemistry of Mn^{3+}
728 in the clino- and orthozoisite structure types, $Ca_2M^{3+}{}_3[OH/O/SiO_4/Si_2O_7]$: A structural and
729 spectroscopic study of some natural piemontites and "thulites" and their synthetic
730 equivalents. Zeitschrift für Kristallographie 217, 563-580.
731 Larson, A.C., Von Dreele, R.B., 1994. General Structure Analysis System (GSAS): Los Alamos
732 National Laboratory Report LAUR, p. 86-748.
733 Lasaga, A.C., Rye, D.M., 1993. Fluid flow and chemical reaction kinetics in metamorphic systems.
734 American Journal of Science 293, 361-404.
735 Le Bail, A., Duroy, H., Fourquet, J.L., 1988. Ab initio structure determination of $LiSbWO_6$ by X-
736 ray powder diffraction. Materials Research Bulletin 23, 447-452.
737 Lee, C.T.A., Leeman, W.P., Canil, D., Li, Z.X.A., 2005. Similar V/Sc systematics in MORB and
738 arc basalts: implications for the oxygen fugacities of their mantle source regions. Journal of
739 Petrology 46, 2313–2336
740 Lee, C.-T.A., Luffi, P., Le Roux, V., Dasgupta, R., Albarede, F., Leeman, W.P., 2010. The redox
741 state of arc mantle using Zn/Fe systematics. Nature. 468, 681-685.
742 Luth, R.W., Virgo, D., Boyd, F.R., Wood, B. J., 1990. Ferric iron in mantle-derived garnets;
743 implications for thermobarometry and for the oxidation state of the mantle. Contributions to
744 Mineralogy and Petrology. 104, 56–72.

745 Malaspina, N., Poli, S., Fumagalli, P., 2009. The oxidation state of metasomatized mantle wedge:
746 insights from C-O-H-bearing garnet peridotite. Journal of Petrology 50, 1533-1552.
747 Malaspina, N., Scambelluri, M., Poli, S., Van Roermund, H.L.M., Langenhorst, F., 2010. The
748 oxidation state of mantle wedge majoritic garnet websterites metasomatised by C-bearing
749 subduction fluids. Earth and Planetary Science Letters 298, 417–426.
750 Malaspina, N., Langenhorst, F., Fumagalli, P., Tumiati S., Poli, S., 2012. Fe^{3+} distribution between
751 garnet and pyroxenes in mantle wedge carbonate-bearing garnet peridotites (Sulu, China)
752 and implications for their oxidation state. Lithos 146-147, 11-17.
753 Manheim, F.T., 1978. Marine manganese deposits. Elsevier, Amsterdam.
754 Maresch, W.V., Mottana, A., 1976. The pyroxmangite-rhodonite transformation for the MnSiO3
755 composition. Contributions to Mineralogy and Petrology. 55, 69-79.
756 Marschall, H.R., Schumacher, J.C., 2012. Arc magmas sourced from mélange diapirs in subduction
757 zones. Nature Geosciences 5, 862-867.
758 Martin, S., Kienast, J.-R., 1987. The HP-LT manganesiferous quartzites of Praborna, Piedmont
759 ophiolite nappe, Italian western Alps. Schweizerische Mineralogische und Petrographische
760 Mitteilungen 67, 229-360.
761 Martin, S., Rebay, G., Kienast, J.-R., Mevel, C., 2008. An eclogitised oceanic palaeo-hydrothermal
762 field from the St. Marcel Valley (Italian Western Alps). Ofioliti. 33, 1-15.
763 Mattinson, C.G., Zhang, R.Y., Tsujimori, T., Liou, J.G., 2004. Epidote-rich talc-kyanite-phengite
764 eclogites, Sulu terrane, eastern China: *P-T-f*O_2 estimates and the significance of the epidote-
765 talc assemblage in eclogite. American Mineralogist 89, 1772-1783.
766 McMurdie, H.F., Sullivan B.M., Mauer, F.A., 1950. High-temperature X-ray study of the system
767 Fe_3O_4-Mn_3O_4. Journal of Research of the National Bureau of Standards, 45, 35-41.
768 Merkel, S., Jephcoat, A.P., Shu, J., Mao, H.K., Gillet, P., Hemley, R.J., 2002. Equation of state,
769 elasticity, and shear strength of pyrite under high pressure. Physics and Chemistry of
770 Minerals 29, 1-9.

771 Miletich, R., Allan, D.R., Angel, R.J., 1998. Structural control of polyhedral compression in
772 synthetic braunite $Mn^{2+}Mn^{3+}{}_6O_8SiO_4$. Physics and Chemistry of Minerals 25, 1983-1992.
773 Mori, M., 2002. Irreversible expansion behavior of $Mn_3O_{4+\delta}$ spinel and shrinkage behavior of
774 $La_{0.6}Sr_{0.4}MnO_3$ composites with the spinel during thermal cycling in O_2 atmosphere. Journal
775 of the Electrochemical Society 149, A995-A1000.
776 Muan, A., 1959. Stability relations among some manganese minerals. American Mineralogist 44,
777 946-960.
778 Ohashi, M., Tashiro, A., Oomi, G., Maeda, E., Zeng, X.G., 2006. Effect of pressure on the magnetic
779 phase transition in cupric oxide. Physical Review B 73, 134421.
780 Paris, E., Ross, C.R., Olijnyk, H., 1992. Mn_3O_4 at high-pressure – a diamond-anvil cell study and a
781 structural modelling. European Journal of Mineralogy 4., 87-93.
782 Proyer, A., Dachs, E., McCammon, C., 2004. Pitfalls in geothermobarometry of eclogites: Fe^{3+} and
783 changes in the mineral chemistry of omphacite at ultrahigh pressures. Contributions to
784 Mineralogy and Petrology. 147, 305-318.
785 Reinecke, T., 1998. Prograde high- to ultrahigh-pressure metamorphism and exhumation of oceanic
786 sediments at Lago di Cignana, Zermatt-Saas Zone, Western Alps. Lithos 42, 147-189.
787 Robertson, E.C., 1988. Thermal properties of rocks. U. S. Geological Survey Open-File Report, 88-
788 441.
789 Robie, R., Hemingway, B.S., 1995. Thermodynamic properties of minerals and related substances
790 at 298.15 K and 1 bar (10^5 Pascals) pressure and at higher temperatures. U.S. Geological
791 Survey Bulletin 2131, 461 pp.
792 Rupp, B., 1988. XLAT – Least square refinements of cell constants. Scripta Metallurgica. 22, 1.
793 Sherman, D.M., 1990. Molecular orbital (SCF-Xα-SW) theory of Fe^{2+}-Mn^{3+}, Fe^{3+}-Mn^{2+} charge
794 transfer and magnetic exchange in oxides and silicates. American Mineralogist 75, 256-261.
795 Shi, P., 1992. Fluid fugacities and phase equilibria in the Fe-Si-O-H-S system. American
796 Mineralogist 77, 1050-1066.

797 Smyth, J.R., Jacobsen, S.D., Hazen, R.M., 2000. Comparative crystal chemistry of dense oxide
798 minerals. Reviews in Mineralogy 40, 157-186.
799 Spear, F.S., Rumble III, D., Ferry, J.M., 1982. Linear algebraic manipulation of n-dimensional
800 composition space. Reviews in Mineralogy 10, 53-104.
801 Tumiati, S., 2005 (A). Geochemistry, mineralogy and petrology of the eclogitized manganese
802 deposit of Praborna (Valle d'Aosta, Western Italian Alps) [Ph.D. thesis]: Università
803 dell'Insubria (Como)–Université Denis Diderot (Paris-7).
804 Tumiati, S., Godard, G., Martin, S., Nimis, P., Mair, V., Boyer, B., 2005 (B). Dissakisite-(La) from
805 the Ulten zone peridotite (Italian Eastern Alps): A new end-member of the epidote group.
806 American Mineralogist 90, 1177-1185.
807 Tumiati, S., Godard, G., Masciocchi, N., Martin, S., Monticelli, D., 2008. Environmental factors
808 controlling the precipitation of Cu-bearing hydrotalcite-like compounds from mine waters.
809 The case of the "Eve verda" spring (Aosta Valley, Italy). European Journal of Mineralogy
810 20, 73-94.
811 Tumiati, S., Martin, S., Godard, G., 2010. Hydrothermal origin of manganese in the high-pressure
812 ophiolite metasediments of Praborna ore deposit (Aosta Valley, Western Alps). European
813 Journal of Mineralogy 11, 577-594.
814 Tumiati, S., Fumagalli, P., Tiraboschi, C., Poli, S., 2013. An experimental study on COH-bearing
815 peridotite up to 3.2 GPa and implications for crust-mantle recycling. Journal of Petrology
816 54, 453-479.
817 Wang, Z., Pischedda, V., Saxena, S.K., Lazor, P., 2002. X-ray diffraction and Raman spectroscopic
818 study of nanocrystalline CuO under pressures. Solid State Communications 121, 275-279.
819 Wood, B.J., Bryndzia, L.T., Johnson, K.E., 1990. Mantle oxidation state and its relation to tectonic
820 environment. Science. 248, 337–345.
821 Yamanaka, T., Nagai, T., Okada, T., Fukuda, T., 2005. Structure change of Mn_2O_3 under high
822 pressure and pressure-induced transition. Zeitschrift für Kristallographie 220, 938-945.

823

824 **Tables**

825 Table 1: Representative compositions of major minerals forming the assemblages of Praborna
826 occurring in the basal levels, upper levels, HP veins and the SiO_2-undersaturated sample C4.

827 Table A-1: Thermodynamic database used for calculations.

828 Table A-2: *V-T* data of braunite**.**

829 Table A-3: *V-T* data of pyrolusite**.**

830

831 **Figure captions**

832 Figure 1: Appearance of two-phase field (A + B) between two one-phase fields (A, B) in a unary
833 system, when the molar quantity nO_2 is introduced instead of its conjugate potential μO_2. Vertical
834 lines in *b* are isothermal tie-lines accounting for the difference in molar quantity nO_2. Redrawn
835 from Hillert (1985).

836

837 Figure 2. Geological sketch map of the Saint-Marcel valley showing the Praborna mine (45.6796°
838 lat. N; 7.4495° long. E) and the principal lithologies occurring in the area.

839

840 Figure 3. Schematic section of the Mn ore. Basal levels are highly fractured and show pervasive
841 veining. The enlargement shows a stockwork of quartz- and feldspar-filled veins cutting the
842 massive ore mainly consisting of braunite (black) and piemontite (purple) (orange crusts are
843 lichens). Note that the growth of "pegmatoid" piemontite crystals is perpendicular to the fracture
844 walls (black arrow). Basal levels and veins contain omphacite in equilibrium with quartz and are in
845 contact with glaucophanites. The upper part of the ore gradates into garnet + quartz ± pyroxmangite
846 assemblages, and is overlaid by Mn-poor micaschists.

847

Figure 4. Representative mineral assemblages characterizing the Mn ore of Praborna. (a) Colorized Back Scattered Electron (CBSE) image of braunite (blue), pyroxmangite (green) and hematite (violet) coexisting with quartz in the basal level. (b) Transmitted Light Photomicrograph (TLP) of the vein containing Mn-rich purple omphacite (violan) in equilibrium with quartz, braunite and piemontite. (c) TLP of hematite in equilibrium with garnet, pyroxmangite and quartz in the silica-rich assemblages of the upper level. (d) CBSE image of quartz-free sample from the upper level, showing the replacement of pyroxmangite (yellow) + braunite (blue) by tephroite (blue-green) and hausmannite (violet). Rhodochrosite (red) is a late mineral.

Figure 5. Raman spectra of $MnSiO_3$ in selected samples (basal levels: SM93; upper levels: 16/01) compared with those of reference pyroxmangite and rhodonite from the mineralogical collection of the *Muséum National d'Histoire Naturelle* in Paris. These spectra show that $MnSiO_3$ at Praborna is the high-pressure pyroxmangite polymorph.

Figure 6. As- and Sb-bearing minerals characterizing the parageneses at Praborna. (a) basal levels; zoned apatite crystal richer in As at the rim (cathodoluminescence image); (b) basal levels; ardennite-(As) $(Mn,Ca,Mg)_4(Al,Mg,Fe)_6(SiO_4)_2(Si_3O_{10})(AsO_4,VO_4)(OH)_6$ in equilibrium with garnet and rutile showing a Sb-rich rim (BSE image); (c) basal levels; romeite $(Ca,Fe,Mn,Na)_2(Sb,Ti)_2O_6(O,OH,F)$ showing oscillatory zoning (BSE image); (d) upper levels; hematite associated to Sb-rich pyrophanite ($MnTiO_3$) (BSE image).

Figure 7. Thermodynamic model of the system $MnO–SiO_2–O_2$, calculated for P = 2.1 GPa and T = 550 °C. (a) μO_2 (kJ•mol^{-1}) and log (fO_2/1 bar) vs. $SiO_2/(MnO+SiO_2)$ phase diagram. Compositions are represented in barycentric mole fractions. Considered phases are: quartz (qtz); manganosite (mang); pyroxmangite (pxmn); tephroite (teph); hausmannite (hsm); braunite (braun); bixbyite (bxb); pyrolusite (not stable at these conditions). In addition to μO_2 (right vertical axis), the

874 corresponding log (fO_2/1 bar) and ΔFMQ values (black and grey numbers, respectively, on the left
875 vertical axis) are also reported for comparison. Dashed grey lines are the univariant equilibria
876 piemontite = garnet + H_2O + O_2, CuO = Cu_2O + O_2, Cu_2O = Cu+O_2, $FeSO_4$ = pyrite + hematite +
877 O_2, hematite = magnetite + O_2, and magnetite + quartz = fayalite + O_2. The red and blue horizontal
878 lines indicate the associations quartz–braunite–pyroxmangite (basal levels) and braunite–
879 haussmanite–tephroite (upper levels), respectively. Shaded fields represents in grey scale the ratio
880 Mn^{3+}/Mn_{tot} as suggested by Figure 7b. (b) Ternary chemography of the system MnO–SiO_2–O_2.
881 Compositions are represented in barycentric mole fractions (i.e., sum of coordinates = 1). The
882 diagram is stretched vertically (the upper O_2 vertex is not shown) in order to highlight the
883 assemblages without oxygen as a free phase. nO_2 represents the excess of O_2 component with
884 reference to the Mn^{3+}-free system SiO_2–MnO. μO_2 (kJ•mol^{-1}) is reported for each divariant field.
885 Thick dotted lines are Mn^{3+}/Mn_{tot} isopleths, whereas horizontal dotted lines are nO_2 isopleths. The
886 quartz–O_2, braunite–O_2 and bixbyite–O_2 tie-line (dotted arrows) are virtual, because O_2 is not
887 thought to be a real phase at these conditions. The coloured fields correspond to the typical
888 Praborna assemblages as in Figure 7a. Black arrow is a hypothetical metasomatic path from SiO_2-
889 poor to SiO_2-enriched assemblages, where nO_2 and the ratio Mn^{3+}/Mn_{tot} decrease while μO_2
890 increases.
891
892 Figure 8. Thermodynamic model of the system MnO–FeO–SiO_2–O_2 calculated for P = 2.1 GPa and
893 T = 550 °C. Compositions are represented in barycentric mole fractions. nO_2 represents the excess
894 of component O_2 with reference to the Fe^{3+}- and Mn^{3+}-free system FeO–SiO_2–MnO. ΔFMQ is
895 reported for each 4-phases assemblage (e.g., +12.7 for pyroxmangite–quartz–braunite–hematite).
896 The grey plane represents the locus of points at constant value of nO_2 and intersects all the
897 assemblages, with ΔFMQ ranging from -18.1 (wüstite–fayalite–magnetite–manganosite, light green
898 volume), to +9.7 (tephroite–hausmannite–braunite–hematite, blue volume, upper levels), and to
899 +12.7 (braunite–quartz–pyroxmangite–hematite, red volume, basal levels).

Figure 9. Oxygen in the subduction channel. Cartoon redrawn after Konrad-Schmolke et al. (2011) showing a patchy and heterogeneous distribution of fO_2 (see ΔFMQ; see also Fig. 12 in Foley, 2011), but a more regular gradient of nO_2 (i.e. the quantity of oxygen in excess compared to Fe^{3+}- and Mn^{3+}-free systems). In terms of nO_2, the mélange appears as a metasomatic front from the more oxidized slab to the less oxidized mantle wedge. Oxygen can be transported along fractures and veins through dissolution-reprecipitation of oxides and silicates fluxed by fluids. See text for further details.

Figure 1

Click here to download high resolution image

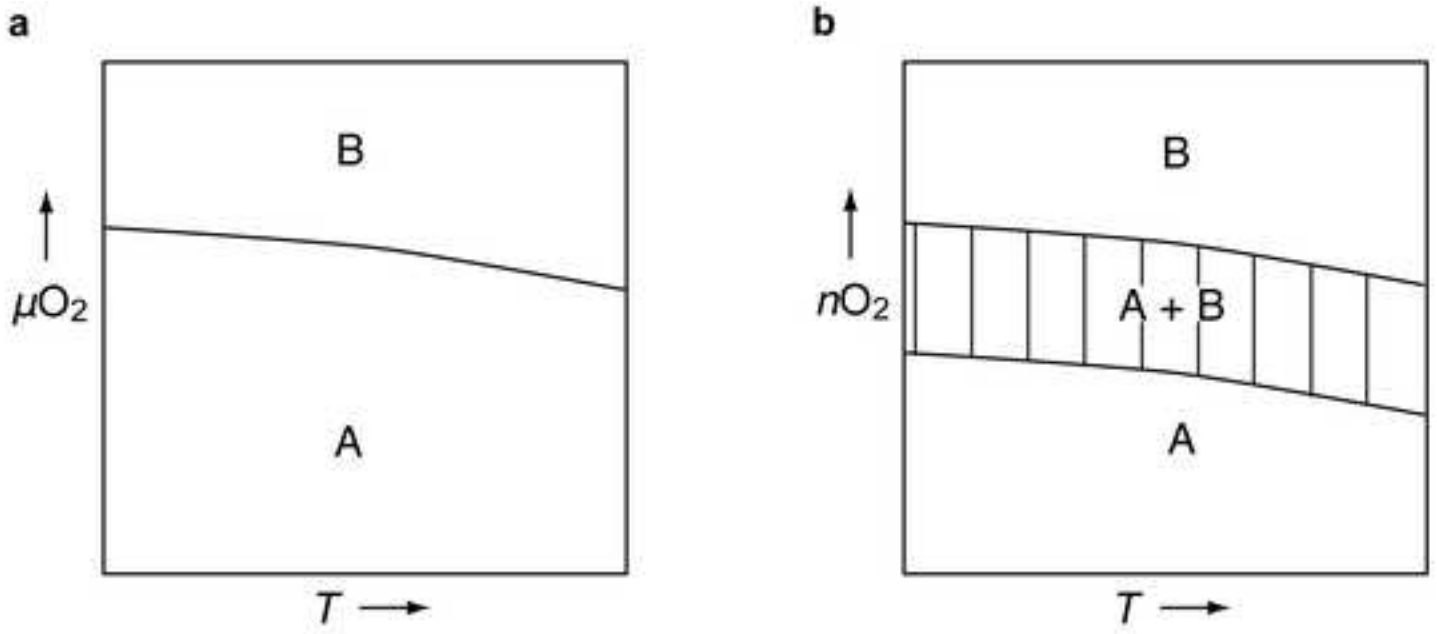

Figure 2

Click here to download high resolution image

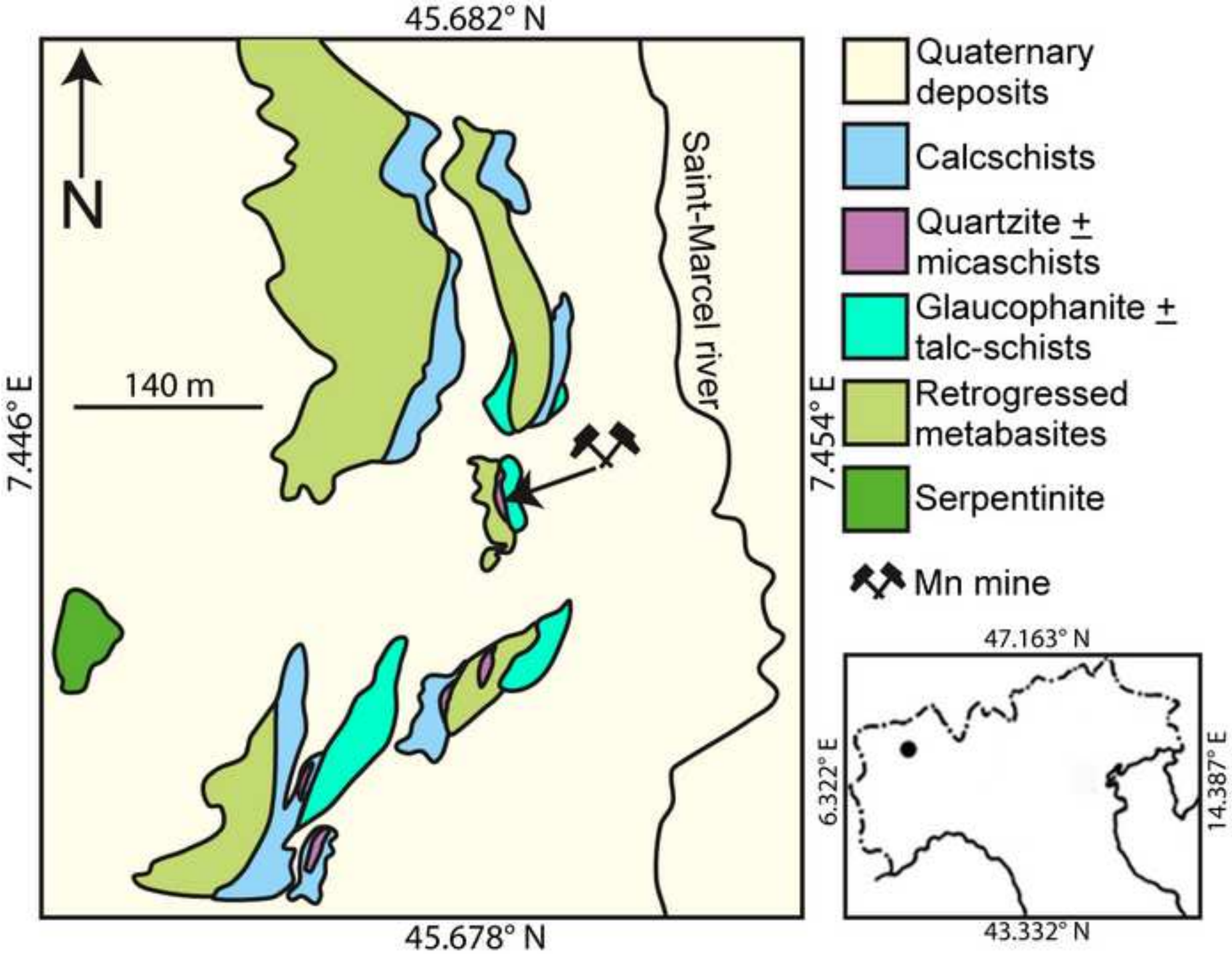

Figure 3

Click here to download high resolution image

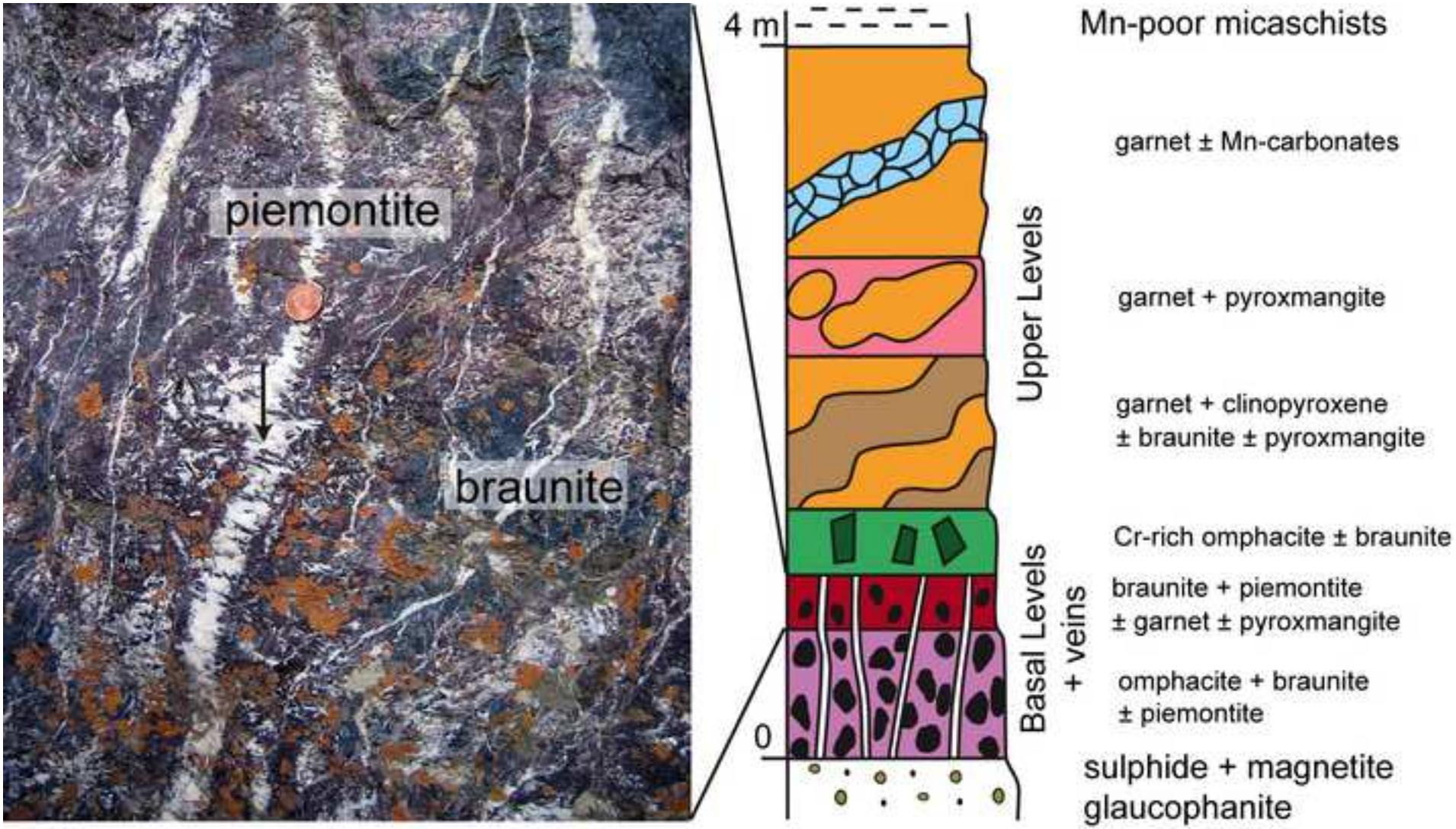

Figure 4

Click here to download high resolution image

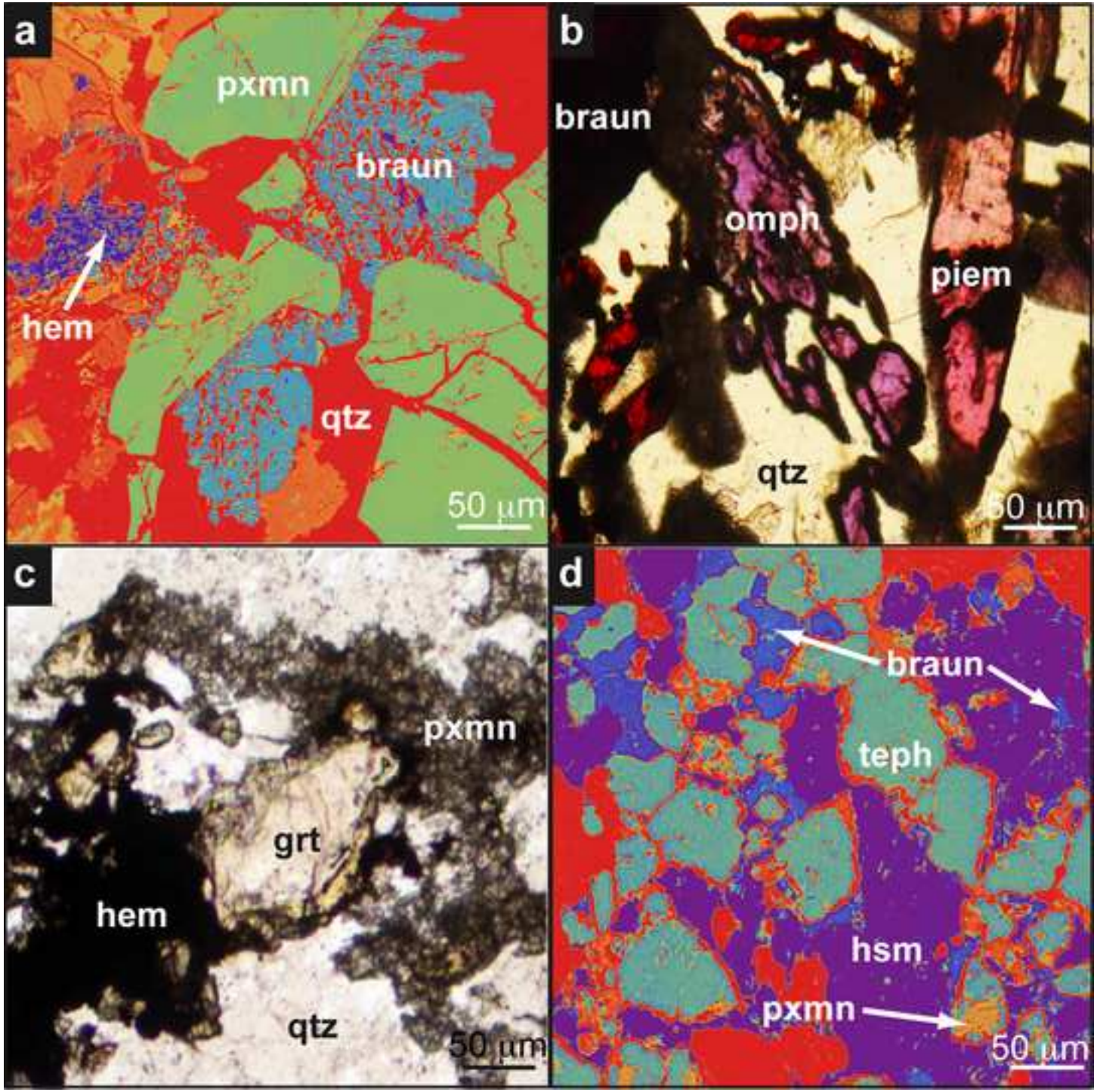

Figure 5

Click here to download high resolution image

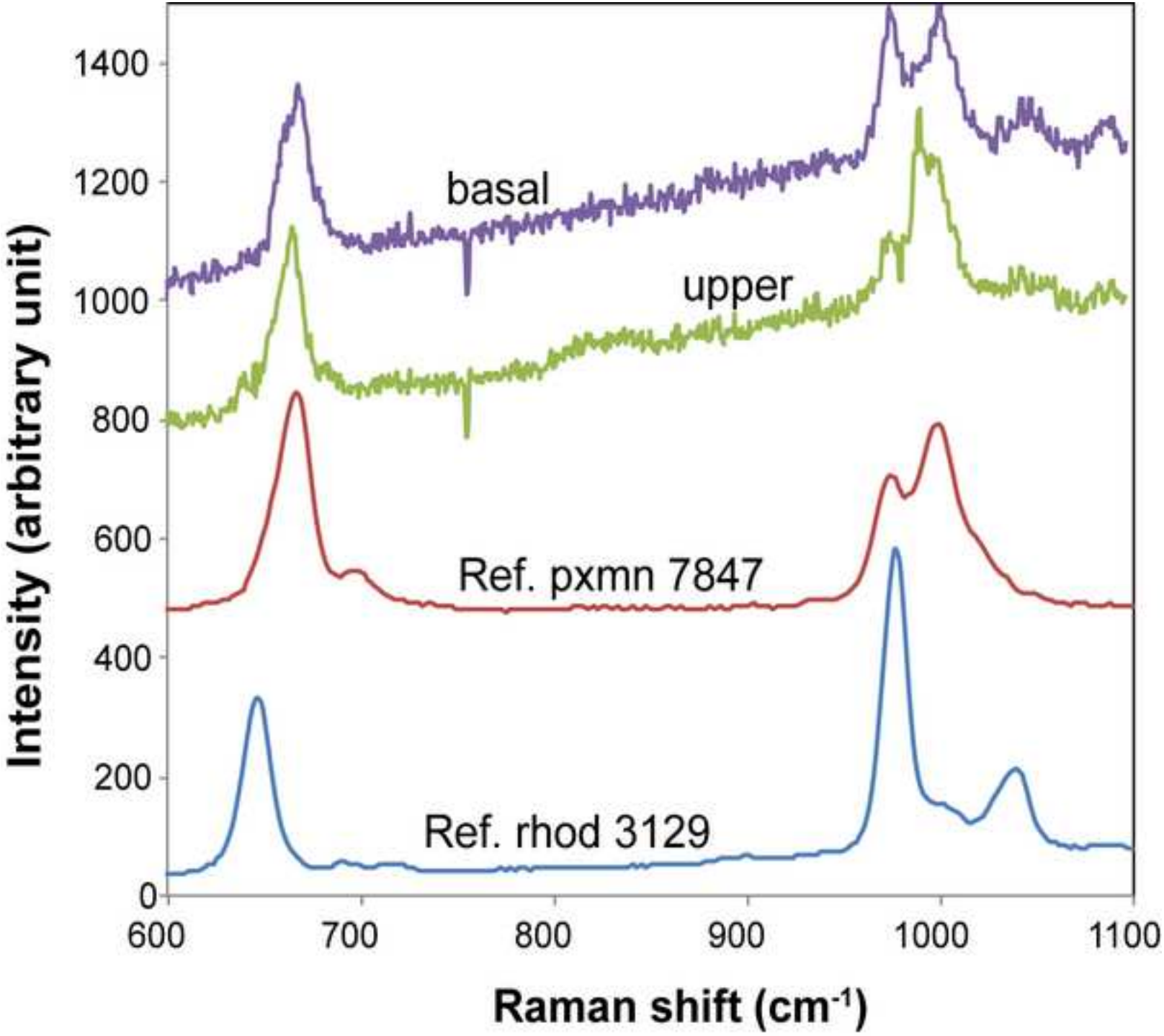

Figure 6

Click here to download high resolution image

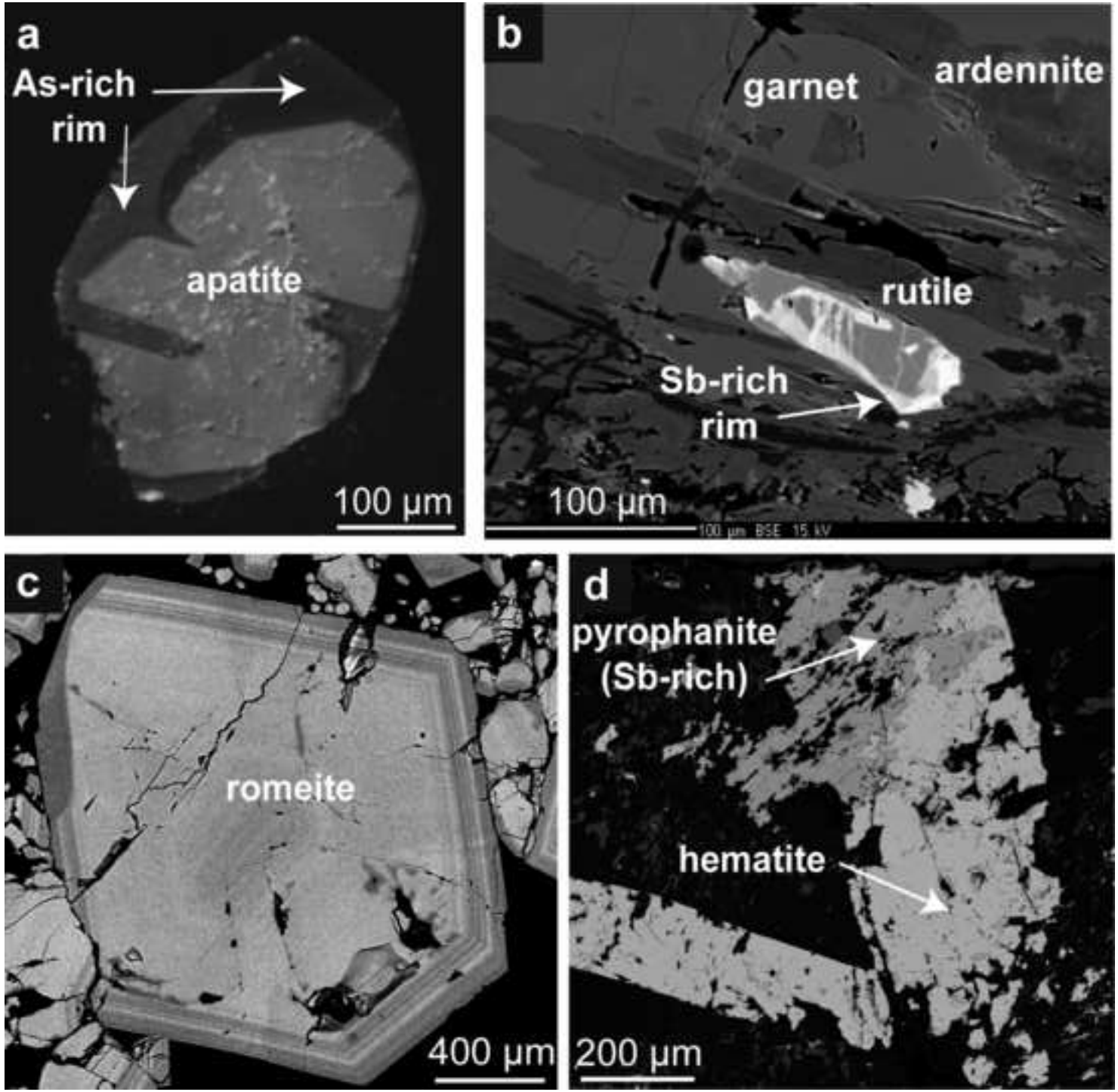

Figure 7

Click here to download high resolution image

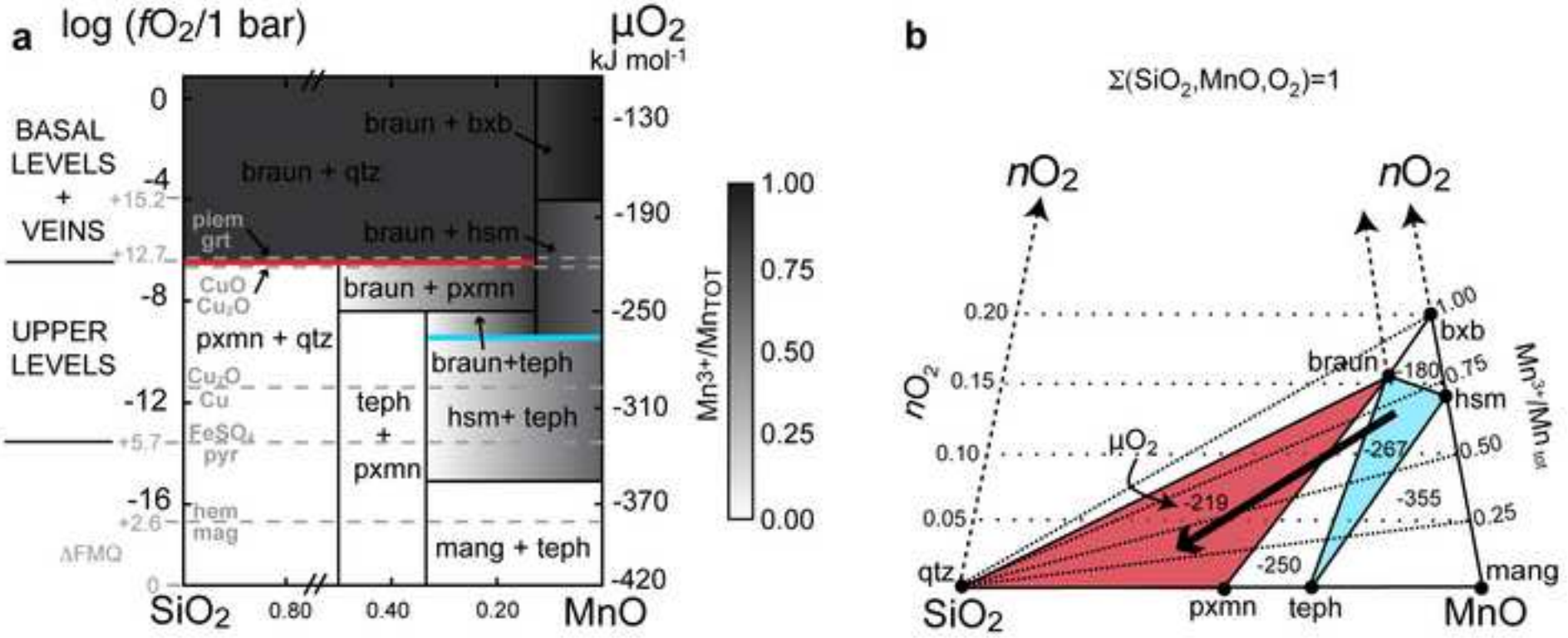

Figure 8

Click here to download high resolution image

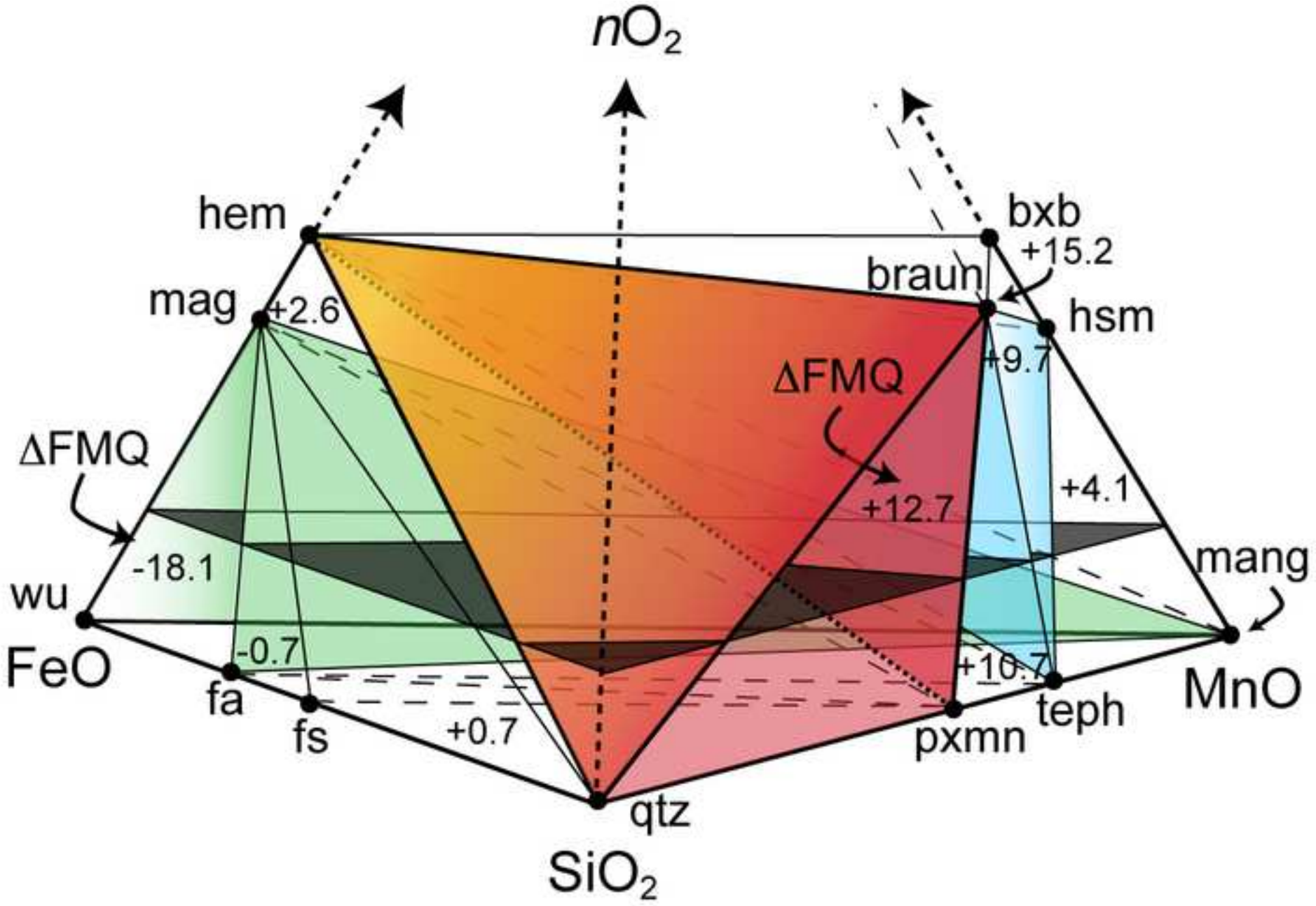

Figure 9

Click here to download high resolution image

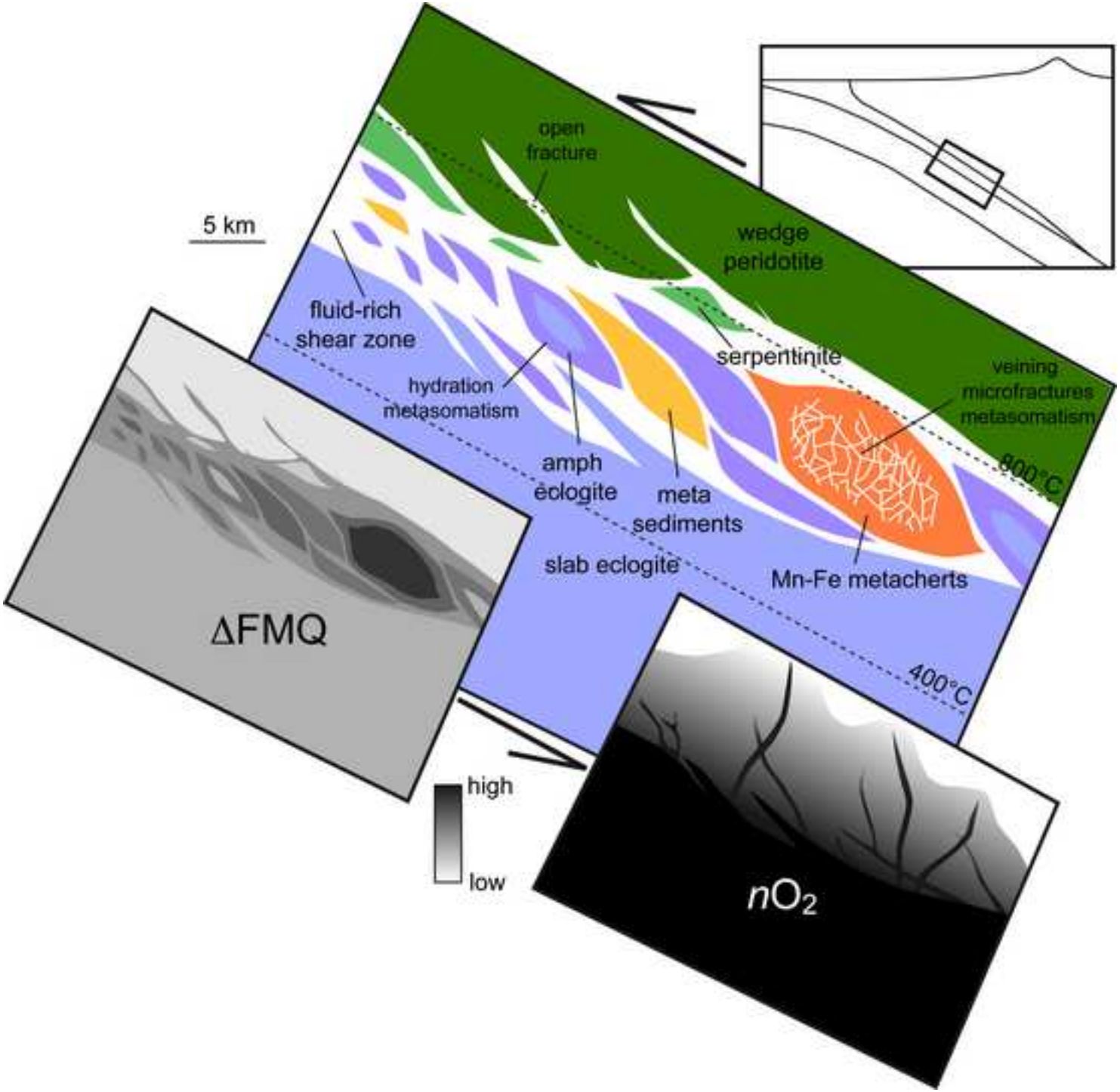

Table 1

Click here to download Table: Table 1.xlsx

Table 1. Representative mineral compositions of Praborna

	Basal levels			
Samples	SM-viol	SM-viol	SM-viol	SM93
wt.%	braunite	piemontite	clinopyroxene (violet)	pyroxmangite
SiO_2	10.01	35.91	57.64	47.70
TiO_2	0.00	0.01	0.03	0.04
Al_2O_3	0.17	16.80	15.16	0.04
Cr_2O_3	0.00	0.00	0.00	0.00
Fe_2O_3[a]	1.34	1.23	7.19	0.00
Mn_2O_3[a]	79.18	18.90	1.18	0.00
FeO	0.00	0.00	0.00	0.70
MnO	9.20	1.96	0.95	42.99
MgO	0.79	0.02	2.75	0.55
CaO	0.76	19.50	4.01	8.82
SrO	0.07	2.31	0.00	0.01
Na_2O	0.05	0.03	12.45	0.07
K_2O	0.01	0.01	0.07	0.01
Total	101.57	96.66	101.43	100.93
a.p.f.u.				
Si	0.984	3.024	2.000	1.002
Ti	0.000	0.001	0.001	0.001
Al	0.020	1.667	0.620	0.001
Cr	0.000	0.000	0.000	0.000
Fe^{3+}	0.099	0.078	0.188	0.000
Mn^{3+}	5.922	1.211	0.031	0.000
Fe^{2+}	0.000	0.000	0.000	0.012
Mn^{2+}	0.766	0.140	0.028	0.765
Mg	0.115	0.003	0.142	0.017
Ca	0.080	1.759	0.149	0.198
Sr	0.004	0.113	0.000	0.000
Na	0.009	0.005	0.837	0.003
K	0.001	0.001	0.003	0.000
Total cations	7.999	8.000	4.000	1.999
Charges	23.998	25.000	11.999	6.000

a: by stoichiometry

n.d.: not determined

Table A-1

Click here to download Table: Table A-1 def.docx

Table A-1. Thermodynamic database used for calculations.

Phase	manganosite	hausmannite	braunite	bixbyite	pyrolusite	piemontite	pyrite	Fe-sulfate	cuprite	tenorite	copper
Formula	MnO	Mn_3O_4	Mn_7SiO_{12}	Mn_2O_3	MnO_2	$Ca_2Al_2MnSi_3O_{12}(OH)$	FeS_2	$FeSO_4$	Cu_2O	CuO	Cu
$\Delta_f G^0$ (J mol^{-1})	-362816[a]	-1282434[c]	-3944653[c]	-882042[c]	-465018[c]	-6143680[e]	-160068[f]	-815331[f]	-147797[c]	-128330[c]	0[c]
$\Delta_f H^0$ (J mol^{-1})	-385150[a]	-1384500[c]	-4260000[c]	-959000[c]	-520000[c]	-6531850[e]	-171544[f]	-919330[f]	-170600[c]	-156100[c]	0[c]
S^0 (J mol^{-1} K^{-1})	59.70[a]	164.10[c]	416.4[c]	113.7[c]	52.8[c]	328.06[e]	52.93[f]	120.957[f]	92.4[c]	42.6[c]	33.14[c]
V^0 (J bar^{-1})	1.322[a]	4.695[c]	12.508[c]	3.137[c]	1.661[c]	13.87[d]	2.394[f]	5.0633[f]	2.3437[c]	1.222[c]	0.7113[c]
Coefficients for heat-capacity equation $C_p = c1 + c2\,T + c3/T^2 + c4\,T^2 + c5/T^{0.5}$											
c1	59.8[a]	-7.4[c]	430.1[c]	162.4[c]	290.4[c]	610.0[a*]	72.1[f]	142.7[f]	426.0[c]	31.0[c]	60.8[c]
c2	3.60E-03[a]	9.49E-02[c]	1.11E-01[c]	1.21E-02[c]	-1.44E-01[c]	2.48E-02[a]	1.79E-06[f]	1.59E-06[f]	-2.51E-01[c]	1.37E-02[c]	-2.88E-02[c]
c3	-3.14E+04[a]	-6.71E+06[c]	-7.33E+06[c]	1.05E+06[c]	2.01E+06[c]	-1.12E+07[a]	-2.04E+07[f]	2.40E+06[f]	4.90E+06[c]	-1.26E+06[c]	3.33E+05[c]
c4	0[a]	0[c]	0[c]	3.46E-06[c]	4.54E-05[c]	0[a]	3.42E-06[f]	-8.32E-07[f]	9.24E-05[c]	0[c]	1.42E-05[c]
c5	-282.6[a]	3396.0[c]	0[c]	-1317.0[c]	-3787.0[c]	-1192.1[a]	-0.4[f]	0.0[f]	-6078.0[c]	369.3[c]	-567.1[c]
Volumetric thermal expansion coefficient $V_{1,T} = V_{1,298}\,(1 + b1\,(T\text{-}298) - 20\,b1\,(T^{0.5} - 298^{0.5}))$											
b1 (a^0) (K^{-1})	6.300E-05[a]	4.450E-05[g]	4.900E-05[u]	4.380E-05[v]	1.315E-05[u]	5.05E-05[a]	3.40E-05[w]	1.10E-04[a]	1.150E-05[q]	4.260E-05[r]	1.124E-04[s]
Parameters for the third order Birch-Murnaghan Equation of State (Perplex EOS = 2) $V_{298,P} = V_{298,1} \cdot (1 - b8 \cdot P/(b8 \cdot P + b6))^{1/b8}$											
b6 (K) (GPa)	148.0[b]	137.0[h]	180.7[k]	169.1[l]	328.0[m]	123.3[a]	133.5[o]	120.0[a]	131.0[b]	80.0[p]	143.7[t]
b8 (K')	4.0[b]	4.0[h]	6.5[k]	7.4[l]	4.0[m]	4.0[a]	5.7[o]	4.0[a]	5.7[b]	4.0[p]	5.3[t]
Landau model parameters											
t1 (T_c) (K)	-	1443[i]	-	-	1261[n]	-	-	-	-	-	-
t2 (S_{max}) (J mol^{-1} K^{-1})	-	14.53[i]	-	-	11.5[n*]	-	-	-	-	-	-
t3 (V_{max}) (J bar^{-1})	-	0.160[j]	-	-	-	-	-	-	-	-	-

$\Delta_f G^0$ is the Gibbs free energy of formation from the elements in the standard state (298 K; 1 bar) calculated from the enthalpy of formation $\Delta_f H^0$ and the entropy in the standard state S^0; V^0 is the molar volume in the standard state; *b1* is the volumetric thermal expansion parameter; *b6* is the bulk modulus and *b8* the pressure derivative of the bulk modulus; *t1* is the temperature at which the phase becomes fully disordered at the reference pressure; *t2* is the maximum entropy change of disorder; *t3* is the maximum volume change of disorder.

a: Holland and Powell (1998) and references therein (Perple_X 2004 update, database HP04ver.dat). The thermal expansion and compressibility parameters of Fe-sulfate are mutuated from siderite. Heat capacity, thermal expansion and compressibility parameters of piemontite are mutuated from epidote, apart from the *c1* parameter (a*) that was adjusted in order to be consistent with the piemontite-garnet transition found experimentally by Keskinen and Liou (1979).

b: Smyth et al. (2000) and references therein; c: Robie and Hemingway (1995) and references therein; d: Langer et al. (2002); e: Tumiati (2005 A), estimated using the "polyhedral model" (see details on this method in the review of Hazen, 1985); f: Shi (1992); g: Mori (2002); h: Paris et al. (1992); i: temperature of transition from distorted tetragonal to cubic structure (Irani et al., 1958); j: calculated from the cubic cell parameters given by McMurdie et al. (1950); k: Miletich et al. (1998); l: Yamanaka et al. (2005); m: Heines et al. (1995); n: Curie temperature given by Krist et al. (1992) (n* is the contribution of the magnetic effect to S^0 calculated as $R\ln(2s+1)$ (cf. Holland,1989), where *s*

is the spin quantum number (1.5 for Mn^{4+})); o: Merkel et al. (2002); p: Wang et al. (2002); q: Dapiaggi et al. (2003); r: Ohashi et al. (2006); s: Kazanc et al. (2006); t: Greeff et al. (2006); u: this study (see Appendix); v: Geller and Espinosa (1970); w: Robertson (1988).

Table A-2

Click here to download Table: Table A-2 def.docx

Table A-2: *V*-*T* data of braunite.

T (°C)	*V* (Å^3)	σ	*molar V* (J bar^{-1})	σ
25	1659.4	0.3	12.491	0.002
25	1659.0	2.0	12.488	0.015
25	1659.0	1.0	12.488	0.008
25	1659.0	3.0	12.488	0.023
25	1659.0	2.0	12.488	0.015
100	1662.4	0.7	12.514	0.005
200	1666.0	0.7	12.541	0.005
300	1671.0	1.0	12.578	0.008
400	1675.6	0.5	12.613	0.004
400	1675.6	0.4	12.613	0.003
400	1675.2	0.6	12.610	0.005
400	1675.8	0.4	12.615	0.003
500	1680.4	0.6	12.649	0.005
600	1686.0	1.0	12.691	0.008

Table A-3
Click here to download Table: Table A-3.docx

Table A-3. *V-T* data of pyrolusite.

T (°C)	*V* (Å^3)	σ	*molar V* (J bar^{-1})	σ
25	55.808	0.005	1.680	0.0002
100	55.831	0.003	1.681	0.0001
150	55.871	0.005	1.682	0.0002
200	55.902	0.005	1.683	0.0002
250	55.908	0.005	1.683	0.0002
300	55.935	0.005	1.684	0.0002
350	55.975	0.005	1.685	0.0002
400	55.962	0.004	1.685	0.0001
450	55.972	0.005	1.685	0.0002
500	55.986	0.004	1.686	0.0001
550	56.016	0.005	1.687	0.0002
600	56.027	0.005	1.687	0.0002

Background dataset for online publication only

Click here to download Background dataset for online publication only: supplementary material def.pdf

Ultra-oxidized ~~redox conditions~~rocks in subduction mélanges? Decoupling between oxygen fugacity and oxygen availability in a Mn-rich metasomatic environment

Simone Tumiati[a,*], Gaston Godard[b], Silvana Martin[c], Nadia Malaspina[d] and Stefano Poli[a]

[a] *Dipartimento di Scienze della Terra "Ardito Desio", Università degli Studi di Milano, via Mangiagalli 34, I-20133 Milano, Italy; simone.tumiati@unimi.it*

[b] *Institut de Physique du Globe de Paris, Sorbonne Paris Cité, Université Paris Diderot, UMR 7154 CNRS, 1 rue Jussieu, F-75252 Paris, France*

[c] *Dipartimento di Geoscienze, Università degli Studi di Padova, via Giotto 1, 35137 Padova, Italy*

[d] *Dipartimento di Scienze dell'Ambiente e del Territorio e di Scienze della Terra, Università degli Studi di Milano Bicocca, piazza della Scienza 4, 20126 Milano, Italy*

ABSTRACT

The manganese ore of Praborna (Italian Western Alps) is embedded within a metasedimentary sequence belonging to a subduction mélange equilibrated at high-pressure (HP) conditions ~~(~~(ca. 2 GPa) during the Alpine orogenesis. The pervasive veining of the ore and the growth of "pegmatoid" HP minerals suggest ~~an open system with large fluid/rock ratio and a strong interaction with slab-derived fluids. This rock association provides an excellent natural laboratory to constrain the redox state in subducting oceanic slab mélanges at HP, fluid-present conditions. The Mn-rich~~that these Mn-rich rocks strongly interacted with slab-derived fluids during HP metamorphism. These rocks are in textural and chemical equilibrium with the veins and in contact with sulphide- and magnetite-bearing metabasites at the bottom of the sequence. They contain braunite ($Mn^{2+}Mn^{3+}{}_6SiO_{12}$~~) +~~), quartz~~ +~~, pyroxmangite ($Mn^{2+}SiO_3$), and minor hematite, omphacite, ~~Mn-rich epidote (~~piemontite~~)~~ and spessartine-rich garnet. Sulphides are absent in the Mn-rich rocks, whereas sulphates (barite,

celestine) occur together with As- and Sb-oxides and silicates. This rock association provides an excellent natural laboratory to constrain the redox conditions in subducting oceanic slab mélanges at HP and fluid-present conditions. Similarly to Fe-bearing minerals, Mn oxides and silicates can be regarded as natural redox-sensors. ~~On the basis of~~ A thermodynamic dataset for these Mn-bearing minerals is built, using literature data as well as new thermal expansion parameters for braunite aud pyrolusite, derived from experiments. Based on this dataset and the observed assemblages~~, new~~ at Praborna, thermodynamic calculations show that these mélange rocks are characterized by ~~unrealistic~~ ultra-oxidized ~~states~~conditions (ΔFMQ up to +12.7) if the chemical potential of oxygen (or the oxygen fugacity fO_2) is accounted for. On the other hand, if the molar quantity of oxygen is ~~considered~~ used as the independent state variable to quantify the bulk oxidation state ~~of~~, the ore~~,~~ ~~then this~~ appears only moderately oxidized~~,~~ and comparable to typical subduction-slab mafic eclogites. Such ~~a decoupling~~an apparent contradiction may ~~result when~~happen in rock systems whenever oxygen is improperly considered as a perfectly mobile component ~~in rock systems.~~. In the Earth's mantle, redox reactions take place mainly between solid oxides and silicates, because ~~oxygen~~O_2 is a negligible species ~~even in the most favourable conditions within~~ the ~~presence of a~~ fluid phase. Therefore, the description of the redox ~~state~~conditions of most petrological systems ~~would require~~requires the introduction of ~~the~~an extensive variable, namely the oxygen molar quantity~~.~~ (nO_2). As a consequence, the ~~conjugate~~ oxygen chemical potential, and ~~therefore~~thus fO_2, becomes a dependent state variable, not univocally indicative of the redox ~~state~~conditions of the entire rock column of a subduction zone, from the dehydrating oceanic crust to the overlying mantle wedge. On a more general basis, the comparison of ~~fO_2s~~fO_2 retrieved from different bulk compositions and different phase assemblages ~~may lead to apparent redox heterogeneities.~~is sometimes challenging and should be undertaken with care. From the study of mélange rocks ~~of~~at Praborna, the distribution of oxygen at subduction zones could be modelled as ~~a continuous~~an oxidation ~~front, moving~~gradient, grading from a maximum in the subducted altered oceanic crust to a minimum in the overlying peridotites of the mantle hanging-wall.

Keywords: manganese, oxidation, oxygen fugacity, subduction, mantle wedge, slab, eclogite

Highlights:

- The manganese-rich rocks of Praborna are high-pressure metacherts belonging to a slab mélange.
- Rocks are veined pervasively suggesting a strong interaction at HP with slab-derived fluids.
- Mn-rich mineral associations suggest ultra-high fO_2 conditions up to ΔFMQ +12.7.
- In terms of quantity of O_2, the same rocks display a moderate oxidation state.
- The decoupling between intensity and extensity of O_2 in metasomatic rocks is highlighted.

1. Introduction

The reduction-oxidation (redox) ~~state in~~conditions of rocks ~~is~~are known to affect phase relationships, speciation of volatile elements, trace element partitioning, diffusivity, electrical conductivity and mechanical properties (Arculus, 1985). ~~Variability in~~ Redox conditions are traditionally described using the intensive variable oxygen fugacity (fO_2). Variability in fO_2 at subduction zones has been debated since a long time (Gill, 1981; Wood et al., 1990; Foley et al., 2011). ~~Exception done for few works (e.g., Chinner, 1960; Evans, 2006), the redox state of rocks is traditionally described by the intensive variable oxygen fugacity (fO_2), which is in turn a function of the chemical potential of oxygen (μO_2).~~ Compared to the asthenospheric and lithospheric ~~mantle~~mantles, relatively high ~~fO_2s have~~fO_2 has been proposed for subducted slab materials, sub-arc mantle and arc magmas (Hirschmann, 2009; Kelley and Kottrell, 2009; Malaspina et al., 2009, 2010; Groppo and Castelli, 2010; Evans, 2012). However, trace-element and isotope systematics, aimed to constrain the variation of fO_2 in the mantle (Canil, 2002~~,~~; Lee et al., 2005, 2010), challenge such conclusion, ~~emphasising~~emphasizing a discrepancy between the fO_2 calculated by oxygen thermobarometry~~,~~ and that inferred from V/Sc data on arc lavas.

~~The choice to describe a redox system in terms of fO_2 (or μO_2) is entirely valid only if oxygen can be considered a "perfectly mobile" component. As already explained by Korzhinskii in 1959 (page~~The redox conditions of rocks could be also expressed in terms of ratios of cations occurring in different oxidation states, such as Fe^{2+} and Fe^{3+}. However, paucity of thermodynamic data on Fe^{3+} end-members~~ 16), the behaviour of a chemical component in a rock system could be "inert" or "perfectly mobile", depending on its mobility between the system and an external medium. As an example, during a fluid/rock interaction, where the system is the rock and the external medium is a fluid phase flushing the rock, those rock components that are not readily transported by the fluid are considered inert or "immobile", whereas components that can dissolve into the fluid can be considered "mobile" and rapidly react with the surrounding rock. On this principle, the quantity of inert components has a fundamental role to attain the equilibrium, while it can be neglected for mobile components. Therefore, from a thermodynamic point of view, during the equilibration between a rock and a fluid phase, the quantity of material (moles) should be considered as independent parameter for inert components, whereas chemical potential must be used as independent parameter for perfectly mobile components (Korzhinskii, 1959). A complication arises when we consider the component oxygen in the Earth's interior, because redox reactions take place mainly among solid oxides and silicates, where oxygen is bonded to relatively "inert" components such as Fe (e.g. Fe_2O_3) and Mn (e.g. Mn_2O_3) while occurs in very limited amounts in fluids. Therefore, oxygen cannot be considered unequivocally a perfectly mobile component. It could well be that, in many cases, oxygen is better regarded as an "inert" component, so that its molar quantity (from now on, nO_2) should be the independent variable, while its chemical potential (μO_2) the dependent variable. When these two parameters are considered for thermodynamic calculations in rock systems, it must be stressed that the introduction of nO_2 (which is the conjugate variable of μO_2 concerning the thermodynamic material parameters) instead of μO_2, modifies the inspection of phase relationships (e.g., Hillert, 1985). In particular, when a molar quantity is introduced as an axis instead of its conjugate potential, one-phase fields wills separate from each other thus leaving room

~~for the two-phase field, and the distance is equal to the difference in their molar quantity (Fig. 1). In addition, when molar quantities other than nO_2 are not constant, μO_2 (and fO_2) is not a simple, monotonically increasing function of the quantity of oxygen. Therefore, the reconstruction of the extensive property (nO_2) from the intensive variable (fO_2 or μO_2) can be a very inaccurate procedure in natural, multi-component systems (see Malaspina et al., 2009, 2012).~~

~~Paucity of thermodynamic data on Fe^{3+} endmembers~~ of minerals and analytical difficulties in retrieving Fe^{3+}/Fe^{2+} in fine-grained, texturally complex volatile-rich rocks have hindered so far the quantitative assessment of redox conditions in the slab-mantle mixing zone in terms of Fe^{3+}/Fe^{2+} ratio (Bebout, 2007). ~~Sedimentary material involved in subduction mélanges shows large compositional variability, but~~On the other hand, Mn-rich nodules and crusts, though volumetrically very limited, are nearly ubiquitous on the seafloor (Manheim, 1978) and contain highly oxidized Mn^{4+}-bearing phases, such as amorphous MnO_2, pyrolusite, birnessite, and todorokite (e.g., Ostwald and Frazer, 1973). Upon metamorphism, a variety of Mn^{3+} and Mn^{2+} oxides and silicates may form in subduction mélanges, depending on *P*–*T*–*X* conditions (e.g., Dasgupta, 1997~~).~~; Tumiati et al., 2010). The variable oxidation states of manganese~~, as it is for iron in oxides and silicates,~~ make Mn minerals extremely useful sensors to constrain redox conditions of rocks.

The present study ~~concerns~~takes advantage of the manganese ore of Praborna, cropping out in the Italian western Alps, and consisting of Mn-rich metasediments embedded within meta-ophiolites (Tumiati et al., 2010). This ore displays a complex variety of Mn- and Fe-rich mineral assemblages, formed at eclogite-facies conditions in a subduction mélange. Swarms of stockwork high-pressure (HP) veins are cutting the Mn-rich rocks, suggesting an interaction with slab-derived fluids at very high fluid-rock ratio, as expected for such very thin, veined, metasedimentary sequences (Bebout et al., 2013). Praborna represents an excellent natural laboratory for the study of the behaviour of the component oxygen in terms of mobility in oceanic slab mélanges subducted at ~~high-pressure (~~HP~~)~~ conditions and flushed by fluids. This particular case should be considered as paradigmatic, because

it draws the attention to the choice of ~~fO_2 (μO_2) vs. nO_2 as~~ the independent ~~variable~~parameter capable of describing the redox ~~state~~conditions of ~~the system~~rocks in a metasomatic environment.

2. Concepts and definitions

Oxidation and reduction are defined in general chemistry as loss and gain of electrons, respectively. Since oxygen is the most common electron acceptor in natural systems, because of its high electronegativity, oxidation and reduction generally mean gain and loss of oxygen, by exchange with the external medium. Thus, the redox condition of rocks is described by considering a variable that can potentially rule this exchange. Exception done for a few works (e.g., Chinner, 1960; Evans, 2006), the variable traditionally considered in Earth sciences is the oxygen fugacity (fO_2). However, O_2 is not expected to be a major gaseous/fluid species in the Earth's interior, and the chemical potential of oxygen (either μO or μO_2) could appear more appropriate. In this study, we use both variables fO_2 and μO_2 considered as equivalent.

The fugacity of a gaseous species is the theoretical partial pressure that this gas would have if it would obey the ideal-gas law ($P \times V = n \times R \times T$). This means that fugacity is equal to partial pressure only in ideal gases (i.e., for $P \rightarrow 0$ bar). At higher pressures, gases strongly diverge from the ideal gas law, and a fugacity coefficient ($\Phi = f / P$) is introduced accounting for the non-ideal behaviour. The fugacity of a gas is in turn a function of the chemical potential of the relative component. For the component O_2, this relationship is expressed by the following equation:

$$\mu O_2 = G^0_{f,T,O2} + R \times T \times \ln fO_2/f^0O_2$$

where

- μO_2 (J•mol^{-1}) is the chemical potential of the component O_2 at P and T of interest;
- $G^0_{f,T,O2}$ (J•mol^{-1}) is the molar Gibbs energy of formation of pure oxygen (O_2) at P^0 = 1 bar and T;
- R (J•K^{-1}•mol^{-1}) is the gas constant;
- fO_2 (bar) is the fugacity of pure oxygen at P and T of interest;

- f^0O_2 is the fugacity of pure oxygen at the standard-state pressure P^0 (f^0O_2 = 1 bar at all T).

As for any other component of a petrological system, μO_2, and thus fO_2, is ideally homogenous in all phases at equilibrium and independent of the phase abundance; in other terms, it is an intensive variable. The O_2 molar quantity (nO_2) is the conjugate extensive variable of μO_2, since the product ($\mu O_2 \times nO_2$) has the dimension of an energy ($J \cdot mol^{-1} \times mol = J$), similarly to other couples of intensive and extensive variables like ($P \times V$) and ($T \times -S$).

While considering an oxidised system, the set of basis vectors that generate the compositional vector space (i.e. the set of independent components) could be either {Si, Fe, Mn, ..., O} or {SiO_2, FeO, MnO, ..., O_2}. We have chosen here the latter set of independent components, so that μO_2 and nO_2 have to be considered instead of μO and nO. In that case, nO_2 represents the coordinate for the basis vector O_2; it equals zero when all Fe and Mn occur in their divalent oxidation state, i.e. as FeO and MnO (see Fig. 7).

The choice to describe a redox system in terms of intensive variables (fO_2 or μO_2) is entirely valid only if O_2 can be considered a "perfectly mobile" component. As already explained by Korzhinskii (1959, p. 16), the behaviour of a chemical component in a rock system could be "inert" or "perfectly mobile", depending on its mobility between the system and an external medium. As an example, during a fluid-rock interaction, where the system is the rock and the external medium is a fluid phase flushing the rock, those rock components that are not readily transported by the fluid are considered inert or "immobile", whereas components that can dissolve into the fluid can be considered "mobile" and rapidly react with the surrounding rock. On this principle, the quantity of inert components has a fundamental role to attain the equilibrium, while it can be neglected for mobile components. Therefore, from a thermodynamic point of view, during the equilibration between a rock and a fluid phase, the molar quantity of material should be considered as an independent state variable for inert components, whereas chemical potential must be used as an independent state variable for perfectly mobile components (Korzhinskii, 1959).

A complication arises when we consider the component O_2 in the Earth's interior, because redox reactions take place mainly between solid oxides and silicates, where oxygen is bonded to relatively inert components such as FeO (forming, for example, Fe_2O_3) and MnO (forming, for example, Mn_2O_3), while it occurs in very limited amounts in fluids. Therefore, O_2 cannot be considered unequivocally a perfectly mobile component. It could well be that, in many cases, O_2 is better regarded as an inert component, so that nO_2, rather than μO_2, becomes an independent thermodynamic state variable imposed upon the system.

Considering the variable nO_2 instead of μO_2 modifies the inspection of phase relationships (e.g., Hillert, 1985). In particular, when a molar quantity is introduced as an axis instead of its conjugate chemical potential, two one-phase fields will separate from each other, thus leaving room for the two-phase field, and their distance will be equal to the difference in the molar quantity between the two phases (Fig. 1). In addition, when molar quantities other than nO_2 are not constant, μO_2 (and fO_2) is not a simple, monotonically increasing function of the quantity of oxygen. Therefore, the reconstruction of the extensive property (nO_2) from the intensive variable (fO_2 or μO_2) can be a very inaccurate procedure in natural, multi-component systems (see Malaspina et al., 2009, 2012).~~2~~

3. The Praborna manganese ore

Slices of Mn-rich metasediments are commonly hosted in meta-ophiolites of the Western Alps. Praborna (Saint-Marcel valley, Italy; Fig. 2) is the largest Mn deposit in the Zermatt-Saas unit, which is interpreted as part of the Jurassic oceanic lithosphere of the Tethys, subducted during the Alpine orogeny (e.g., Dal Piaz, 2001). In the Zermatt-Saas unit, Mn-rich rocks from Lago di Cignana (Valtournanche) preserve coesite (Reinecke, 1998) and microdiamonds (Frezzotti et al., 2011), suggesting that the oceanic sediments underwent ultrahigh-*P* (UHP) metamorphism. HP metamorphic peak conditions of 2.1 GPa and 550 °C were recorded also in the meta-ophiolite of the Saint-Marcel valley (Martin et al., 2008), which are the country rocks of the Praborna deposit.

The disused mine of Praborna, known since 1415 ~~AD~~CE (Castello, 1982), is world-famous for its peculiar rocks and minerals. In particular, it is the type locality of five mineralogical species, namely piemontite, braunite, romeite, strontiomelane, and manganiandrosite-(Ce) (Ciriotti et al., 2009 and references therein). The Praborna deposit displays a continuous change in mineralogy from the basal contact with metabasites (now glaucophanites) towards the upper contact with Mn-poor metasediments (Figs. 2, 3), and consists of boudinaged Mn-rich metasediments cropping out in a "mélange" composed of serpentinite, ophicarbonate breccias, metagabbro and metabasalt with N-MORB affinity (Fig. 2; Martin and Kienast, 1987; Martin et al., 2008; Tumiati et al., 2010). Swarms of stockwork HP veins cut the Mn-rich rocks especially near the basal contact (Fig. 3), suggesting an interaction with slab-derived fluids. On the basis of the mineralogical composition, several "levels" have been recognized (Martin and Kienast, 1987; Tumiati et al., 2010). Basal levels and veins contain braunite (the ore mineral), piemontite and jadeite-rich Mn-bearing omphacite, whereas upper levels are characterised by the abundance of garnet ± pyroxmangite ± jadeite-poor clinopyroxene. Quartz is generally abundant in all the levels. In Table 1, we report representative mineral compositions of the basal and upper levels, the HP ~~vein~~veins and the SiO_2-undersaturated assemblages found at Praborna. Other details concerning mineralogy and petrography of the ore are provided in Section ~~4 and~~5, as ~~Supplemetary~~Supplementary Material~~.~~ (SM), and in Tumiati et al. (2010).

~~3. Material~~4. Materials and methods

Several thin sections of the basal and upper levels (Table SM-1 in the Supplementary Material) have been analysed at the petrographic and scanning electron microscopes. Chemical analyses reported in Table 1 were performed using the Cameca SX100 (Paris) and JEOL 8200 (Milano) wavelength-dispersive electron microprobes (EMP), at 15-kV accelerating potential, 15-nA sample current and 1-μm beam diameter. Standards used were albite (Na), diopside (Ca, Mg and Si), Fe_2O_3

(Fe), orthoclase (Al and K), $MnTiO_3$ (Mn and Ti), Cr_2O_3 (Cr) and barite (Ba). A counting time of 30 s was applied for all elements.

The Fe^{3+}/Fe_{TOT} and Mn^{3+}/Mn_{TOT} ratios in minerals have been calculated by stoichiometry. Because of ~~their electronic configuration,~~ the relative electronegativity of Fe and Mn, the pair Fe^{3+}–Mn^{2+} is more stable than the pair Fe^{2+} ~~towards oxidation to its +3 state. This assumption is confirmed by the fact that the pair Fe^{2+}-$^{+}$–Mn^{3+}~~, which has never been reported in minerals (Sherman, 1990). In fact, values of standard redox potential (or electromotive force) are 0.77 V for the pair Fe^{3+}–Fe^{2+} and 1.51 V for Mn^{3+}–Mn^{2+}. Therefore, the charges were calculated iteratively, by adjusting first Fe^{3+}/Fe_{TOT}, and then, if necessary, Mn^{3+}/Mn_{TOT}. In any case, this study is mainly focused on simple manganese oxides and silicates characterized by fixed Mn^{3+}/Mn_{TOT}, so that uncertainties related to this procedure do not affect the conclusions provided here.

For more complex phases, crystal chemistry has been evaluated mostly using the principal component analysis (PCA). In particular, this method was used to unravel substitution vectors in solid solutions. PCA is a statistical procedure that transforms a number of possibly correlated variables into the same number of uncorrelated variables given by the eigenvectors of the covariance matrix, and called principal components. The first principal component (F1) account for as much of the variability in the data as possible, and thus corresponds to the highest eigenvalue of the covariance matrix; each of the succeeding components (F2, F3…) accounts for as much of the remaining variability as possible. For other details and examples of PCA applied to EMP data, refer to Tumiati et al. (2005 A, 2005 B, 2008, 2013).

Raman spectroscopy of selected samples has been carried out using a green (514 nm) laser radiation, at the *Muséum National d'Histoire Naturelle* of Paris. In particular, Raman spectroscopy was required for the identification of the ~~high-pressure~~HP $MnSiO_3$ polymorph pyroxmangite.

~~4~~5. Mineralogy and petrography of the Praborna ore

~~4~~5.1 Basal levels

The basal levels (Fig. 3; Table 1) are in contact with glaucophanite made up of glaucophane + garnet + chloritoid + chlorite + paragonite ~~- bearing glaucophanite,~~and showing pseudomorphs after lawsonite (Martin et al., 2008). These basal levels mainly contain braunite ($Mn^{2+}Mn^{3+}_6SiO_{12}$) and piemontite (Fig. 3), minor quartz, omphacite, garnet, phengite and pyroxmangite, the HP polymorph of $Mn^{2+}SiO_3$ (Fig. 4A; see Raman spectrum of sample SM93 in Fig. 5). Hematite is the stable iron oxide (Fig. 4a), while magnetite ~~has~~was never ~~been~~ observed. Rutile and As-bearing apatite (Fig. 6a) are common accessories. Sulphides were not observed, although they are reported in the host metabasites of the Saint-Marcel valley, where Fe–Cu ores have been exploited in the past centuries (mines of Servette and Chuc; e.g. Martin et al., 2008; Tumiati et al., 2008).

Omphacite in these levels is dark purple and known as ~~*violan*,~~ a semiprecious stone called *violan* (Bondi et al., 1978). It is a solid solution of jadeite (up to Jd_{64}), diopside and aegirine, with minor contents in johansennite ($CaMn^{2+}Si_2O_6$) and namansilite ($NaMn^{3+}Si_2O_6$), often showing a complex zoning. PCA ~~suggests~~indicates that the main substitution vector in omphacite, represented by the first principal component F1 (79.55 % of the total eigenvalues), concerns augite (elements Ca, Mg, Fe^{2+}, Mn^{2+}) vs. jadeite + aegirine + namansilite (elements Na, Al, Fe^{3+}, Mn^{3+}). The second principal component F2 (18.98 % of the eigenvalues) mainly represents the jadeite (Al) and namansilite (Mn^{3+}) vs. aegirine (Fe^{3+}) substitution.

Omphacite always coexists with braunite and piemontite, forming cm-sized boudinaged bands hosted by massive quartz. Braunite crystals can contain ~~inclusions~~included and/or ~~exsolutions of~~exsolved barite and hollandite ($BaMn^{3+}_2Mn^{4+}_6O_{16}$), suggesting a possible presence of Ba in the initial braunite. Tumiati et al. (2010) reported up to 194 ppm (µg/g) of Ba in these crystals, in addition to other trace elements (e.g. 2015 ppm Cu, 1101 ppm Zn, 272 ppm Sr, 2543 ppm Co and 404 ppm Ni). Piemontite is typically Sr-bearing and shows oscillatory zoning, following the coupled piemontite-(Sr) vs. Fe-epidote substitution. Tumiati et al. (2010) have shown that the Sr-rich parts of piemontite contain up to 459 ppm As, 361 ppm Zn, 937 ppm P, 508 ppm Ni and 767 ppm Ba. In some samples, epidote ~~displays~~ group minerals display Mn-poor cores and Mn-rich

piemontite rims. The transition between the two compositions is ~~continuous~~gradual without an obvious solution gap, and follows the substitution $Mn^{3+}_{+2}Al^{3+}_{-1}Fe^{3+}_{-1}$.

Garnet is a solid solution of spessartine and grossular with minor contents in calderite ($Mn^{2+}_3Fe^{3+}_2Si_3O_{12}$) and pyrope. The garnet crystals are generally only slightly zoned in these levels.

~~4~~5.2 *High-P veins*

Veins crosscutting the basal levels are quartz-rich and contain piemontite, omphacite, braunite (Fig. 4b; ~~Tab.~~Table 1), pyroxmangite and hematite. Piemontite is euhedral and commonly displays oscillatory zoning with REE and Sr substituting for Mn following the exchange 2 Ca^{2+}_A + 1 Mn^{3+}_M = 2 Sr^{2+}_A + 1 REE^{3+}_M (first eigenvector of the PCA; 80.4% of the total eigenvalues). The maximum contents in REE and Sr observed are 0.24 atoms per formula unit (a.p.f.u~~.~~.) (Ce/La = 2.36) and 0.17 a.p.f.u., respectively~~.~~ (for 12.5 equivalent O). These oscillatory zones are sharp and superimposed to a weaker and more regular zoning involving Fe^{3+} *vs*. Mn^{3+}, suggesting an increase of the piemontite endmember from core to rim (second eigenvector of the PCA; 15.0% of the total eigenvalues).

Veins often contain pink Mn-bearing phengite, known as *alurgite*. Occasionally, As and Sb silicates and oxides occur, in particular ardennite (a rare hydrous silico-arseniate of aluminium and manganese; Fig. 6B) and the calcium antimonate romeite (Fig. 6c). ~~Sulphides have never been observed, although they are reported in the host metabasites of the Saint-Marcel valley, where Fe-Cu ores have been exploited in the past years (mines of Servette and Chuc; e.g. Martin et al., 2008; Tumiati et al., 2008).~~

A quartz-rich vein, between the basal braunite/piemontite-rich and the upper garnet-rich levels (Fig. 3), contains emerald-green omphacite (Jd_{70}), minor Cr-rich phengite and (Cr, REE)-rich ~~epidotes.~~epidote-group minerals. Accessory minerals are Cr-bearing hematite (up to 3.51 wt% Cr_2O_3) and braunite (up to 0.52 wt% Cr_2O_3). As-bearing apatite (up to 9.22 wt% As_2O_3), native Au and ~~(Ca, REE)~~ -vanadates (wakefieldite; M. Merlini pers. comm.; details provided elsewhere) have been found as accessory phases.

~~4~~5.3 *Upper levels*

Upper levels (Fig. 3; ~~Tab.~~Table 1) are dominated by garnet and quartz associated with hematite, pyroxmangite (Fig. 4c; see Raman spectrum of sample 1601 in Fig. 5) and/or an aegirine-rich Mn-bearing clinopyroxene known as *schefferite*. Garnet is zoned with grossular- and/or calderite-rich core and spessartine-rich rim (cf. also Cenki-Tok and Chopin, 2006). In the Fe^{3+}-rich core, Cr is present up to $Uv_{1.1}$ (0.022 a.p.f.u.~~;~~. per 12 equivalent O; 0.32 wt% Cr_2O_3~~) in the Fe^{3+} rich core.~~). The epidote-group mineral manganiandrosite-(Ce) occurs instead of piemontite as an accessory phase (Cenki-Tok et al. 2006). Sb-rich pyrophanite ($MnTiO_3$) ~~has~~was also ~~been~~ observed (Fig. 6d). In one sample, dominated by tephroite, hausmannite and rhodochrosite, we observed a peculiar quartz-free assemblage, where braunite and pyroxmangite show resorption microstructures (Fig. 4d; ~~Tab.~~Table 1).

~~5~~6. Thermodynamic modelling

~~. Discussion~~

At Praborna, the occurrence of omphacite + quartz and of pyroxmangite (e.g. Maresch and Mottana, 1979) confirms that these Mn-rich metasediments equilibrated at HP conditions in the eclogite facies. Jadeite-rich omphacite in equilibrium with quartz occurs also in the pervasive veins ~~crosscutting~~that crosscut the basal layers, suggesting that an interaction with vein-forming fluids occurred also at HP. These fluids are likely derived from the dehydration of the slab and flushed the mélange rocks ~~forming~~, like the serpentinite and ~~the~~ glaucophanite now cropping out at the bottom of the sequence. This is the best of all possible ~~scenarios~~environments to be considered, ~~in order to verify~~for verifying the mobility of the component oxygen in the slab. ~~If oxygen could be considered a "perfectly mobile" component, the redox state of the system should be described in terms of μO_2 (or fO_2).~~ The importance of fO_2 in controlling the phase relationships of Mn-rich systems was first recognised by Muan (1959) and Huebner (1967), who demonstrated that, analogously to the Fe–O

system, Mn-oxides can be used as oxygen buffers because Mn shows changes in the oxidation state from +2 to +4. Also, the presence of piemontite requires very high fO_2 to be stabilized over garnet, as experimentally demonstrated by Anastasiou and Langer (1977), and Keskinen and Liou (1979). However, such systems have been rarely adopted as redox sensors in HP rocks, because the available experimental data are currently restricted to the ~~MnO~~MnO–SiO_2–O_2 and Al_2O_3–~~MnO-~~MnO–SiO_2–O_2 systems at 0.4–2.5 GPa (Abs-Wurmbach et al., 1983; Abs-Wurmbach and Peters, 1999).

At Praborna, the basal levels are characterised by the assemblage braunite + quartz, the stability of which requires very high fO_2 ($\Delta FMQ = \log (fO_2^{sample} ~~- \log fO_2^{FMQ}~~ / fO_2^{fayalite+magnetite+quartz})$) = +11 at 0.8 GPa and 500 °C, estimated by Brown et al., 1978). These high fO_2 values have been interpreted as indicative of highly oxidized rocks, inheriting the ~~fO_2s~~fO_2 of the sedimentary protolith. In this ~~study~~section, we ~~re-discuss~~quantify the ~~concept of oxidation degree of these slab metasediments, emphasizing the difference between the choice of intensive (μO_2 or, fO_2) and extensive (nO_2) independent parameters~~ variables at Praborna, using a specific thermodynamical dataset customized for Mn-rich systems and presented in Appendix.

~~5~~6.1 ~~Thermodynamic~~ *Modelling of the MnO–SiO_2–O_2 system*

The MnO–SiO_2–O_2 is the simplest petrological system that describes the phase relations between Mn-silicates and oxides. Pure phases belonging to this system are: quartz, manganosite ($Mn^{2+}O$), tephroite ($Mn^{2+}{}_2SiO_4$), pyroxmangite ($Mn^{2+}SiO_3$), rhodonite ($Mn^{2+}SiO_3$), hausmannite ($Mn^{2+}Mn^{3+}{}_2O_4$), braunite ($Mn^{2+}Mn^{3+}{}_6SiO_{12}$), bixbyite ($Mn^{3+}{}_2O_3$) and pyrolusite ($Mn^{4+}O_2$). Solid solutions are not expected in this system. Using literature (Table A-1 in Appendix) and ~~unpublished~~new experimentally derived thermodynamic data for these phases (~~see~~Table A-2 and A-3 Appendix ~~A~~), we were able to construct two diagrams (Figs. ~~6A~~7a and ~~6B~~7b), calculated at P ~~=~~ = 2.1 GPa and T = 550 °C, i.e. at the metamorphic conditions recorded by the slab lithologies in the Saint-Marcel valley (Martin et al., 2008). Diagrams ~~6A~~7a and ~~6B~~7b consider, respectively, the

component ~~oxygen~~O_2 as "perfectly mobile" (i.e., ~~intensity~~ μO_2 and fO_2 are intensive independent state variables) and "inert" (~~extensity~~ nO_2 is ~~the~~an extensive independent state variable). We recall that in these diagrams and in the following calculations, nO_2 is set to zero value for rocks in which all Fe and Mn occur exclusively in their divalent oxidation state. Therefore, nO_2 could be regarded as extra moles of the component O_2 relative to a Fe^{3+}- and Mn^{3+}-free reference composition (see also Section 2).

Figure 7a displays ~~logfO_2/μ~~log (fO_2/1 bar) – μO_2 vs. X_{SiO2} (=SiO_2/(~~MnO~~$Mn^{2+}O$+SiO_2)). The bulk Mn^{3+}/Mn_{tot} ratio is also reported (shaded areas in Fig. 7a and black dotted isopleths in Fig. 7b).~~7b) is also reported.~~ For comparison, reference redox ~~equilibria~~buffers, such as ~~FMQ~~, hematite ~~–~~+ magnetite, pyrite –+ Fe-sulphate and piemontite –+ garnet~~,~~ are shown in Figure 7a~~.~~, where they are expressed as ΔFMQ, i.e. with reference to the fayalite + magnetite + quartz buffer (FMQ).

The braunite + quartz + pyroxmangite assemblage of the basal levels at Praborna is stable for almost the entire X_{SiO2} range (except for very low SiO_2 contents, where quartz disappears) at very high fO_2 (ΔFMQ~~=+~~ = +12.7), above the hematite–magnetite buffer and slightly above the piemontite–garnet ~~(PG) equilibrium~~buffer. This is consistent with the occurrence of piemontite and hematite in basal levels (Figs. 4a, b).

The upper levels of Praborna are characterised by the equilibrium between pyroxmangite, quartz, garnet~~,~~ and hematite (Figs. 3, 4c), which are stable at ΔFMQ~~<+~~ < +12.7 and X_{SiO2}~~>~~ > 0.5 according to Figure 7a. In one quartz-free sample, we observed the assemblage braunite + hausmannite + tephroite (blue fields in Figs. 7a, b; ~~cf.~~see also Fig. 4d) with relics of pyroxmangite. This latter assemblage can be attained only for X_{SiO2}~~<~~ < 0.33 and ~~logfO_2~~log (fO_2/1 bar) between ~~Δ~~FMQ+4.1 and ~~Δ~~FMQ+9.7. A further constraint is given by the occurrence of sulphates at Praborna (e.g. barite and celestine), and the absence of sulphides. Chalcophile elements, such as Sb and As, ~~form solely~~partitionate into silicates, phosphates and oxides (Fig. 6), suggesting that the fO_2 at Praborna is higher than the pyrite–$FeSO_4$ buffer (i.e. ΔFMQ~~>+~~ > +5.~~5~~7), even in the most retrograde assemblages. Values of ~~logfO_2~~log (fO_2/1 bar) in the range ~~of Δ~~from FMQ+5.~~5~~ 7 to FMQ+12~~,~~.7

widely exceed ~~the range of logfO_2~~those previously evaluated for subduction environments (see Introduction and Section ~~5.4~~7.2 below). ~~This highlights the complexities in relating the chemical potential to the redox state of slab rocks even in the case of fluid flushing.~~

Figure 7b is the ternary chemography of the system ~~MnO~~$Mn^{2+}O$–SiO_2–O_2. Compositions are portrayed in barycentric mole fractions. This diagram plots the relative positions of the phase assemblages shown in Figure 7a, therefore unravelling the relationships between μO_2 (or fO_2~~; here dependent variable), Mn^{3+}/Mn_{tot}~~) and the ~~amount~~conjugate variable nO_2 (see also Fig. 1). In terms of ~~the component oxygen.~~nO_2, the most reduced possible assemblages (i.e., ~~poor~~the poorest in component O_2) ~~possible associations~~ consist of tephroite + manganosite, pyroxmangite + tephroite, and quartz + pyroxmangite, depending on $X SiO_2$ (Fig. 7a). These associations fall on the join SiO_2–~~MnO of Figure 6B, which represents a reference state~~$Mn^{2+}O$, where ~~the barycentric molar quantity of the component O_2 (nO_2)~~ is null~~.~~ and Mn^{3+}/Mn_{tot} = 0. On the other hand, the most oxidized assemblage (i.e., ~~rich~~the richest in component O_2) ~~association~~ is braunite + bixbyite, for which nO_2 and Mn^{3+}/Mn_{tot} range from 0.16 to 0.20 and from 0.86 to 1.~~0~~00, respectively, depending on the ~~relative~~ phase ~~proportion~~proportions. The assemblage bixbyite + hausmannite and bixbyite + hausmannite + braunite can therefore ~~display~~have the same Mn^{3+}/Mn_{tot} ratio, provided that the abundance of hausmannite is sufficiently low. The Mn^{3+}/Mn_{tot} ratio and nO_2 values are directly proportional only on the ~~MnO~~$Mn^{2+}O$–O_2 ~~side~~subspace of the chemographic diagram ~~(MnO–O_2 subsystem).~~. As a consequence, the equilibrium tie-lines of Figure 7b, which delimit the phase fields with identical chemical potentials, crosscut the ~~isopleths of~~ nO_2 and ~~of~~ Mn^{3+}/Mn_{tot} isopleths at high angle. This translates into a decoupling between μO_2, nO_2 and Mn^{3+}/Mn_{tot}, when comparing Figures 7a and 7b. To better understand this concept, we reported a hypothetical metasomatic path represented by the black arrow of Figure 7b~~, which delineates the addition~~. Evolution of ~~a SiO_2-rich component in the system. The addition of this component moves~~ the bulk composition along this path from the ~~blue field, where the stable~~ starting point to the ending point induces a change of the assemblage ~~is~~ hausmannite + braunite + tephroite (blue field: Mn^{3+}/Mn_{tot}~~=~~ = 0.70; μO_2 = -267

kJ•mol^{-1}; nO_2~~=~~ = 0.13~~), towards the SiO_2 rich side of the diagram, where~~) to the assemblage braunite + pyroxmangite + quartz ~~is stable in the~~ (red field~~ (:~~ Mn^{3+}/Mn_{tot}~~=~~ = 0.30; μO_2 = -219 kJ•mol^{-1}; nO_2~~=~~ = 0.03). Counter-intuitively, it is therefore possible to *increase* μO_2 (and fO_2), while nO_2 and ~~also the~~ Mn^{3+}/Mn_{tot} ~~ratio~~ actually ~~*decreases*~~*decrease*. In this case, ~~"~~oxidation~~",~~ in terms of an increase of the intensive variable μO_2 (or fO_2~~),)~~ actually corresponds to a decrease in nO_2 and Mn^{3+}/Mn_{tot}, ~~therefore~~and thus to a ~~net~~ bulk reduction. The Mn^{3+}/Mn_{tot} ~~data are~~ratio is also depicted ~~graphically also~~ in Figure 7a~~, profiting of the Mn^{3+}/Mn_{tot} isopleths shown in the chemography of Figure 7b. In Figure 7a,~~ by greyscale ~~areas grade~~tones grading from black (Mn^{3+}/Mn_{tot}~~=~~ = 1) to white (Mn^{3+}/Mn_{tot}~~=~~ = 0), ~~and areas characterized by the same grey tone (i.e.~~showing that the same Mn^{3+}/Mn_{tot} ratio~~)~~ can be found at different μO_2 conditions. Figures 7a and 7b show that the decrease in fO_2 from the basal (red) to the upper (blue) levels of Praborna does not necessarily correspond to an increase in bulk Mn^{3+}/Mn_{tot} as one would expect. The Mn^{3+}/Mn_{tot} ratio is also a function of phase abundances, which cannot be evaluated using ~~chemical potential~~μO_2 (or fO_2) diagrams. Therefore, the high fO_2 values observed at Praborna cannot be considered a straightforward sign of high degrees of oxidation.

~~5~~6.2 *Comparison with the ~~system~~ FeO–SiO$_2$–O$_2$* system

The peculiarity of the MnO–SiO_2–O_2 system is mostly related to the occurrence of braunite, a compound that does not have an analogue in the well known FeO–SiO_2–O_2 system. In order to explore differences and similarities between Mn- and Fe-bearing assemblages, we have constructed a four-component, FeO–MnO–SiO_2–O_2, compositional space shown in Figure 8. Analogously to Figure 7b, also in this diagram the quantity of the component oxygen (nO_2) is treated as an independent state variable, and fO_2 (expressed as ΔFMQ in the figure) is dependent. Every Mn-bearing phase has a corresponding Fe-bearing phase, except braunite. While hematite and magnetite can coexist with quartz, hausmannite and bixbyite cannot, because of the stability of braunite. In Figure 8, the high-fO_2 phase assemblage braunite + pyroxmangite + quartz + hematite of the basal

levels (red volume) can be accessed from the low-fO_2 braunite + hausmannite + tephroite + hematite assemblage of the upper levels (blue volume) just by adding silica (e.g. via a metasomatic agent), even decreasing nO_2, similarly to what displayed in Figure 7b. The grey plane in Figure 8 represents the surface where nO_2 is constant and is drawn to highlight the decoupling between oxygen intensity (fO_2) and extensity~~.~~ (nO_2). Moving along this plane it is possible to cross ultra ~~"oxidized"~~ high fO_2 (e.g. red volume, ΔFMQ = +12.7) and ultra ~~"reduced"~~ low fO_2 (e.g. light green, ΔFMQ = -~~19~~18.1) assemblages at constant nO_2, which means without changing the bulk "redox budget" (Evans, 2006) of the rock.

Therefore, although the braunite + pyroxmangite + quartz + hematite assemblage of the basal levels of Praborna shows an ultra-oxidized redox state in terms of intensive redox parameters (ΔFMQ = +12.7), it could have the same quantity of ~~oxygen~~O_2 component as magnetite- and even ultra-reduced wüstite-bearing assemblages.

7. Discussion

~~5.3~~In this section, we re-discuss the concept of oxidation degree of slab rocks, emphasizing the choice between intensive (μO_2 or fO_2) and extensive (nO_2) parameters to describe properly redox conditions. In general, we will demonstrate that the oxidation degree of rocks is definitely a relative concept, dependent on the variable used to describe it.

7.1 Oxygen chemical potential versus oxygen molar quantity: is oxygen a "perfectly mobile" or an "inert" component?

The rocks of Praborna clearly suggest that even in the presence of pervasive flux of fluids, the homogenization of ~~the chemical potential of oxygen~~μO_2 was not attained. In fact, if oxygen ~~was~~had been perfectly mobile, ~~the~~ μO_2 (and fO_2 ~~should be~~) would have been constant but, on the contrary, while the country-rock pyrite-magnetite-bearing glaucophanite records ΔFMQ < +2 ~~according to Figure~~.6 (Fig. 7a ~~(they contain pyrite and magnetite.),~~), the adjacent basal Mn-rich quartzites ~~jump~~

~~to an apparently unrealistic ultra-high "oxidation state" of~~attain ΔFMQ ≥+12.~~5,~~ 7. Moreover, we recognised a mineralogical variability between the basal and upper levels, reflecting ΔFMQ down to +5.~~5, without necessarily changing the actual amount of oxygen in the system.~~7. These observations suggest that, in these rocks, oxygen can hardly be considered a "perfectly mobile" component ~~in these rocks~~, as defined by Korzhinskii (1959~~), and~~); thus, the description of the redox ~~state~~conditions of such petrological systems should not be described by ~~the oxygen chemical potential~~μO_2 (or fO_2) as an *independent* state variable. The introduction of its conjugate ~~oxygen molar quantity~~variable nO_2 is instead required, ~~the oxygen chemical potential~~μO_2 becoming ~~a~~ *dependent* ~~variable~~of nO_2. Figures 7a, 7b and 8 ~~warns~~warn against the undiscriminating use of μO_2 (or fO_2) as univocal indicator of the redox state of a rock system. Especially in multi-component and metasomatic systems, the ~~quantity of the oxygen component and the oxygen fugacity~~nO_2 and μO_2 (or fO_2) could be well decoupled.

~~5.4~~In order to enlighten this concept, we can make a comparison with a more intuitive analogue: *P* and *V* is a couple of intensive and extensive variables similar to μO_2 and nO_2, respectively. Pressure *P* (like μO_2 or fO_2) is generally considered as an independent variable imposed upon the system by its environment, to which the system responds by adapting the conjugate variable *V* (similarly to nO_2), in order to reach the state of equilibrium. However, in a few particular cases, like fluid inclusions, *V* is imposed by the surroundings, which may induce local *P* heterogeneities, like overpressures at the inclusion scale; in that case, *V* should be considered as the independent variable and *P* the conjugate dependent variable. This occurs when volumes cannot adjust as easily as pressures. In our case, nO_2, in part inherited from the sedimentary protolith, cannot adjust itself easily – in other terms, O_2 not a "perfectly mobile" component. This generates local μO_2 heterogeneities, and nO_2 should be considered as the independent variable that determines the redox state.

7.2 Consequences for fO_2 estimates in ~~high-pressure rocks~~subduction zones

In a multi-component system, the chemical ~~potentials~~potential of ~~all the components~~each component, including oxygen, ~~are constant~~is ideally homogeneous, i.e. equal in all the phases at equilibrium. As seen in Figures 7a, 7b and 8, different mineralogical associations will be characterised by different chemical potentials, including μO_2, and thus fO_2, even when they display the same ~~oxygen molar quantity~~nO_2 or the same Fe^{3+}/Fe^{2+} ~~–~~ and Mn^{3+}/Mn^{2+} ~~ratios.~~ contents. In fact, ~~it should be noted that~~ two variables in a conjugate pair, such as μO_2 (or fO_2) and nO_2, ~~follow the same trend~~are coupled, i.e. both increase or both decrease, only if all the other molar quantities are kept at constant values ~~(Fig. 7b).~~ The addition of SiO_2 or FeO components, for example via a metasomatic process, can produce assemblages characterised by different ~~fO_2s~~fO_2 without necessarily ~~change~~changing the redox ~~state~~budget. This consideration warns against the indiscriminate comparison of fO_2 data ~~of~~for rocks ~~belonging to~~characterized by different ~~petrological systems~~bulk composition or simply ~~displaying~~by different mineral assemblages, because it may lead to apparent redox heterogeneities, wherever μO_2 cannot be considered as an independent variable (i.e., where O_2 is not "perfectly mobile" and therefore rocks could be not in equilibrium to each other). Therefore, heterogeneities in fO_2 do not necessarily require the mobility of redox species.

~~For example, oxygen fugacities~~In subduction zones, fO_2 corresponding to a range of ΔFMQ ~~ranging~~ from 0 to +2 ~~have~~has been estimated on carbonate-bearing mantle-wedge peridotite from the Sulu UHP terrane (China) by Malaspina et al. (2009~~). However,~~), whereas eclogites from the same area are characterised by ΔFMQ from +2.5 (Cao et al., 2011; massive lawsonite eclogite~~),~~) to ~~~~ca. +4 (Cao et al., 2011; foliated clinozoisite + glaucophane eclogite) and ~~~~ca. +4.5 (amphibole eclogite; Mattinson et al., 2004). Difference in ~~oxygen fugacity~~fO_2 between peridotite and eclogite are reported also in the Western Gneiss Region of Norway, where Malaspina et al. (2010) estimated ΔFMQ ~~=~~of -2~~——~~0 for garnet websterites, while Donohue and Essene (2000) and Boundy et al.

(2002) estimated ΔFMQ ~~≈~~in the range +2.5– +3.0 for eclogite-facies marbles.

Although it is unclear, at present, whether heterogeneities in ~~fO_2~~ fO_2 in the slab (see also Foley, 2011) should be ascribable ~~entirely~~ to differences in chemical ~~and~~ mineralogical composition, to lack of μO_2 equilibration, or ~~they correspond to real~~to differences in redox ~~states~~budget, the case of Praborna appears paradigmatic and suggests that metasomatic processes could lead to ultra-high fO_2 conditions despite a modest, if any, bulk oxidation~~.~~ in terms of nO_2.

In order to compare the Praborna metasediments with other slab rocks and the corresponding mantle wedge, we need to evaluate ~~their~~the oxidation states of representative rocks in terms of nO_2. Unlike for μO_2 (or fO_2), the quantification of nO_2 depends on the mineral abundances. Typically, nO_2 may vary in an oxygen buffer assemblages (i.e., oxygen can be added or subtracted) without a change of μO_2 (or fO_2). For example, the addition of oxygen to a hematite + magnetite assemblage leads thus to an increase in the abundance of hematite, an increase of Fe^{3+}/Fe_{tot} and an increase of nO_2, without changing fO_2, as long as both minerals are present. The system is therefore buffered at constant fO_2 (and μO_2).

Estimates of nO_2 provided below take into account the mineral mode in different subduction-related rock types. They should be regarded as an attempt to assess the magnitude of the redox budget of the subducting slab pile and its overlying mantle wedge. Concerning HP rocks, only few analytical data ~~are reported in literature~~ allowing a mass balance of the component oxygen~~.~~ are reported in literature. We profit of the case of HP rocks from Sulu (China), a unique ~~locality~~region where the Fe^{3+} contents of garnet and clinopyroxene have been measured both in wedge peridotite (Malaspina et al., 2009; 2012) and in slab eclogite (Proyer et al., 2004).

For peridotite mineral assemblages, the contribution of garnet to nO_2 (cf. Fig. 7b and 8) is the amount of excess oxygen with reference to a Fe^{3+}-free system, provided by the skiagite ($Fe^{3+}_2Fe^{2+}_3Si_3O_{12}$) component. In the following idealized mass balance, oxygen (~~nO_2~~ O_2) is not regarded as a phase or species but merely as a component and therefore can be made explicit:

$1.00 \times (FeO)_{0.59}\bullet(SiO_2)_{0.35}\bullet(O_2)_{0.06}$ [skiagite] =

$0.71 \times (FeO)_{0.67}\bullet(SiO_2)_{0.33}$ [fayalite] + $0.24 \times (FeO)_{0.50}\bullet(SiO_2)_{0.50}$ [ferrosilite] + 0.06 O_2 (Eq. 1~~)~~).

This ~~equality~~equation, after Luth et al. (1990~~)~~), has been rewritten here expressing compounds ~~in barycentric mole~~as molar fractions ~~(cf.~~of the independent components SiO_2, FeO, MnO and O_2 (see Section 2; Spear et al., 1982~~) of Fe^{3+} - and Mn^{3+} -free oxides and O_2;~~), allowing a direct comparison ~~between~~of the excess O_2 ~~in~~with different barycentric ~~systems (cf.~~ representations (Figs. 7b and 8). In the discussion below, we will use the same convention to express chemical compositions of minerals and rocks.

According to Eq. 1, one mole of pure skiagite would lead to 0.06 ~~moles~~mole of excess O_2. Because Malaspina et al. (2009) reported ~~garnets~~garnet containing up to 6 mol% of skiagite ~~molecule, the excess oxygen contribution of~~, one mole of garnet from Sulu peridotite ~~is therefore~~contributes for the 6 percent of 0.06 ~~moles~~mole of O_2, i.e. for 3.6 millimoles of excess O_2.

In mafic eclogites, a model redox mass balance for skiagite can be written as:

$1.00 \times (FeO)_{0.59}\bullet(SiO_2)_{0.35}\bullet(O_2)_{0.06}$ [skiagite] = $+1.37 \times (FeO)_{0.43}\bullet(Al_2O_3)_{0.14}\bullet(SiO_2)_{0.43}$ [almandine] - $0.39 \times (Al_2O_3)_{0.5}\bullet(SiO_2)_{0.5}$ [kyanite] - 0.04 SiO_2 [quartz/coesite] + 0.06 O_2 (Eq. 2~~)~~).

The coefficients for O_2 are the same in ~~Equation~~Equations 1 and ~~Equation~~ 2, suggesting that in both mafic and ultramafic rocks the excess oxygen is 0.06 ~~moles~~mole of O_2 per 1 mole of skiagite component.

Profiting of the garnet composition reported by Proyer et al. (2004), containing up to 5 mol% of skiagite, the contribution of one mole of garnet from Sulu ~~eclogites~~eclogite is therefore the 5 percent of 0.06 moles of O_2 (v. Eq. 2), i.e~~.,~~. 3.0 millimoles of excess O_2 per 1 mole of garnet.

As peridotitic and eclogitic garnets display comparable skiagite content (~5% in eclogite and ~6% in peridotite), the nO_2s for one mole of garnet are also comparable (3.6 ~~mmol~~and 3.0 millimoles in

peridotite and ~~3.0 mmol in~~ eclogite, respectively).

The contribution of clinopyroxene to the bulk oxidation can be evaluated on the basis of the aegirine ($NaFe^{3+}Si_2O_6$) component, which can be expressed in the following way, for peridotite (Eq. 3) and eclogite (Eq. 4) assemblages respectively ~~(Eq. 4).~~

$$1.00 \times (Na_2O)_{0.13}\bullet(FeO)_{0.27}\bullet(SiO_2)_{0.53}\bullet(O_2)_{0.07}\ [\text{aegirine}] = 0.80 \times (Na_2O)_{0.17}\bullet(Al_2O_3)_{0.17}\bullet(SiO_2)_{0.67}\ [\text{jadeite}] - 0.80 \times (FeO)_{0.50}\bullet(SiO_2)_{0.50}\ [\text{ferrosilite}] + 0.13 \times (FeO)_{1.00}\bullet(SiO_2)_{1.00}\bullet(Al_2O_3)_{-1.00}\ [\text{Fe Tschermak}] + 0.80 \times (FeO)_{0.67}\bullet(SiO_2)_{0.33}\ [\text{fayalite}] + 0.07\ O_2 \qquad \text{(Eq. 3~~)~~).}$$

$$1.00 \times (Na_2O)_{0.13}\bullet(FeO)_{0.27}\bullet(SiO_2)_{0.53}\bullet(O_2)_{0.07}\ [\text{aegirine}] = 0.80 \times (Na_2O)_{0.17}\bullet(Al_2O_3)_{0.17}\bullet(SiO_2)_{0.67}\ [\text{jadeite}] + 0.53 \times (FeO)_{0.50}\bullet(SiO_2)_{0.50}\ [\text{ferrosilite}] - 0.13\ SiO_2\ [\text{quartz/coesite}] - 0.27 \times (Al_2O_3)_{0.5}\bullet(SiO_2)_{0.5}\ [\text{kyanite}] + 0.07\ O_2 \qquad \text{(Eq. 4~~)~~).}$$

Similarly to equalities involving garnet in Equations 1 and 2, the coefficients of O_2 in Equations 3 and 4 are identical and independent on the system chosen, accounting for 0.07 ~~moles~~mole of excess O_2 per 1 mole of pure aegirine. Clinopyroxene from Sulu peridotite contains 5 mol% of aegirine ~~molecule~~endmember (Malaspina et al., 2012), while clinopyroxene from eclogite contains 6 mol% of aegirine (Proyer et al., 2004~~),~~). Therefore, one mole of clinopyroxene contributes to 3.5 and to 4.2 millimoles of excess O_2 in peridotites and mafic eclogites, respectively.

On the basis of the above considerations ~~above~~, a bimineralic eclogite composed of 50 mol% of garnet and 50 mol% of clinopyroxene would be characterized by 3.6 millimoles of excess O_2 per mole of a rock, whose composition is expressed ~~in barycentric mole~~as molar fractions of oxides. On the other hand, ~~a peridotite,~~ assuming 5 mol% of garnet and 5 mol% of clinopyroxene, a peridotite would be characterized by 0.36 millimoles of excess O_2 per mole of rock, ~~that~~which means one order of magnitude less. ~~Unlike calculation of intensive variables (e.g. μO_2), the quantification of nO_2 obviously depends on the mineral abundances. Estimates provided here should be therefore~~

~~regarded as an attempt to assess the magnitude of the oxidation degree of the subducting slab pile, and of the overlying mantle wedge.~~

Metasedimentary rocks at Praborna display ~~nO_2s~~nO_2 that can be estimated on the basis of the proportions between pyroxmangite, braunite and quartz (~~cf.~~see Fig. 7b). Considering the bulk chemical and mineralogical compositions reported by Tumiati et al. (2010), we estimated ~~by mass-balance~~ average contents of ~~~~ca. 95 mol% of quartz and ~~~5 mol% of pyroxmangite + braunite. Although the available data are not sufficient to determine the pyroxmangite/braunite ratio, we can estimate that the braunite abundance equals that of pyroxmangite, being the first mineral more abundant in the basal levels and the second ~~more abundant~~ in the upper levels. Braunite and pyroxmangite can be written ~~in barycentric mole fractions of Mn^{3+} free oxides~~ respectively as $(MnO)_{0.74}$•$(SiO_2)_{0.11}$•$(O_2)_{0.16}$ and $(MnO)_{0.50}$•$(SiO_2)_{0.50}$ (~~cf.~~see Fig. 7b). Therefore, only braunite can contribute to the excess O_2 of the Mn-rich metasediments of Praborna, at the rate of 2.5% of 0.16 moles of excess O_2, i.e. 4.0 millimoles of excess O_2 per 1 mole of rock. This value is nearly identical to the excess O_2 of the Sulu eclogite, suggesting that the Mn-rich metasediments of a subduction mélange can display ~~a moderate degree of oxidation,~~towards the mantle an oxidizing power comparable to ~~the~~that of slab rocks, ~~even in~~despite the presence of ultra-high fO_2 mineral assemblages.

As a consequence, a likely scenario for the slab-mantle interface in natural geodynamic environments is illustrated in Figure 9. Mass transport and metasomatism are supported by chemical gradients, notably by gradient in nO_2 across rocks of the subduction channel towards the mantle hanging-wall. Dehydration processes trigger fluid flow, which is localized in shear zones, and open fractures and pervasive microfractures~~.~~. While ~~the fO_2s are~~ΔFMQ is likely very inhomogeneous, reflecting the different bulk chemical–mineralogical compositions and the ~~poor~~limited mobility of oxygen, the oxidation degree of the subduction channel, expressed in terms of nO_2, is expected to be much smoother. In the conceptual model of Figure 9, a sort of metasomatic front develops from the slab to the overlying mantle wedge~~.~~ passing through a

transitional layer of mélange rocks. Although fluids cannot transport oxygen as a major volatile species, they are expected to promote mass transfers and to affect the attainment of equilibrium and kinetics of reactions (Lasaga and Rye, 1993~~).~~; Marschall and Schumacher, 2012). Therefore, oxygen is expected to be transported, especially along fractures and veins (see inset of Fig. 9), possibly through mechanisms of dissolution-reprecipitation of O-enriched oxides and silicates. The front ~~might be~~is possibly sustained also by the strong inverse thermal gradient across the slab surface, which is ~~numerically~~ evaluated to be in the order of -20 °C/km (Arcay et al., 2007). Whether a thermophoretic effect at the slab–mantle interface is able to contribute to the ~~oxygen (~~O_2 component~~)~~ redistribution ~~at the slab–mantle interface~~ or mass-transport ~~should be entirely ascribed to gravity~~ is driven mainly by chemical potential gradients and to advective processes (e.g., Gerya and Yuen, 2003; Marschall and Schumacher, 2012) is an open challenge for understanding rock diversity at subduction zones.

~~6~~8. Conclusions

Praborna ~~high-pressure,~~HP veined Mn-rich rocks record environmental conditions typical for a subducting slab setting. Although veining and growth of "pegmatoid" HP minerals might suggest an open system, characterized by large fluid-rock ratios~~ and thus "externally controlled" redox conditions~~, the extremely high ~~oxygen fugacities~~fO_2 deduced from Mn–Fe-rich mineral assemblages clearly ~~indicate~~indicates that oxygen can ~~be~~ hardly be considered as a perfectly mobile component~~, even in the most favourable conditions~~. As a consequence, μO_2, and therefore fO_2, should not be regarded as long-range properties, indicative of the redox state of the entire rock column of a subduction zone, from the dehydrating oceanic crust to the overlying mantle wedge. On a more general basis, the comparison of ~~fO_2~~sfO_2 retrieved from different bulk compositions and ~~different~~ phase assemblages may ~~lead to apparent~~suggest redox heterogeneities~~. On the contrary,~~ in subduction zones, even if the distribution of oxygen is expected to be much more continuous ~~moving~~, ranging from a maximum in the ~~subducted~~ mafic eclogites, ~~formed~~derived from the altered

oceanic basalts and gabbros, and in the sediments of the slab, down ~~(upward)~~ to a minimum in the overlying peridotites of the mantle hanging-wall.

~~This observation may partly reconcile differences in assessing the redox state of the Earth interior, when approached from different oxybarometers.~~

Acknowledgements

The authors are indebted to the reviewers H. Marschall and A. Korsakov for their useful suggestions. M. Fialin and A. Risplendente supported the work at EMP. ~~The authors are indebted to~~ F. Zorzi and S. Carbonin, and N. Masciocchi and G. Tagliabue are acknowledged for the acquisition and the refinement of XRD data of braunite and pyrolusite, respectively. P. Mietto, C. Micaglio and E. A. Perseil are thanked for providing some interesting samples. D. Smith is acknowledged for the access to Raman facility. This work was supported by the Italian Ministry of Education, University and Research (MIUR) [PRIN-2012R33ECR].

Appendix A. Thermodynamic calculations and supplementary data

Phase diagrams of Figures 6 and 7 have been drawn on the basis of thermodynamic calculation performed with the Perple_X computer package (http://www.perplex.ethz.ch; Connolly, 1990) using a specifically compiled thermodynamic dataset of ~~manganese~~Mn-rich minerals and oxygen buffers (see Table ~~SM-4 in Supplementary data~~A-1). Thermodynamic parameters are available in the literature apart from the thermal expansion coefficients of braunite and pyrolusite, unknown as far as we are aware, ~~so that~~and which we derived ~~them~~ experimentally ~~on the basis of~~from their cell-volume changes during heating (cf. Tables ~~SM~~A-2 and ~~SM~~A-3 ~~in Supplementary data~~). The dataset used has proven to be robust in reproducing the results of the HP experiments of Abs-Wurmbach et al. (1983).

Thermal expansion of braunite

Braunite at Praborna is invariably polycrystalline. Consequently, powder X-ray diffraction methods rather than single crystal methods were used to measure the thermal expansion of this mineral. Average composition ~~(standard deviation in parenthesis)~~ of 11 analyses can be expressed on the basis of 8 cations and 12 O as~~:~~ (standard deviation in parenthesis):

$Mn^{3+}_{5.92(8)}\ Mn^{2+}_{0.82(6)}\ Mg_{0.13(2)}\ Fe^{3+}_{0.06(3)}\ Ca_{0.05(2)}\ Al_{0.03(1)}\ Si_{0.99(5)}\ O_{12}$.

Powder diffraction patterns were recorded on a Philips X'Pert PRO automatic powder diffractometer, using a normal focus Cu X-ray tube operating at 40 kV and 40 mA**.** The vertical goniometer in Bragg-Brentano geometry (~~θ-θ~~ with 240 mm radius) was equipped with a first divergence slit, a Soller ~~slits in incident~~slit and ~~diffracted beam paths,~~ a 0.2 mm receiving slit~~, and~~ upstream of a curved graphite diffracted-beam monochromator PW3123/10. For high temperature data collection, the diffractometer was equipped with a heating camera Anton Paar HTK16.

The powder was spread as a thin film directly on the platinum thermocouple (heating strip) and the beam impingement area was restricted to a narrow central section of the strip, so that thermal gradients through and across the sample were minimized. The expansion of Al_2O_3 NIST standard reference material 676 was used for temperature calibration. We estimate the uncertainty of temperature measurement at the sample to be 10 °C.

A first data collection performed in continuous mode in the 16~~-~~–120° 2θ range revealed the good crystallinity and the purity of the phase. Successively~~,~~ data ~~collections~~ were ~~performed step by step~~collected with ~~an~~a step increment of 0.02° and a step counting time of 5 seconds in the 90~~-~~–120° 2θ range.

The position of each Bragg peak was measured by means of "X'pert high score" program and indexed by comparison with the calculated pattern obtained by GSAS program (Larson and Von Dreele, 1994). Angular values and respective ~~indices~~crystallographic planes were used to refine lattice parameters *a* and *c* by means of the XLAT program (Rupp, 1988). Diffractometer alignment was repeatedly checked by carrying out data collection of NBS640B silicon standard and obtaining *a* values of 5.4308(1) and 5.4310(1) Å.

In Table ~~SM~~A-2~~ (Supplementary data),~~ we reported the molar volume of braunite at *T* ranging from 25 to 600 °C. These data have been fitted with the expression reported in Table ~~SM-4 (Supplementary data),~~A-1, in order to obtain the volumetric expansion parameter *b1*.

Thermal expansion of pyrolusite

Although pyrolusite has proven to be unstable at the investigated conditions, this mineral was included in calculations because it belongs to the investigated petrological system. Thermal expansion data were collected in Bragg-Brentano mode on a Bruker AXS D8 Advance, operating in θ:θ geometry equipped with Nickel filtered Cu-Kα radiation and a position-sensitive Lynxeye detector. Generator settings ~~are~~were 40 kV and 40 mA. Reagent-grade MnO_2 was deposited in the aluminium sample holder of a custom-made heating chamber, operating in air, supplied by *Officine Elettrotecniche di Tenno*, Ponte Arche, Italy. A series of scans, lasting ca. 30 min each, were collected in isothermal conditions, in the ~~25-600°~~ *T* range 100–600 °C at 50 °C steps.

Cell parameters were refined by the whole pattern structureless refinement technique (Le Bail et al., 1988) with the aid of the TOPAS-R program (V. 3.0, Bruker AXS, Karlsruhe, Germany). Estimated standard deviations were computed under the assumption that, in the absence of systematic effects, errors followed a normal distribution. Similarly to braunite, cell volume data (Table ~~SM~~A-3~~ in Supplementary data~~) have been fitted with the expression reported in Table ~~SM-4 (Supplementary data),~~A-1, in order to obtain the volumetric expansion parameter *b1*.

References

Abs-Wurmbach, I., Peters, T., Langer, K., Schreyer, W., 1983. Phase relations in the system Mn–Si–O: an experimental petrological study. Neues Jahrbuch für Mineralogie Abhandlungen 14, 258-279.

Abs-Wurmbach, I., Peters, T., 1999. The Mn-Al-Si-O system: an experimental study of phase relations applied to parageneses in manganese-rich ores and rocks. European Journal of

722 Mineralogy 11, 45-68.
723 Anastasiou, P., Langer, K., 1977. Synthesis and physical properties of piemontite, $Ca_2Al_{3-p}Mn^{3+}_p(Si_2O_7/SiO_4/O/OH)$. Contributions to Mineralogy and Petrology. 60, 225-245.
725 Arcay, D., Tric, E., Doin, M.P., 2007. Slab surface temperature in subduction zones: Influence of
726 the interpolate decoupling depth and upper plate thinning processes. Earth and Planetary
727 Science Letters 255, 324-338.
728 Arculus, R.J., 1985. Oxidation status of the mantle–Past and present. Annual Review of Earth and
729 Planetary Sciences13, 75–95.
730 Bebout, G.E., 2007. Metamorphic chemical geodynamics of subduction zones. Earth and Planetary
731 Science Letters 260, 373–393.
732 Bebout, G.E., Agard, P., Kobayashi, K., Moriguti, T., Nakamura, E., 2013. Devolatilization history
733 and trace element mobility in deeply subducted sedimentary rocks: Evidence from Western
734 Alps HP/UHP suites. Chemical Geology 342, 1-20.
735 Bondi, M., Mottana, A., Kurat, G., Rossi, G., 1978. Cristallochimica del violano e della schefferite
736 di St. Marcel (Valle d'Aosta). Rendiconti della Società Italiana di Mineralogia e Petrologia.
737 34, 15-25.
738 Boundy, T.M., Donohue, C.L., Essene, E.J., Mezger, K., Austrheim, H., 2002. Discovery of
739 eclogite facies carbonate rocks from the Lindås Nappe, Caledonides, Western Norway.
740 Journal of Metamorphic Geology 20, 649-667.
741 Brown, P., Essene, E.J., Peacor, D., 1978. The mineralogy and petrology of manganese-rich rocks
742 from St. Marcel, Piedmont, Italy. Contributions to Mineralogy and Petrology. 67, 227-232.
743 Canil, D., 2002. Vanadium in peridotites, mantle redox and tectonic environments: Archean to
744 present. Earth and Planetary Science Letters 195, 75–90.
745 Cao, Y., Song, S.G., Niu, Y.L., Jung, H., Jin, Z.M., 2011. Variation of mineral composition, fabric
746 and oxygen fugacity from massive to foliated eclogites during exhumation of subducted
747 ocean crust in the North Qilian suture zone, NW China. Journal of Metamorphic Geology

29, 699-720.

Castello, P., 1982. Il giacimento di Praborna (S. Marcel-AO). Rivista Mineralogica Italiana. 3, 87-92.

Cenki-Tok, B., Ragu, A., Armbruster, T., Chopin, C., Medenbach, O., 2006. New Mn- and rare-earth-rich epidote-group minerals in metacherts: manganiandrosite-(Ce) and vanadoandrosite-(Ce). European Journal of Mineralogy 18, 569–582.

Cenki-Tok, B., Chopin, C., 2006. Coexisting calderite and spessartine garnets in eclogite-facies metacherts of the Western Alps. Mineralogy and Petrology 88, 47-68.

Chinner, G. A., 1960. Pelitic gneisses with varying ferrous/ferric ratios from Glen Clova, Angus, Scotland. Journal of Petrology 1, 178-217.

Ciriotti, M. E., Fascio, L., Pasero, M., 2009. Italian type minerals: Edizioni Plus, Pisa.

Connolly, J.A.D., 1990. Multi-variable phase diagrams: an algorithm based on generalized thermodynamics. American Journal of Science 290, 666-718.

Dal Piaz, G.V., 2001. History of tectonic interpretations of the Alps. J. Geodyn. 32, 99-114.

Dapiaggi, M., Tiano, W., Artioli, G., Sanson, A., Fornasini, P., 2003. The thermal behaviour of cuprite: An XRD-EXAFS combined approach. Nuclear Instruments and Methods in Physics Research B 200, 231-236.

Dasgupta, S., 1997. P-T-X relationships during metamorphism of manganese-rich sediments: Current status and future studies. Geological Society Special Publication 199, 327-337.

Donohue, C.L., Essene, E.J., 2000. An oxygen barometer with the assemblage garnet-epidote. Earth and Planetary Science Letters 181, 459-472.

Evans, K.A., 2006. Redox decoupling and redox budgets: Conceptual tools for the study of earth systems. Geology. 34, 489-492.

Evans, K.A., 2012. The redox budget of subduction zones. Earth-Science Reviews 113, 11-32.

Foley, S., 2011. A reappraisal of redox melting in the Earth's mantle as a function of tectonic setting and time. Journal of Petrology 52, 1363-1391.

774 Frezzotti, M.L., Selverstone, J., Sharp, Z.D., Compagnoni, R., 2011. Carbonate dissolution during
775 subduction revealed by diamond-bearing rocks from the Alps. Nature Geosciences 4, 703-
776 706.
777 Geller, S., Espinosa, G.P., 1970. Magnetic and crystallographic transitions in Sc^{3+}, Cr^{3+}, and Ga^{3+}
778 substituted Mn_2O_3. Physical Review B 1, 3763-3769.
779 Gerya, T., Yuen, D.A., 2003. Rayleigh-Taylor instabilities from hydration and melting propel 'cold
780 plumes' at subduction zones. Earth and Planetary Science Letters 212, 47-62.
781 Gill, J., 1981. Orogenic Andesites and Plate Tectonics: New York, Springer-Verlag.
782 Greeff, C.W., Boettger, J.C., Graf, M.J., Johnson, J.D., 2006. Theoretical investigation of the Cu
783 EOS standard. Journal of Physics and Chemistry of Solids 67, 2033-2040.
784 Groppo, C., Castelli, D., 2010. Prograde P-T Evolution of a Lawsonite Eclogite from the Monviso
785 Meta-ophiolite (Western Alps): Dehydration and Redox Reactions during Subduction of
786 Oceanic FeTi-oxide Gabbro. Journal of Petrology 51, 2489-2514.
787 Hazen, R.M., 1985. Comparative crystal chemistry and the polyhedral approach. Reviews in
788 Mineralogy 14, 317-345.
789 Heines, J., Leger, J.M., Hoyau, S., 1995. 2^{nd}-order rutile-type to $CaCl_2$-type phase-transition in
790 beta-MnO_2 at high-pressure. Journal of Physics and Chemistry of Solids 56, 965-973.
791 Hillert, M., 1985. Principles of phase diagrams. International Metals Review 30, 45-67.
792 Hirschmann, M.M., 2009. Ironing out the oxidation state of Earth's mantle. Science 325, 545–546.
793 Holland, T.J.B., 1989. Dependence of entropy on volume for silicate and oxide minerals: A review
794 and a predictive model. American Mineralogist 74, 5-13.
795 Holland, T.J.B., Powell, R., 1998. An internally consistent thermodynamic data set for phases of
796 petrological interest. Journal of Metamorphic Geology 16, 309-343.
797 Huebner, J., 1967. Stability relations of minerals in the system Mn–Si–C–O [Ph.D. thesis]:
798 Baltimore, John Hopkins University.

Irani, K.S., Sinha, A.P.B., Biswas, A.B., 1958. Entropy of hausmannite to spinel transformation. Proceedings of the Physical Society 71, 270-271.

Kazanc, S., Çiftci, Y.Ö., Çolakoğlu, K., Ozgen, S., 2006. Temperature and pressure dependence of the some elastic and lattice dynamical properties of copper: a molecular dynamics study. Physica B 381, 96-102.

Kelley, K.A., Cottrell, E., 2009. Water and the oxidation state of subduction zone magmas. Science 325, 605–607.

Keskinen M., Liou, J.G., 1979. Synthesis and stability relations of Mn-Al piemontite, $Ca_2MnAl_2Si_3O_{12}(OH)$. American Mineralogist 64, 317-328.

Konrad-Schmolke, M., O'Brien, P.J., Zack, T.,2011. Fluid migration above a subducted slab – Constraints on amount, pathways and major element mobility from partially overprinted eclogite-facies rocks (Sesia Zone, Western Alps). Journal of Petrology 52, 457-486.

Korzhinskii, D.S., 1959. Physicochemical basis of the analysis of the paragenesis of minerals: New York, Consultants bureau, inc.

Krist, P., Bohem, J., Gerber, R., Kelland, D.R., 1992. OGMS of cryogenically enhanced magnetics. IEEE Transactions on Magnetics 28, 2412-2414.

Langer, K., Tillmanns, E., Kersten, M., Almen, H., Arni, R.K., 2002. The crystal chemistry of Mn^{3+} in the clino- and orthozoisite structure types, $Ca_2M^{3+}{}_3[OH/O/SiO_4/Si_2O_7]$: A structural and spectroscopic study of some natural piemontites and "thulites" and their synthetic equivalents. Zeitschrift für Kristallographie 217, 563-580.

Larson, A.C., Von Dreele, R.B., 1994. General Structure Analysis System (GSAS): Los Alamos National Laboratory Report LAUR, p. 86-748.

Lasaga, A.C., Rye, D.M., 1993. Fluid flow and chemical reaction kinetics in metamorphic systems. American Journal of Science 293, 361-404.

Le Bail, A., Duroy, H., Fourquet, J.L., 1988. Ab initio structure determination of $LiSbWO_6$ by X-ray powder diffraction. Materials Research Bulletin 23, 447-452.

825 Lee, C.T.A., Leeman, W.P., Canil, D., Li, Z.X.A., 2005. Similar V/Sc systematics in MORB and
826 arc basalts: implications for the oxygen fugacities of their mantle source regions. Journal of
827 Petrology 46, 2313–2336
828 Lee, C.-T.A., Luffi, P., Le Roux, V., Dasgupta, R., Albarede, F., Leeman, W.P., 2010. The redox
829 state of arc mantle using Zn/Fe systematics. Nature. 468, 681-685.
830 Luth, R.W., Virgo, D., Boyd, F.R., Wood, B. J., 1990. Ferric iron in mantle-derived garnets;
831 implications for thermobarometry and for the oxidation state of the mantle. Contributions to
832 Mineralogy and Petrology. 104, 56–72.
833 Malaspina, N., ~~Langenhorst, F., Fumagalli, P., Tumiati S., Poli, S., 2012. Fe^{3+} distribution between~~
834 ~~garnet and pyroxenes in mantle wedge carbonate-bearing garnet peridotites (Sulu, China)~~
835 ~~and implications for their oxidation state. Lithos 146-147, 11-17.~~
836 ~~Malaspina, N.,~~ Poli, S., Fumagalli, P., 2009. The oxidation state of metasomatized mantle wedge:
837 insights from C-O-H-bearing garnet peridotite. Journal of Petrology 50, 1533-1552.
838 Malaspina, N., Scambelluri, M., Poli, S., Van Roermund, H.L.M., Langenhorst, F., 2010. The
839 oxidation state of mantle wedge majoritic garnet websterites metasomatised by C-bearing
840 subduction fluids. Earth and Planetary Science Letters 298, 417–426.
841 Malaspina, N., Langenhorst, F., Fumagalli, P., Tumiati S., Poli, S., 2012. Fe^{3+} distribution between
842 garnet and pyroxenes in mantle wedge carbonate-bearing garnet peridotites (Sulu, China)
843 and implications for their oxidation state. Lithos 146-147, 11-17.
844 Manheim, F.T., 1978. Marine manganese deposits. Elsevier, Amsterdam.
845 Maresch, W.V., Mottana, A., 1976. The pyroxmangite-rhodonite transformation for the MnSiO3
846 composition. Contributions to Mineralogy and Petrology. 55, 69-79.
847 Marschall, H.R., Schumacher, J.C., 2012. Arc magmas sourced from mélange diapirs in subduction
848 zones. Nature Geosciences 5, 862-867.

849 Martin, S., Kienast, J.-R., 1987. The HP-LT manganesiferous quartzites of Praborna, Piedmont
850 ophiolite nappe, Italian western Alps. Schweizerische Mineralogische und Petrographische
851 Mitteilungen 67, 229-360.
852 Martin, S., Rebay, G., Kienast, J.-R., Mevel, C., 2008. An eclogitised oceanic palaeo-hydrothermal
853 field from the St. Marcel Valley (Italian Western Alps). Ofioliti. 33, 1-15.
854 Mattinson, C.G., Zhang, R.Y., Tsujimori, T., Liou, J.G., 2004. Epidote-rich talc-kyanite-phengite
855 eclogites, Sulu terrane, eastern China: *P-T-f*O_2 estimates and the significance of the epidote-
856 talc assemblage in eclogite. American Mineralogist 89, 1772-1783.
857 McMurdie, H.F., Sullivan B.M., Mauer, F.A., 1950. High-temperature X-ray study of the system
858 Fe_3O_4-Mn_3O_4. Journal of Research of the National Bureau of Standards, 45, 35-41.
859 Merkel, S., Jephcoat, A.P., Shu, J., Mao, H.K., Gillet, P., Hemley, R.J., 2002. Equation of state,
860 elasticity, and shear strength of pyrite under high pressure. Physics and Chemistry of
861 Minerals 29, 1-9.
862 Miletich, R., Allan, D.R., Angel, R.J., 1998. Structural control of polyhedral compression in
863 synthetic braunite $Mn^{2+}Mn^{3+}_6O_8SiO_4$. Physics and Chemistry of Minerals 25, 1983-1992.
864 Mori, M., 2002. Irreversible expansion behavior of $Mn_3O_{4+\delta}$ spinel and shrinkage behavior of
865 $La_{0.6}Sr_{0.4}MnO_3$ composites with the spinel during thermal cycling in O_2 atmosphere. Journal
866 of the Electrochemical Society 149, A995-A1000.
867 Muan, A., 1959. Stability relations among some manganese minerals. American Mineralogist 44,
868 946-960.
869 Ohashi, M., Tashiro, A., Oomi, G., Maeda, E., Zeng, X.G., 2006. Effect of pressure on the magnetic
870 phase transition in cupric oxide. Physical Review B 73, 134421.
871 Paris, E., Ross, C.R., Olijnyk, H., 1992. Mn_3O_4 at high-pressure – a diamond-anvil cell study and a
872 structural modelling. European Journal of Mineralogy 4., 87-93.

Proyer, A., Dachs, E., McCammon, C., 2004. Pitfalls in geothermobarometry of eclogites: Fe^{3+} and changes in the mineral chemistry of omphacite at ultrahigh pressures. Contributions to Mineralogy and Petrology. 147, 305-318.

Reinecke, T., 1998. Prograde high- to ultrahigh-pressure metamorphism and exhumation of oceanic sediments at Lago di Cignana, Zermatt-Saas Zone, Western Alps. Lithos 42, 147-189.

Robertson, E.C., 1988. Thermal properties of rocks. U. S. Geological Survey Open-File Report, 88-441.

Robie, R., Hemingway, B.S., 1995. Thermodynamic properties of minerals and related substances at 298.15 K and 1 bar (10^5 Pascals) pressure and at higher temperatures. U.S. Geological Survey Bulletin 2131, 461 pp.

Rupp, B., 1988. XLAT – Least square refinements of cell constants. Scripta Metallurgica. 22, 1.

Sherman, D.M., 1990. Molecular orbital (SCF-Xα-SW) theory of Fe^{2+}-Mn^{3+}, Fe^{3+}-Mn^{2+} charge transfer and magnetic exchange in oxides and silicates. American Mineralogist 75, 256-261.

Shi, P., 1992. Fluid fugacities and phase equilibria in the Fe-Si-O-H-S system. American Mineralogist 77, 1050-1066.

Smyth, J.R., Jacobsen, S.D., Hazen, R.M., 2000. Comparative crystal chemistry of dense oxide minerals. Reviews in Mineralogy 40, 157-186.

Spear, F.S., Rumble III, D., Ferry, J.M., 1982. Linear algebraic manipulation of n-dimensional composition space. Reviews in Mineralogy 10, 53-104.

Tumiati, S., 2005 (A). Geochemistry, mineralogy and petrology of the eclogitized manganese deposit of Praborna (Valle d'Aosta, Western Italian Alps) [Ph.D. thesis]: Università dell'Insubria (Como)–Université Denis Diderot (Paris-7).

Tumiati, S., Godard, G., Martin, S., Nimis, P., Mair, V., Boyer, B., 2005. (B). Dissakisite-(La) from the Ulten zone peridotite (Italian Eastern Alps): A new end-member of the epidote group. American Mineralogist 90, 1177-1185.

Tumiati, S., Godard, G., Masciocchi, N., Martin, S., Monticelli, D., 2008. Environmental factors

controlling the precipitation of Cu-bearing hydrotalcite-like compounds from mine waters. The case of the "Eve verda" spring (Aosta Valley, Italy). European Journal of Mineralogy 20, 73-94.

Tumiati, S., Martin, S., Godard, G., 2010. Hydrothermal origin of manganese in the high-pressure ophiolite metasediments of Praborna ore deposit (Aosta Valley, Western Alps). European Journal of Mineralogy 11, 577-594.

Tumiati, S., Fumagalli, P., Tiraboschi, C., Poli, S., 2013. An experimental study on COH-bearing peridotite up to 3.2 GPa and implications for crust-mantle recycling. Journal of Petrology 54, 453-479.

Wang, Z., Pischedda, V., Saxena, S.K., Lazor, P., 2002. X-ray diffraction and Raman spectroscopic study of nanocrystalline CuO under pressures. Solid State Communications 121, 275-279.

Wood, B.J., Bryndzia, L.T., Johnson, K.E., 1990. Mantle oxidation state and its relation to tectonic environment. Science. 248, 337–345.

Yamanaka, T., Nagai, T., Okada, T., Fukuda, T., 2005. Structure change of Mn_2O_3 under high pressure and pressure-induced transition. Zeitschrift für Kristallographie 220, 938-945.

Tables

Table 1: Representative compositions of major minerals forming the assemblages of Praborna occurring in the basal levels, upper levels, HP veins and the SiO_2-undersaturated sample C4.

Table A-1: Thermodynamic database used for calculations.

Table A-2: *V-T* data of braunite**.**

Table A-3: *V-T* data of pyrolusite**.**

Figure captions

Figure 1: Appearance of two-phase field (A + B) between two one-phase fields (A, B) in ~~an~~a unary system, when the molar quantity nO_2 is introduced instead of its conjugate potential μO_2. Vertical

lines in *b* are isothermal tie-lines accounting for the difference in molar quantity nO_2. Redrawn from Hillert (1985).

Figure 2. Geological sketch map of the Saint-Marcel valley showing the Praborna mine (45.6796° lat. N; 7.4495° long. E) and the principal lithologies occurring in the area.

Figure 3. Schematic section of the Mn ore. Basal levels are highly fractured and show pervasive veining. The enlargement shows a stockwork of quartz- and feldspar-filled veins cutting the massive ore mainly consisting of braunite (black) and piemontite (purple~~), with minor pyroxmangite and garnet.~~) (orange crusts are lichens). Note that the growth of "pegmatoid" piemontite crystals is perpendicular to the fracture walls~~.~~ (black arrow). Basal levels and veins contain omphacite in equilibrium with quartz and are in contact with glaucophanites. The upper part of the ore gradates into garnet + quartz ± pyroxmangite assemblages, and ~~are~~is overlaid by Mn-poor micaschists.

Figure 4. Representative mineral assemblages characterizing the Mn ore of Praborna. (a) Colorized Back Scattered Electron (CBSE) image of braunite (blue), pyroxmangite (green) and hematite (violet) coexisting with quartz in the basal level. (b) Transmitted Light Photomicrograph (TLP) of the vein containing Mn-rich purple omphacite (violan) in equilibrium with quartz, braunite and piemontite. (c) TLP of hematite in equilibrium with garnet, pyroxmangite and quartz in the silica-rich assemblages of the upper level. (d) CBSE image of quartz-free sample from the upper level, showing the replacement of pyroxmangite (yellow) + braunite (blue) by tephroite (~~light~~ blue-green) and hausmannite (violet). Rhodochrosite (red) is a late mineral.

Figure 5. Raman spectra of $MnSiO_3$ in selected samples (basal levels: SM93; upper levels: 16/01) ~~and comparison~~compared with those of reference ~~materials~~pyroxmangite and rhodonite from the

mineralogical collection of the *Muséum National d'Histoire Naturelle* in Paris. These spectra show that $MnSiO_3$ at Praborna is the high-pressure pyroxmangite polymorph.

Figure 6. As- and Sb-bearing minerals characterizing the parageneses at Praborna. (a) basal levels; zoned apatite crystal ~~enriched~~richer in As ~~in~~at the rim (cathodoluminescence image); (b) basal levels; ~~(As, Mn, Al)-silicate~~ ardennite-(As) $(Mn,Ca,Mg)_4(Al,Mg,Fe)_6(SiO_4)_2(Si_3O_{10})(AsO_4,VO_4)(OH)_6$ in equilibrium with garnet and ~~a crystal of~~ rutile showing a Sb-~~enriched~~rich rim (BSE image); (c) basal levels; ~~Ca-Sb oxide~~ romeite $(Ca,Fe,Mn,Na)_2(Sb,Ti)_2O_6(O,OH,F)$ showing oscillatory zoning (BSE image); (d) upper levels; hematite ~~with~~associated to Sb-rich pyrophanite ($MnTiO_3$) (BSE ~~images~~image).

Figure 7. Thermodynamic model of the system $MnO–SiO_2–O_2$, calculated for P = 2.1 GPa and T = 550 °C. (a) μO_2 (kJ•mol^{-1}) and log (fO_2/1 bar) vs. $SiO_2/(MnO+SiO_2)$ phase diagram ~~calculated at P = 2.1 GPa and T = 550 °C.~~. Compositions are represented in barycentric mole fractions. Considered phases are: quartz (qtz); manganosite (mang); pyroxmangite (pxmn); tephroite (teph); hausmannite (hsm); braunite (braun); bixbyite (bxb); pyrolusite (not stable at these conditions). In addition to μO_2 (right vertical axis), the corresponding log (fO_2/1 bar) and ΔFMQ values (black and grey numbers, respectively, on the left vertical axis) are also reported for comparison. Dashed grey lines are the univariant equilibria piemontite = garnet + H_2O + O_2, $CuO = Cu_2O + O_2$, $Cu_2O = Cu+O_2$, $FeSO_4$ = pyrite + hematite + O_2, hematite = magnetite + O_2, and magnetite + quartz = fayalite + O_2. The red and blue horizontal lines indicate the associations quartz–braunite–pyroxmangite (basal levels) and braunite–haussmanite–tephroite (upper levels), respectively. Shaded fields represents in grey scale the ratio Mn^{3+}/Mn_{tot} as suggested by Figure ~~b~~7b. (b) Ternary chemography of the system $MnO–SiO_2–O_2$ ~~calculated at P = 2.1 GPa and T = 550 °C.~~. Compositions are represented in barycentric mole fractions~~.~~ (i.e., sum of coordinates = 1). The diagram is stretched vertically (the upper O_2 vertex is not shown) in order to highlight the assemblages without oxygen as a free phase.

977 nO_2 represents the excess of O_2 component with reference to the Mn^{3+}-free system SiO_2–MnO.
978 μO_2sO_2 (kJ•mol^{-1}) areis reported for each divariant field. Thick dotted lines are theMn^{3+}/Mn_{tot}
979 isopleths with constant Mn^{3+}/Mn_{tot}, whereas horizontal dotted lines are thenO_2 isopleths with
980 constant nO_2.. The O_2 vertex is joined with quartz–O_2, braunite–O_2 and bixbyite by dotted–O_2 tie-
981 line (dotted arrows) are virtual, because O_2 is not thought to be a real phase. at these conditions. The
982 coloured fields correspond to the typical Praborna assemblages as in Figure a7a. Black arrow is a
983 hypothetical metasomatic path from SiO_2-poor to SiO_2-enriched assemblages, where nO_2 and the
984 ratio Mn^{3+}/Mn_{tot} decrease while the chemical potential of oxygenμO_2 increases.
985
986 Figure 8. QuaternaryThermodynamic model of the system MnO–FeO–SiO_2–O_2
987 calculated atfor P = 2.1 GPa and T = 550 °C. Compositions are represented in barycentric mole
988 fractions. nO_2 represents the excess of component O_2 with reference to the Fe^{3+}- and Mn^{3+}-free
989 system FeO–SiO_2–MnO. Log fO_2s areΔFMQ is reported for each 4-phases field (manganosite–
990 tephroite–hausmannite–hematite; braunite–hausmannite–bixbyite–hematite; tephroite–
991 hausmannite–braunite–hematite; tephroite–pyroxmangite–braunite–hematite;assemblage (e.g.,
992 +12.7 for pyroxmangite–quartz–braunite–hematite; quartz–magnetite–hematite–pyroxmangite;
993 quartz–ferrosilite–magnetite–manganosite; fayalite–ferrosilite–magnetite–manganosite; wüstite–
994 fayalite–magnetite–manganosite). The grey plane represents the locus of points at constant value of
995 nO_2 and intersects all the assemblages, with ΔFMQ ranging from logfO_2 = –38-18.1 (wüstite–
996 fayalite–magnetite–manganosite, light green volume), to –10+9.7 (tephroite–hausmannite–braunite–
997 hematite, blue volume, upper levels), and to -+12.7 (braunite–quartz–pyroxmangite–hematite, red
998 volume, basal levels).
999
1000 Figure 9. Cartoon illustrating a Oxygen in the subduction channel,. Cartoon redrawn after Konrad-
1001 Schmolke et al. (2011), appearing) showing a patchy in termsand heterogeneous distribution of
1002 oxygen fugacity (cf.fO_2 (see ΔFMQ; see also Fig. 12 in Foley, 2011, Fig. 12), which reflects the

~~different bulk rock compositions~~), but ~~not the net bulk oxidation, represented by~~ a more regular gradient of nO_2~~,~~ (i.e. the quantity of oxygen in excess compared to Fe^{3+}- and Mn^{3+}-free systems~~.~~). In terms of nO_2, the mélange appears as a metasomatic front from the more oxidized slab to the less oxidized mantle wedge. Oxygen can be transported along fractures and veins through dissolution-reprecipitation of oxides and silicates fluxed by fluids. See text for further details.